

AD-A122 403

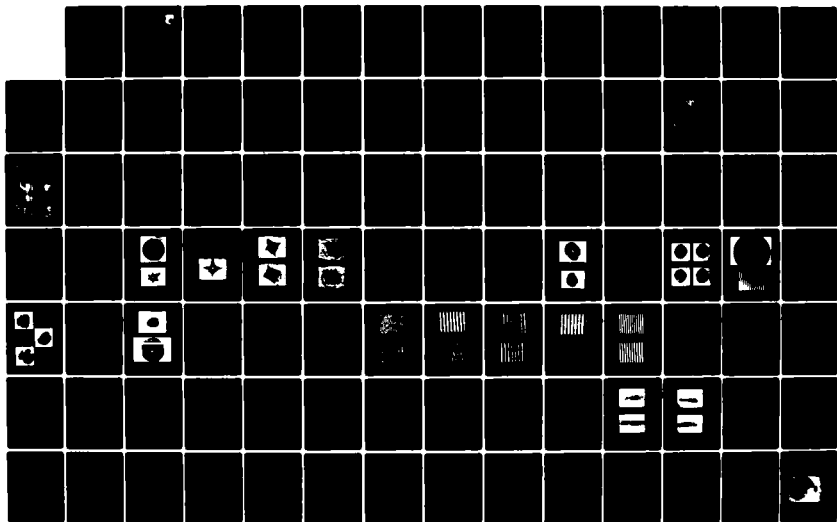
DEVELOPMENT OF NEW NONDESTRUCTIVE TESTING TECHNIQUES  
FOR USE IN BLADED-DI...(U) DAYTON UNIV OH RESEARCH INST  
K G HARDING ET AL. SEP 82 UDR-TR-82-46 AFWAL-TR-82-2081  
F33615-80-C-2011

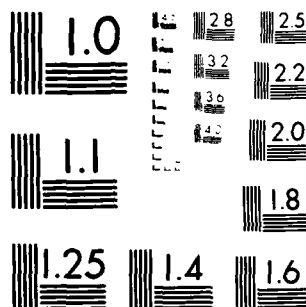
1/2

UNCLASSIFIED

F/G 20/6

NL





MICROCOPY RESOLUTION TEST CHART  
NATIONAL BUREAU OF STANDARDS-1963-A

AD A122403

12

AFWAL-TR-82-2081



DEVELOPMENT OF NEW NONDESTRUCTIVE TESTING  
TECHNIQUES FOR USE IN BLADED-DISK DYNAMICS RESEARCH

Kevin G. Harding and James S. Harris

UNIVERSITY OF DAYTON RESEARCH INSTITUTE

September 1982

Final Report for Period June 1980 to April 1982

Approved for public release; distribution unlimited.

AERO PROPULSION LABORATORY  
AIR FORCE WRIGHT AERONAUTICAL LABORATORIES  
AIR FORCE SYSTEMS COMMAND  
WRIGHT-PATTERSON AIR FORCE BASE, OHIO 45433



FILE COPY

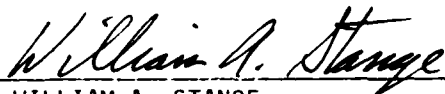
82 14 012

NOTICE

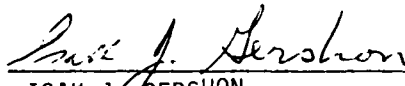
When Government drawings, specifications, or other data are used for any purpose other than in connection with a definitely related Government procurement operation, the United States Government thereby incurs no responsibility nor any obligation whatsoever; and the fact that the government may have formulated, furnished, or in any way supplied the said drawings, specifications, or other data, is not to be regarded by implication or otherwise as in any manner licensing the holder or any other person or corporation, or conveying any rights or permission to manufacture, use, or sell any patented invention that may in any way be related thereto.

This report has been reviewed by the Office of Public Affairs (ASD/TA) and is releasable to the National Technical Information Service (NTIS). At NTIS, it will be available to the general public, including foreign nations.

This technical report has been reviewed and is approved for publication.



WILLIAM A. STANGE  
Project Engineer  
AFWAL/POTA / 52081



ISAK J. GERSHON  
Technical Area Manager  
AFWAL/POTA/52081

FOR THE COMMANDER



H. I. BUSH  
Director  
Turbine Engine Division

"If your address has changed, if you wish to be removed from our mailing list, or if the addressee is no longer employed by your organization, please notify AFWAL/POTA, WPAFB OH 45433 to help us maintain a current mailing list."

Copies of this report should not be returned unless return is required by security considerations, contractual obligations, or notice on a specific document.

UNCLASSIFIED

SECURITY CLASSIFICATION OF THIS PAGE (When Data Entered)

REPORT DOCUMENTATION PAGE		READ INSTRUCTIONS BEFORE COMPLETING FORM
1. REPORT NUMBER AFWAL-TR-82-2081	2. GOVT ACCESSION NO. AD-A122 403	3. RECIPIENT'S CATALOG NUMBER
4. TITLE (and Subtitle) Development of New Nondestructive Testing Techniques for Use in Bladed-Disk Dynamics Research		5. TYPE OF REPORT & PERIOD COVERED Final Report 6/80 - 4/82
		6. PERFORMING ORG. REPORT NUMBER UDR-TR-82-46
7. AUTHOR(s) K. G. Harding, J. S. Harris		8. CONTRACT OR GRANT NUMBER(s) F33615-80-C-2011
9. PERFORMING ORGANIZATION NAME AND ADDRESS University of Dayton Research Institute 300 College Park Dayton, Ohio 45469		10. PROGRAM ELEMENT, PROJECT, TASK AREA & WORK UNIT NUMBERS
11. CONTROLLING OFFICE NAME AND ADDRESS Air Force Wright Aeronautical Laboratory Aero Propulsion Laboratory AFWAL-POTA, Wright-Patterson AFB, Ohio 45433		12. REPORT DATE September 1982
		13. NUMBER OF PAGES 125
14. MONITORING AGENCY NAME & ADDRESS (if different from Controlling Office)		15. SECURITY CLASS. (of this report) Unclassified
		15a. DECLASSIFICATION DOWNGRADING SCHEDULE
16. DISTRIBUTION STATEMENT (of this Report)  Approved for public release; distribution unlimited.		
17. DISTRIBUTION STATEMENT (of the abstract entered in Block 20, if different from Report)		
18. SUPPLEMENTARY NOTES		
19. KEY WORDS (Continue on reverse side if necessary and identify by block number)  Nondestructive Testing, Moire, Speckle, Holography, Interferometry, Turbine Blades, Vibration Analysis		
20. ABSTRACT (Continue on reverse side if necessary and identify by block number)  In this program the University investigated the feasibility of using moire, speckle interferometry, and multiple wavelength contouring in conjunction with the real-time optical derotation system currently in use. Each of these approaches is addressed separately in this report to provide continuity in the text. The first task addressed is an analysis of the current real-time image-derotated holographic interferometry system being used by AFWAL/POTA to present a better understanding of the problems and inherent limitations		

DD FORM 1 JAN 73 1473

EDITION OF 1 NOV 65 IS OBSOLETE

UNCLASSIFIED

SECURITY CLASSIFICATION OF THIS PAGE (When Data Entered)

UNCLASSIFIED

SECURITY CLASSIFICATION OF THIS PAGE(When Data Entered)

BLOCK 20. Abstract

in the system. In particular, the alignment of the derotator and the aberrations of the optical system are addressed. Based on this analysis, Section 2 presents the University's recommendations and actions to improve the current system.

The remainder of this report is dedicated to a discussion of moire, speckle, and multiple wavelength interferometry with particular emphasis on projected fringe moire interferometry. Each approach was evaluated on the basis of the form of data obtained, expense and availability of equipment, range of sensitivity, and possible errors. Section 10 of this report summarizes the results of this program and presents a recommended system for moire interferometry in the AFWAL/POTA facility.

UNCLASSIFIED

SECURITY CLASSIFICATION OF THIS PAGE(When Data Entered)

## PREFACE

This report was prepared by K. G. Harding and J. S. Harris of the University of Dayton Research Institute, Dayton, Ohio 45469. The work described in this report was supported by the Air Force Wright Aeronautical Laboratories, Aero Propulsion Laboratory (AFWAL/POTA) under contract number F33615-80-C-2011 entitled Development of New Nondestructive Testing Techniques for Use in Bladed-Disk Dynamics Research. The period covered by this report is June 1980 through April 1982. The final copy of this report was submitted in September 1982. The Air Force project monitor for this work was William Stange.



Accession For  
NLS MAIL  
FILE NO.  
Volume

A

# TABLE OF CONTENTS

<u>SECTION</u>		<u>PAGE</u>
I	INTRODUCTION . . . . .	1
II	ANALYSIS OF REAL-TIME HOLOGRAPHIC SYSTEM . . . . .	4
	1. ILLUMINATION SYSTEM . . . . .	4
	2. IMAGING SYSTEM . . . . .	5
	3. OTHER IMPROVEMENTS . . . . .	6
III	THEORY . . . . .	8
	1. THEORY OF MOIRE . . . . .	8
	2. OPTICAL PROCESSING . . . . .	12
IV	REVIEW OF MOIRE TECHNIQUES . . . . .	21
	1. SHADOW MOIRE . . . . .	21
	2. REFLECTION MOIRE . . . . .	21
	3. PROJECTION MOIRE . . . . .	23
	4. CONTACT MOIRE . . . . .	23
	5. HOLOGRAPHIC MOIRE . . . . .	27
	6. CONCLUSIONS . . . . .	29
V	INTERFEROMETRY METHODS . . . . .	31
	1. TIME-AVERAGE MOIRE . . . . .	31
	2. REAL-TIME MOIRE . . . . .	37
	3. PULSED MOIRE . . . . .	41
	4. CONCLUSIONS . . . . .	46
VI	DATA RECORDING . . . . .	49
	1. FILM EVALUATION . . . . .	49
	2. MODEL COATING . . . . .	56
VII	DATA INTERPRETATION . . . . .	62
	1. TRANSLATION . . . . .	63
	2. PITCH . . . . .	63
	3. YAW . . . . .	65
	4. DEFLECTION . . . . .	65
	5. MEASUREMENT TECHNIQUES . . . . .	66
	6. EXPERIMENTAL DEMONSTRATION . . . . .	67



# TABLE OF CONTENTS (Continued)

<u>SECTION</u>	<u>PAGE</u>
VIII	SPECKLE INTERFEROMETRY . . . . . 72
	1. BACKGROUND . . . . . 72
	2. CONCLUSIONS . . . . . 78
IX	MULTIPLE WAVELENGTH INTERFEROMETRY . . . . . 80
	1. MULTIPLE WAVELENGTH CONTOURING . . . . . 80
	2. MULTIPLE WAVELENGTH SPECKLE . . . . . 83
	3. RESULTS AND CONCLUSIONS . . . . . 85
X	SUMMARY AND RECOMMENDATIONS . . . . . 88
	1. ANALYSIS OF REAL-TIME SYSTEM . . . . . 88
	2. NEW TECHNIQUES FOR BLADED-DISK DYNAMICS MEASUREMENTS . . . . . 88
	3. SYSTEM RECOMMENDED FOR APL FACILITY INSTALLATION . . . . . 89
REFERENCES	. . . . . 94
APPENDIX A	OBJECT MOTOR SPEED CONTROLLER . . . . . 97
APPENDIX B	MAGNETIC TRANSDUCER, HIGH FORCE, HIGH FREQUENCY . . . . . 108

# LIST OF ILLUSTRATIONS

<u>FIGURE NO.</u>		<u>PAGE</u>
1	Moire by Rotation Mismatch.	9
2	Moire by Pitch Mismatch.	10
3	Schematic of Optical Processor.	13
4	Picture of Optical Processor.	14
5	Diagram of Diffracted Orders from a Straight-Line Grating.	16
6	Picture of Diffracted Orders from a Straight-Line Grating.	17
7	Diagram of Shadow Moire System.	22
8	Diagram of Reflection Moire System.	24
9	Diagram of Projection Moire System.	25
10	Diagram of Contact Moire System.	26
11	Diagram of Holographic Moire System.	28
12	Time-Average Moire Pattern of a Metal Plate.	33
13	Time-Average Moire of a Static Disk.	34
14	Time-Average Moire of a Rotating Disk.	35
15	Schematic of Optical System for Moire Interferometry.	39
16	a. Real-Time Moire of a Static Disk.	40
	b. Real-Time Moire of a Rotating Disk.	40
17	Traveling Wave 2-N Mode Pattern.	42
18	a. Double Exposure Additive Moire.	43
	b. Multiplicative Moire.	43
19	Pulse Moire of a Metal Plate.	45
20	Double Exposure Pulsed Moire.	47
21	Photograph of Grating with Various Films.	51

LIST OF ILLUSTRATIONS (Continued)

<u>FIGURE NO.</u>		<u>PAGE</u>
22	Comparison of Copied Grating Photographs.	57
23	Reflectance Map of Selected Coatings.	60
24	Predicted Moire Pattern of Blade Model.	64
25	Setup to Demonstrate Moire Data Analysis.	68
26	Moire Patterns on a Blade Model.	69
27	System for Multiple Wavelength Contouring.	82
28	Multiple Wavelength Contouring Produced by Ruby Laser.	86
29	Collimating Telescope System for Projected Interference Fringe Moire.	90
30	Single Tilted Lens System for Projected Interference Fringe Moire.	91
A.1 through A.8	Object Motor Speed Controller Drawings.	99 106
A.9	Motor Controller Mother Board Pin Assignment.	107
B.1	Schematic Cross Section of Transducer Showing Coolant Flow.	110
B.2	Magnetic Transducer Core Sheet.	112
B.3	Magnetic Transducer Body.	113
B.4	Magnetic Transducer Outer Barrel.	114
B.5	Magnetic Transducer Coil Form.	115
B.6	Magnetic Transducer End Cap.	116
B.7	Magnetic Transducer Hole Spacing Sketch.	117
B.8	Oersteds vs D.C. Current into Transducer.	118
B.9	Acceleration Response vs D.C. Bias at a Constant A.C. Drive Level.	119

# LIST OF ILLUSTRATIONS (Continued)

<u>FIGURE NO.</u>		<u>PAGE</u>
B.10	Acceleration Response vs A.C. Drive Voltage at a Constant D.C. Bias Current.	120
B.11	Coolant Manifold.	122
B.12	Schematic of Cooling System	123

## LIST OF TABLES

<u>TABLE NO.</u>		<u>PAGE</u>
1	COMPARISON OF MOIRE TECHNIQUES	30
2	COMPARISON OF POSSIBLE FILMS FOR MOIRE PHOTOGRAPHS	50
3	DIFFUSE REFLECTANCE OF VARIOUS MATERIALS AT A WAVELENGTH OF 0.6328 MICRONS	59
4	NORMAL REFLECTION FOR 45 DEGREE INCIDENCE BEAM AT 514.5 nm (NORMALIZED)	61
5	MOIRE MEASUREMENTS COMPARED TO DIAL INDICATOR MEASUREMENTS (IN MILLIMETERS) FOR SIMPLE DEFLECTION OF A BLADE MODEL	71
6	CORRELATION WIDTH MEASUREMENTS	75
7	FRINGE SPACING FOR MULTI-WAVELENGTH CONTOURING	80
8	COMPARISON OF PROJECTED FRINGE OPTICAL SYSTEMS	93

## SECTION I INTRODUCTION

This report describes a program conducted by the University of Dayton under contract to the Air Force Wright Aeronautical Laboratories, Aero Propulsion Laboratory (AFWAL/POTA). The objective of this program was to develop nondestructive testing techniques to extend the sensitivity and range of the real-time holographic system currently being used. Such an extension of the current capability to study rotating disk dynamics is essential to a thorough understanding of the dynamics of full-scale turbine blades and thereby an improvement in dynamic design.

The development and implementation of improved experimental and analytical technology to achieve increased understanding and improved prediction of the dynamic behavior of rotating bladed-disk structures is a prime objective of all turbomachinery developers. This is particularly essential in advanced technology weapons systems where increasing emphasis is placed on achieving higher thrust-to-weight ratios, partially addressed by the use of lightweight, high-work, bladed-disk rotating structures. Typically, bladed-disk failure histories indicate that fatigue failures of these structures can be attributed to blade alone or blade-disk coupled modes characterized by diametrical node lines. These modes are usually complex in nature and typically difficult to characterize using traditional experimental, dynamic structural analysis techniques based solely on current strain gage technology.

Continuous wave and pulsed laser interferometric holography have been used routinely as techniques for establishing the response frequencies and resultant mode shapes of structures. In gas turbine engines, the most common application of holography has been the study of blade airfoils and bladed-disk assemblies under nonrotating conditions. These analyses have greatly improved the understanding of blade and disk interaction under

dynamic conditions. There is a serious drawback, however, which limits this form of analysis: body forces resulting from component spinning cannot be applied in a bench test. The only way to simulate these forces is by actually spinning the component or assembly. In order to analyze these structures under rotating conditions, an optical system incorporating a rotating erector prism with associated controls has been developed, which has sufficient precision to enable interferometric holograms of rotating objects to be constructed.

The optical nondestructive testing techniques investigated previously at the Aero Propulsion Laboratory have used holography. The first approach used a ruby laser and an optical derotator to take a double exposure hologram of a rotating disk. The resulting hologram presents a comparison of the disk at two different instances in time, separated by some set period of time (typically a few microseconds). The short pulses of the ruby laser, a few nanoseconds, freeze all motion associated with the disk as well as any motion in the system being used to make the hologram. Therefore, this system can tolerate many different vibrations in the system and requires a minimal amount of alignment to ensure optical derotation. However, there were a number of limitations to this system. Two of the most important were: only two points in the rotation of the object can be compared and transient modes are difficult to study with this technique. To increase the versatility of the system, the Air Force converted the system to a real-time stroboscopic holographic system. The University of Dayton was responsible for the design and manufacture of the laser modulation system and also worked with the Air Force in the setup and operation of the holographic system. With this system the structural dynamics of a disk can be studied in real-time and at any given rotational position of the disk. The phase and frequency of the strobe can be varied to observe the dynamics of the disk at various positions, at various rotational

speeds, and at various excitation frequencies. All characteristics of the dynamics of the rotating disk can be seen as they happen.

The extension of the derotated, holographic interferometry to a real-time system has significantly extended the range and character of rotating disk dynamics which can be studied. However, any holographic technique is limited in the amplitude of displacements which it can measure. A new testing technique needs to be developed to permit the study of large dynamic displacements (from a few microns and up) of rotating turbine blades.

In this program the University investigated the feasibility of using moire, speckle interferometry, and multiple wavelength contouring in conjunction with the real-time optical derotation system currently in use. Each of these approaches is addressed separately in this report to provide continuity in the text.

The first task addressed is an analysis of the current real-time image-derotated holographic interferometry system being used by AFWAL/POTA to present a better understanding of the problems and inherent limitations in the system. In particular, the alignment of the derotator and the aberrations of the optical system are addressed. Based on this analysis, Section 2 presents the University's recommendations and actions to improve the current system.

The remainder of this report is dedicated to a discussion of moire, speckle, and multiple wavelength interferometry with particular emphasis on projected fringe moire interferometry. Each approach was evaluated on the basis of the form of data obtained, expense and availability of equipment, range of sensitivity, and possible errors. Section 10 of this report summarizes the results of this program and presents a recommended system for moire interferometry in the AFWAL/POTA facility.

## SECTION II

### ANALYSIS OF REAL-TIME HOLOGRAPHIC SYSTEM

The Aero Propulsion Laboratory's real-time derotated holography system is a modification of a system originally developed by United Technologies to do double-pulsed derotated holography of rotating structures.<sup>1</sup> Since the pulsed ruby laser has more than enough energy to make a hologram, the original system did not need to be energy efficient. Therefore, the pulsed system used a lossy 50:50 beam splitter and operated at a very high F-number. Because of the very short pulse of the ruby laser, alignment and optical tolerances needed only to be of interferometric quality over a very limited range.

#### 1. ILLUMINATION SYSTEM

For the real-time system<sup>2</sup> the efficiency needed to be improved by replacing the 50:50 beam splitter with polarizing optics and by using an efficient retroreflecting paper on the object. The polarizing optics yielded nearly a factor of four improvement in light efficiency. The size of the object which could be illuminated was limited by the aperture of these polarizing optics. The alignment tolerances on the optical system were increased by devising a new alignment procedure which ensured close alignment over 360 degrees of rotation of the object. The problems which remained were the ability to illuminate a larger object efficiently, collect the retroreflected light more efficiently, and obtain a higher resolution image. These problems were addressed in this program.

To increase the object area which could effectively be illuminated and to provide more light collection efficiency, the 1-inch (25 mm) polarizing beam splitting cube and 2/3-inch (15 mm) wave plate were replaced with a 4-inch (100 mm) polarizing beam splitting plate and a 2-inch (50 mm) wave plate. The extinction coefficient of the polarizing beam splitting plate is



only about 90 to 1 while the extinction coefficient of the polarizing beam splitting cube was over 500 to 1. This loss in the efficiency of the beam splitter is not a problem. The total loss of the polarizing beam splitting plate (double pass) is only about 20 to 25 percent as opposed to over 75 percent for the 50:50 beam splitter. The light which is lost using the polarizing beam splitting plate rather than the cube is regained in the light collection increase afforded by the larger aperture.

We did not recommend a larger polarizing beam splitting cube simply because of cost considerations. The optical derotator makes all of the stationary optics in the viewing system appear to rotate. A 2-inch thick glass cube will typically have some distortions and a small wedge, and will generally degrade the quality of the image due to spherical aberrations. A high-quality cube of this size is very expensive. The local distortions and wedge would be transformed into movement in the image plane which could not be corrected for by alignment techniques. By using a beam splitting plate and using the plate in reflection for imaging, these problems are completely avoided and a higher quality image is possible.

## 2. IMAGING SYSTEM

The double-pulsed derotator optical system used an infinity corrected 1-inch (25 mm) doublet as a primary imaging element, a similar optic as a field lens behind the derotator, and an inexpensive copy lens for the final imaging. The optical derotator prism itself introduces about 20 microns (almost a mil) of spherical aberration (from theoretical ray trace). The effect of the spherical aberration is to cause a slight spreading (about 5 microns) of any detail in the image plane. The capability of this optical system is about 5 line pairs per millimeter (LP mm) (125 line pairs per inch (LPI)).

The real-time holographic system uses a video system to enlarge the holographic image for easy viewing. On the video

image, the resolution of the optical system translates into about 0.5 LP mm (about 10 LPI) which is a clearly visible degradation. This degradation is mostly cosmetic for the purposes of holography (since the interference fringes are formed behind the derotator) but it could be fatal for certain moire applications. We found that by replacing the double-pulsed system imaging and field lenses with high-quality flat-field enlarger/copy lenses (Rodenstock) the resolution through the derotator could be improved to about 60 LP mm (1500 LPI). This resolution approaches the resolution limit set by the distortions introduced by the derotator prism. By using a 50-mm (2-inch) diameter primary lens, the light collection capability was also improved.

Further improvement in resolution could be realized by designing a Schmidt type corrector plate which would introduce a compensating amount of spherical aberration into the image which the derotator prism would subtract out, leaving little or no spherical aberration. The cost to design and fabricate such an optic would be very expensive and probably gain much less than a factor of two in resolution. Therefore, the cost for further improvement is not warranted until it proves necessary.

### 3. OTHER IMPROVEMENTS

Proper and stable setting of the object rotational speed is a very important factor in real-time study of vibration modes. A small error or drift in the speed can cause the mode to rotate on the object and become unstable, or the object may cease to resonate. Many of these dynamics are of interest in studying disk dynamics, but if the rotation speed has an unknown drift, the results contain an unknown variable.

To correct this problem and permit greater accuracy in setting the speed, the University developed a high-tolerance speed controller for the Aero Propulsion Laboratory System. The speed controller uses a reference signal provided by an optical

encoder attached directly to the object spindle. The speed controller can be set to within 1 rpm and has a drift of less than  $\pm 2$  rpm. A schematic of the speed controller is given in Appendix A of this report.

Another improvement we made to the Aero Propulsion Laboratory facility was the addition of externally cooled magnets for better excitation of the object. An external closed-circuit freon cooling system was employed to prevent overheating of the magnet when used in the AFWAL/POTA vacuum chamber. A DC bias was introduced into the excitation signal to ensure a uniform, sinusoidal excitation signal without the asymmetry usually introduced by crossing zero. These magnets provide about a factor of four more excitation than the magnetic transducers which were previously used. Additional information on the magnets is given in Appendix B.

### SECTION III

#### THEORY

#### 1. THEORY OF MOIRE

Moire interferometry is a full-field, noncontact method of measuring out-of-plane displacements of a structure.<sup>3-5</sup> A moire interference pattern is a series of light and dark fringe lines of equal change in surface position which map out the contour or change in contour of an object the same way a topography map delineates the contour of the land. The tools to create a moire involve well-established photographic equipment and techniques.

Moire interferometry fringes are formed by overlaying two gratings, a specimen or object grating which is viewed or photographed on the object, and a master reference grating. The beat frequency between the two slightly different gratings is what creates the moire pattern. This beat frequency can occur two ways. A rotational mismatch in the position of two like gratings causes the grating lines to intersect at an angle, forming a moire pattern perpendicular to the bisector between the two sets of grating lines as shown in Figure 1. A pitch mismatch between two gratings causes a beat frequency between the two gratings, forming a moire parallel to the grating lines as shown in Figure 2.

This interference phenomenon can be seen mathematically by considering two straight line sinusoidal gratings described by the transmission equations

$$T_1 = a_1 + b_1 \cos (c_1 x)$$

$$T_2 = a_2 + b_2 \cos (c_2 x).$$

Overlaying these two gratings is equivalent to multiplying the two transmission equations which for an initial uniform intensity

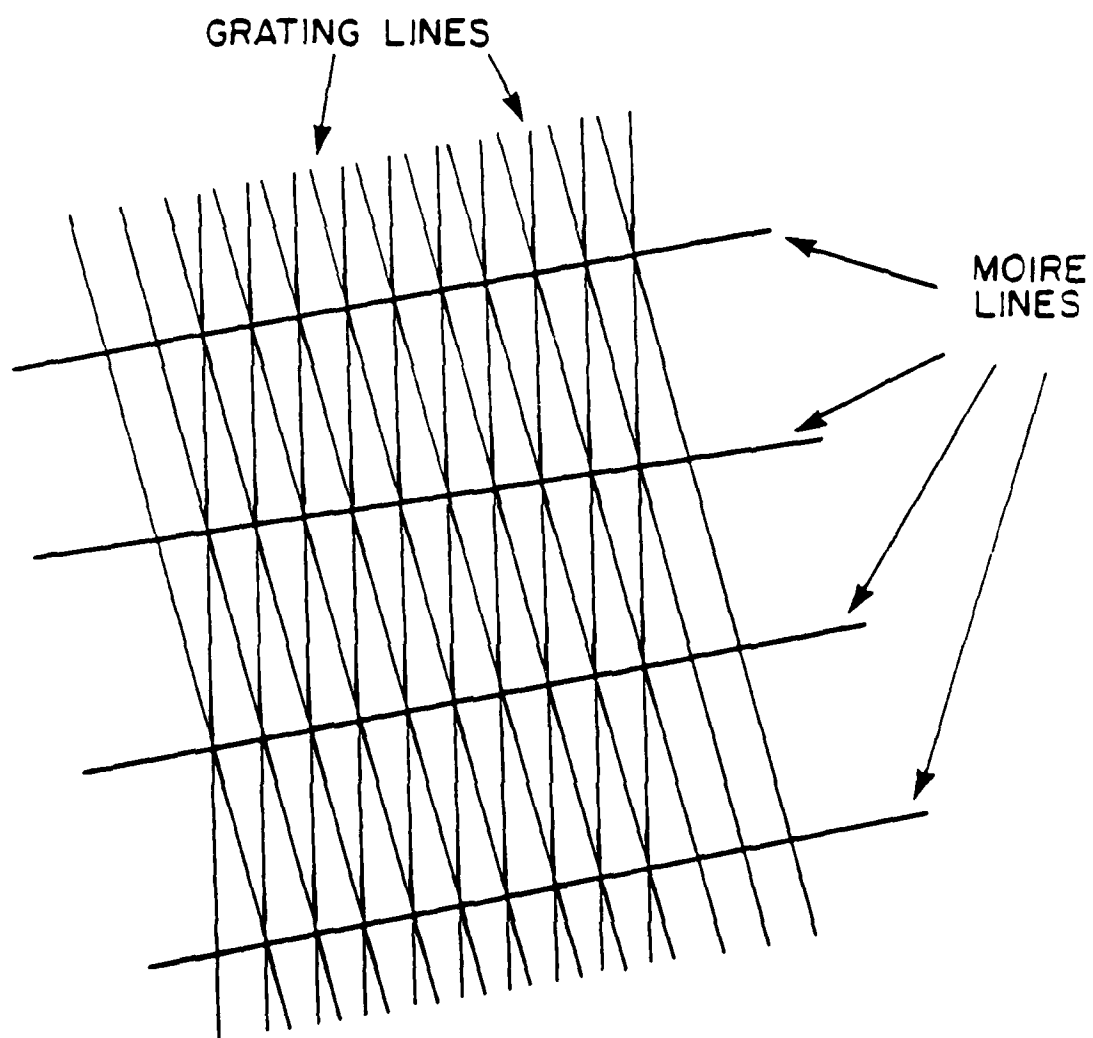


Figure 1. Moire by Rotation Mismatch.

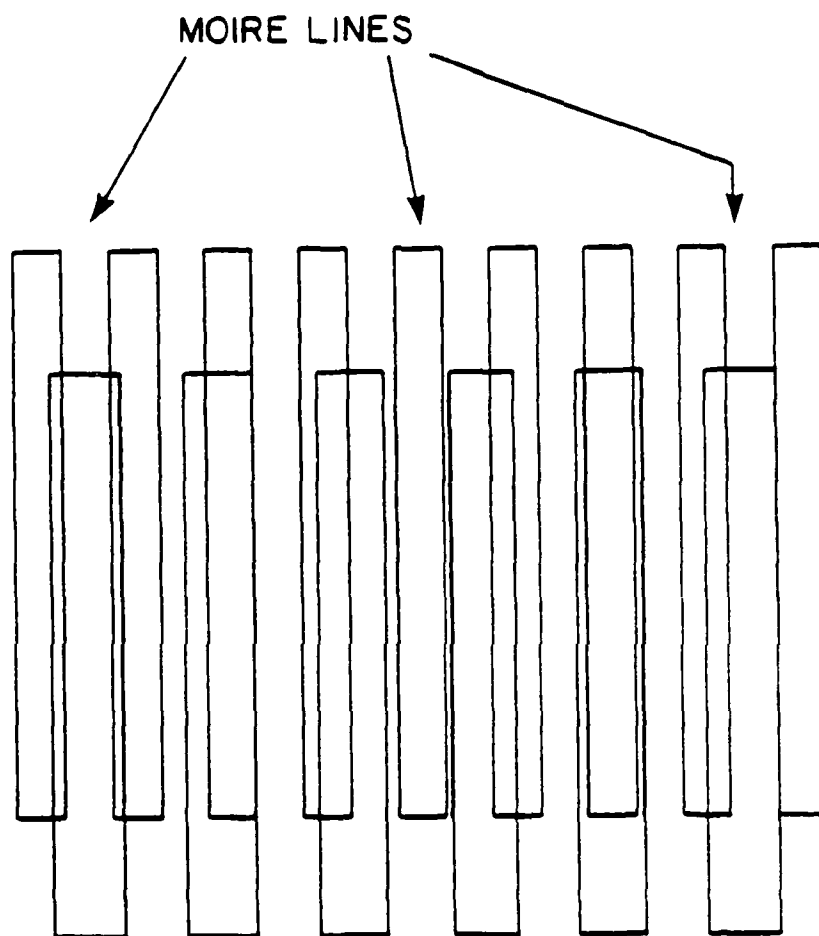


Figure 2. Moire by Pitch Mismatch.

of light of  $I_0$  yields

$$I_t = I_0 T_1 T_2 = I_0 [a_1 a_2 + a_1 b_2 \cos (c_2 x) + a_2 b_1 \cos (c_1 x) + b_1 b_2 \cos (c_1 x) \cos (c_2 x)] .$$

The first term is just the directly transmitted light and the second and third terms are the two original gratings. Expanding the last term of the above equation gives

$$1/2 b_1 b_2 \cos (c_1 + c_2) x + 1/2 b_1 b_2 \cos (c_1 - c_2) x .$$

The first term in the above expression is the sum of the two gratings and the second term is the difference of the two gratings. The difference term is the interference term which describes the resulting beat frequency, analogous to the optical path difference which yields interference fringes in laser interferometry.

If one of the gratings is a specimen or model grating on the surface of an object and the master grating is a straight line grating, the resulting moire pattern will be a contour map of the topography of the object. If the reference or master grating is made by photographing the specimen grating, only changes in surface contour, that is deflections, will create a moire fringe pattern. The specimen grating can be formed by projecting a grating onto the object, in which case the moire is completely insensitive to in-plane motion. Or the grating can actually be contacted onto the object, in which case the grating will move or rotate with the object and in-plane movement can be measured. Contacting the grating to the object permits testing of a moving object referenced to the object coordinate system.

The sensitivity of moire interferometry is given by

$$\Delta Z = P / (\tan \alpha + \tan \beta)$$

where  $P$  is the period of the master grating projected on the object,  $\alpha$  is the angle to the average normal to the object from

which the grating is being projected, and  $\beta$  is the viewing angle. Therefore, the sensitivity of moire interferometry can be tailored to the specific test by simply changing the master grating period, regardless of wavelength. The measurement sensitivity of moire has been demonstrated from 25 micron (0.001 inches) for large areas down to 0.25 microns (0.00001 inches) over small areas (less than 25 millimeters) with no real upper bound on the magnitude of out-of-plane deflections which can be measured.

## 2. OPTICAL PROCESSING

The interference pattern formed in moire interferometry contains a map of the out-of-plane displacement of the model at every point on the model covered by a grating line, even where a moire fringe is not seen. The accuracy to which this information can be measured is determined by the accuracy to which the fringe positions can be measured. Interference fringes can generally be accurately measured manually to one fourth of a fringe. This means that for a moire pattern with a sensitivity of 200 microns (8 mils) of out-of-plane displacement per moire fringe (as calculated from the equation for  $\Delta Z$ ), the displacement can be measured quantitatively to an accuracy of 50 microns (2 mils). This sensitivity can effectively be multiplied by multiplying the number of moire fringes.

Multiplication of the number of moire fringes can be accomplished by multiplying the frequency of the recorded master and model gratings before overlaying them to form the moire. This grating frequency multiplication can be performed in the optical Fourier transform plane.<sup>6,7</sup> A system that will facilitate optical Fourier transform filtering is shown in Figures 3 and 4. The grating photograph is placed in the grating plane and the Fourier transform of that grating is produced in the Fourier transform plane at the focus of lens  $L_3$ . The Fourier transform of a straight-line grating is a series of evenly spaced points.



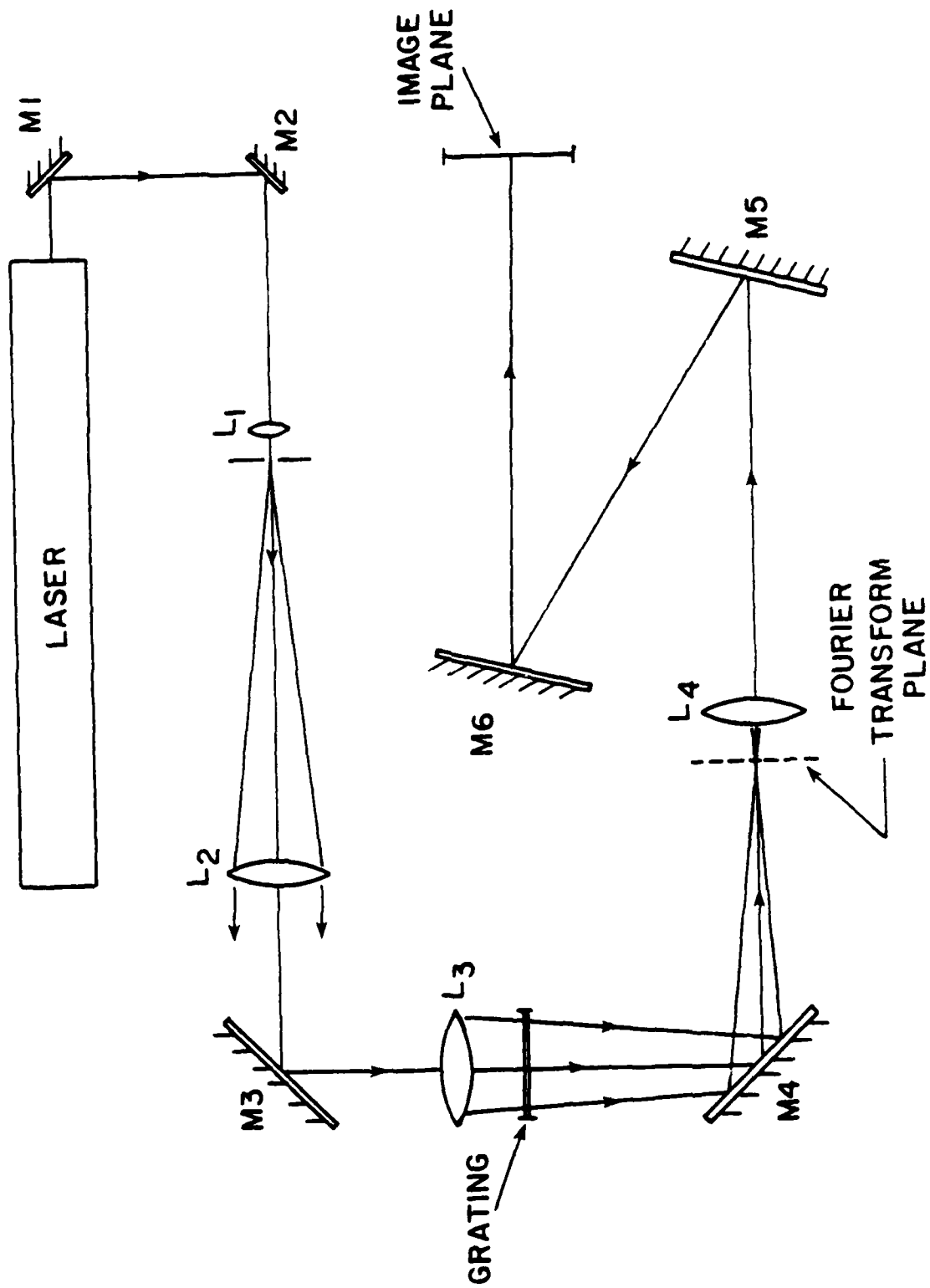


Figure 3. Schematic of Optical Processor.

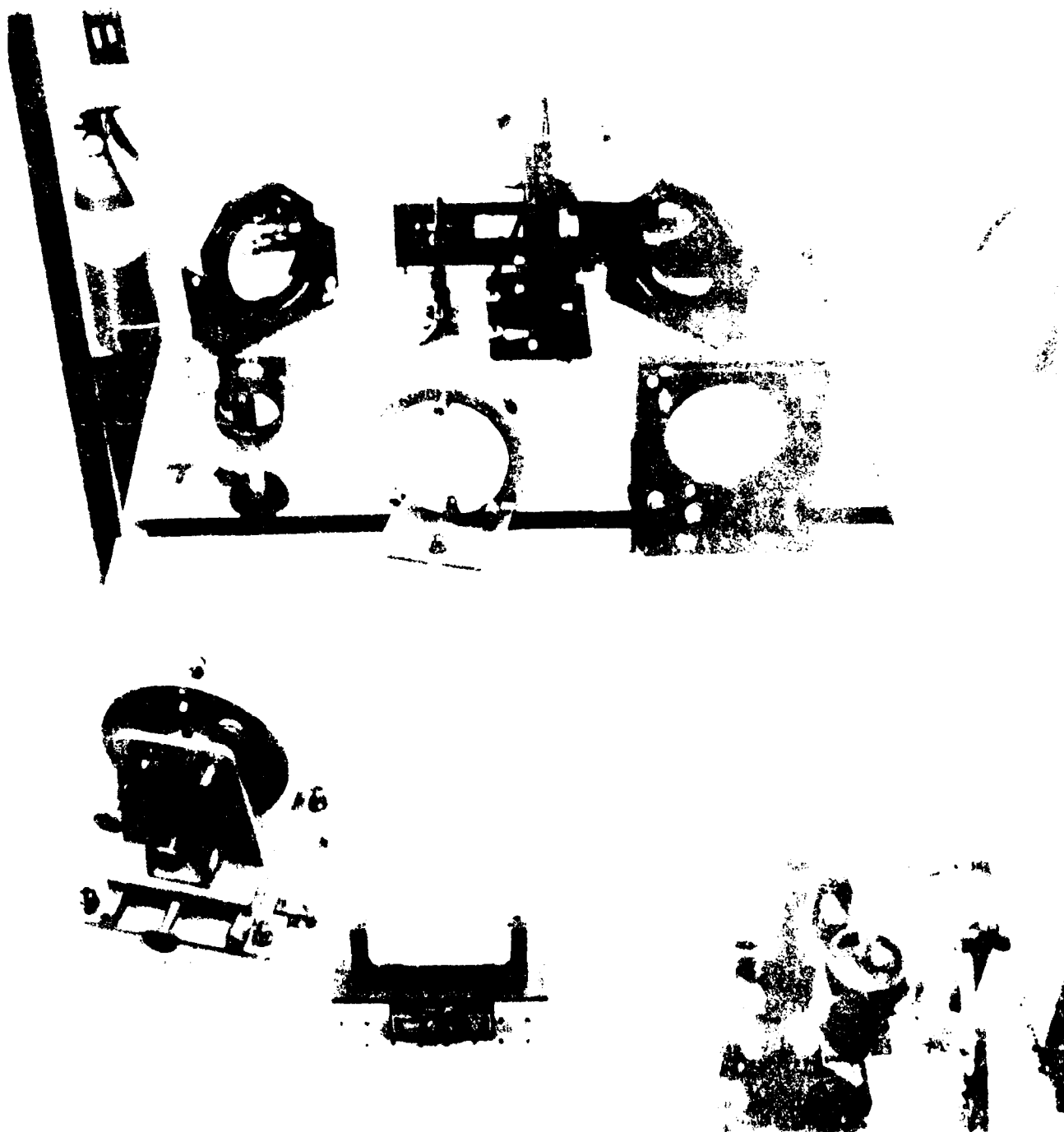


Figure 4. Picture of parts of the engine.

A diagram of the diffracted orders in such a Fourier transform is shown in Figure 5 and a photograph is shown in Figure 6.

The grating period is directly related to the separation,  $d$ , of two adjacent diffracted orders. Considering the simplest case, the light from only 2 points will interfere to create a sinusoidal intensity field described by

$$I = 4 A_0^2 \cos^2 \gamma$$

where

$$\gamma = \frac{\pi}{\lambda} d \sin \theta ,$$

$\lambda$  is the wavelength of light,  $\theta$  is the angle from halfway between the points to the fringes, and  $d$  is the separation of orders. Fringe maxima will occur where

$$d \sin \theta = 0, \lambda, 2\lambda, 3\lambda, \dots .$$

Therefore, as  $d$  increases, the angle  $\theta$  will decrease, giving rise to a higher frequency grating field. In particular, if only the first diffracted orders are passed, the point separation will be twice as far apart as if all orders were passed, and the created grating frequency will be doubled (assuming a small angle approximation for  $\theta$ ). By passing only the second diffracted order (which is four times further apart than any two adjacent diffracted points) and creating the inverse Fourier transform, a new submaster grating with four times the frequency (e.g., 2 lines per millimeter to 8 lines per millimeter) will be formed. This new grating is imaged by lens  $L_4$  and recorded on a photographic plate in the image plane.

All the same information exists in the new grating as in the original. When the model grating is now similarly optically filtered and compared to the multiplied master grating at the image plane of the Fourier transform system, a new moire is formed with four times as many fringes per out-of-plane displacement

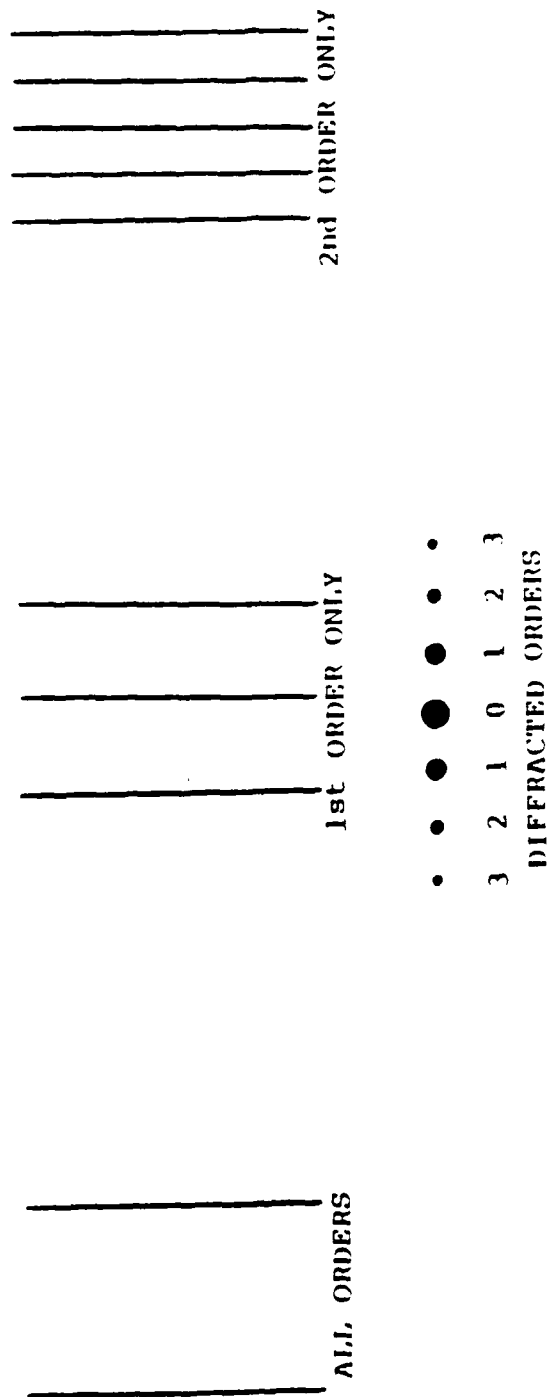


Figure 5. Diagram of Diffracted Orders from a Straight Line Grating.

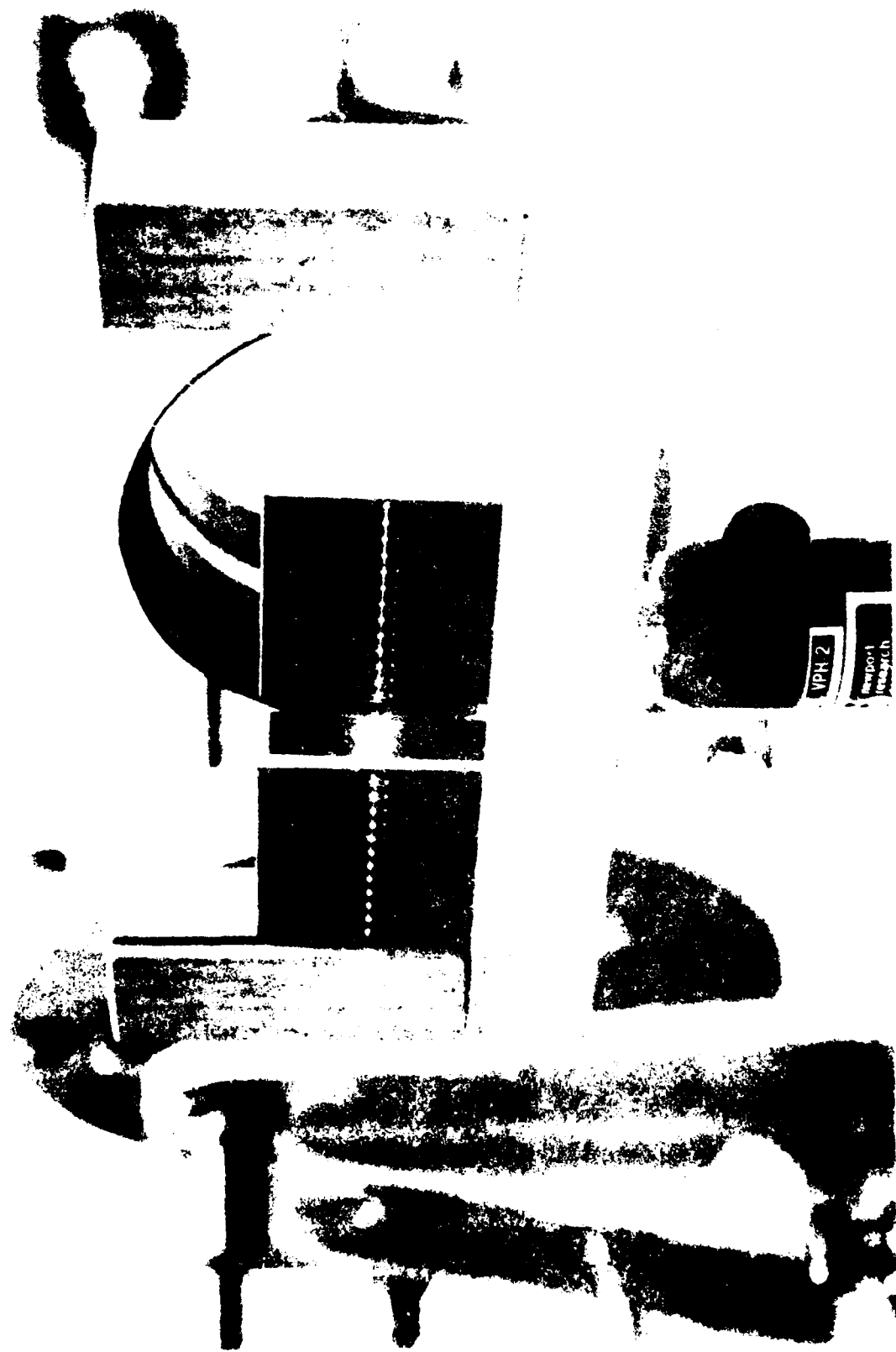


Figure 6. Picture of Diffraction on beam from a 500 nm diode laser.

interval as the original grating. By measuring the new moire pattern to the nearest one fourth fringe, the same sensitivity will be realized as if the original moire were measured to one-sixteenth of a fringe, which is very difficult to do by hand.

This type of optical data processing can be used to measure displacements in specific areas of interest to a high sensitivity, while permitting the full-field map to be a less sensitive and less complicated fringe pattern. Optical processing can also be used to enhance low-fringe contrast which may occur due to mis-focus or lens aberrations encountered when recording the model grating. Fringe contrast enhancement is accomplished by filtering out the undiffracted zero order component in the Fourier transform plane which corresponds to the background light. By removing the D.C. background light, the moire lines will change from shades of gray to all dark and all light, thus improving contrast. Higher frequency noise caused by dirt, film backing, and other factors can also be filtered out to yield a generally clearer image.

The use of optical data processing to multiply sensitivity and enhance contrast permits the requirements on the initial optical test system to be relaxed. A low-frequency grating and moderate quality optics can be used to record the test grating data; then optical processing can be used to increase the sensitivity to the desired value. Optical processing may not always be necessary, but it provides a useful tool to extract data from a test when data have been obscured or are difficult to obtain.

One of the limitations of optical processing of moire data is the inability to view the data and vary the sensitivity in real time. Normally, to vary the sensitivity or enhance the contrast of a moire pattern using optical processing, a photograph of the grating must be recorded and a separate optical system used to process the data. For time-average or pulsed moire application, this extra step is no more work than would normally be required to view the resulting pattern.

Real-time optical filtering would be accomplished by recording the master reference grating with an in-place system and comparing this to the model grating during the test. The complicated part is to optically filter the diffuse master and model grating images before they are compared. Since optical filtering of a diffuse image is difficult to impossible, the image would need to be transformed into a transparency of the object to permit coherent optical processing. This incoherent-to-coherent conversion can be accomplished in real time using an optical light valve.<sup>8,9</sup> A light valve uses either a liquid crystal or an electro-optic crystal (PROM)<sup>10</sup> which responds to an image by producing light and dark areas in the crystal which can be used as a transparency. This system uses a very high technology approach but it does provide for a great deal of flexibility.

A simpler approach to varying the sensitivity of a moire pattern in real time would be to use zoom lenses to vary the projected and/or imaged grating period. To maintain a high-contrast moire, the size of the image of the model on the reference grating would be varied with the change in period of the projected grating. This approach would permit the sensitivity to be varied, although it would not enhance the contrast or quality of the moire.

An alternate approach to increasing the accuracy and dynamic range of a set of moire fringes is to use electronic data processing.<sup>11</sup> A computer can locate and measure the fringe positions more accurately than a person can do it by hand and in less time. The electronics can also be used to enhance fringe data by reducing noise through averaging techniques or by directly subtracting a digitized background.<sup>12</sup> Although electronic digitization eliminates many of the subjective errors associated with the tedium of measuring fringes by hand, it is more costly and has more variables than does optical processing.

If only the moire pattern itself is recorded and not the grating, the moire sensitivity cannot be multiplied using optical processing, although the contrast can still be enhanced. Which process is more appropriate, optical processing or electronic processing, would depend on the volume of data to be analyzed and the form of the data from the particular type of moire used in the test.



## SECTION IV

### REVIEW OF MOIRE TECHNIQUES

We investigated five basic types of moire interferometry: shadow, reflection, projection, contact, and holographic. Each of these techniques will yield a moire fringe pattern by the mechanism of grating superposition as described in Section 3 of this report. The differences in these techniques lie in the mechanism used to overlay the specimen and master gratings.

#### 1. SHADOW MOIRE

Shadow moire is clearly the simplest technique to use.<sup>3</sup> To create a shadow moire, a grating is placed close to the test object which is then illuminated by a point source. The shadow of the grating on the object as viewed through the grating creates a contour moire which maps the topography of the object. This is illustrated in Figure 7. The grating must be close enough to the object to project a sharp shadow. Also, both the grating and the shadow must be maintained in focus simultaneously by the viewing system for the moire to be seen. Because of these last two restrictions (sharp shadow and depth-of-focus) the sensitivity range of shadow moire is typically limited to a contour interval of about one millimeter per fringe for a curved object. In addition to the restriction in sensitivity, the sensitivity to surface topography and the requirement that a grating be placed close to the object make shadow moire unsuitable for testing of rotating turbine blade assemblies, and so it has not been pursued in this study.

#### 2. REFLECTION MOIRE

A reflection moire pattern is created similarly to shadow moire patterns except that the specular reflection of the master grating off a polished subject is used instead of a diffuse shadow.<sup>5</sup> Two possible approaches to projection moire are shown

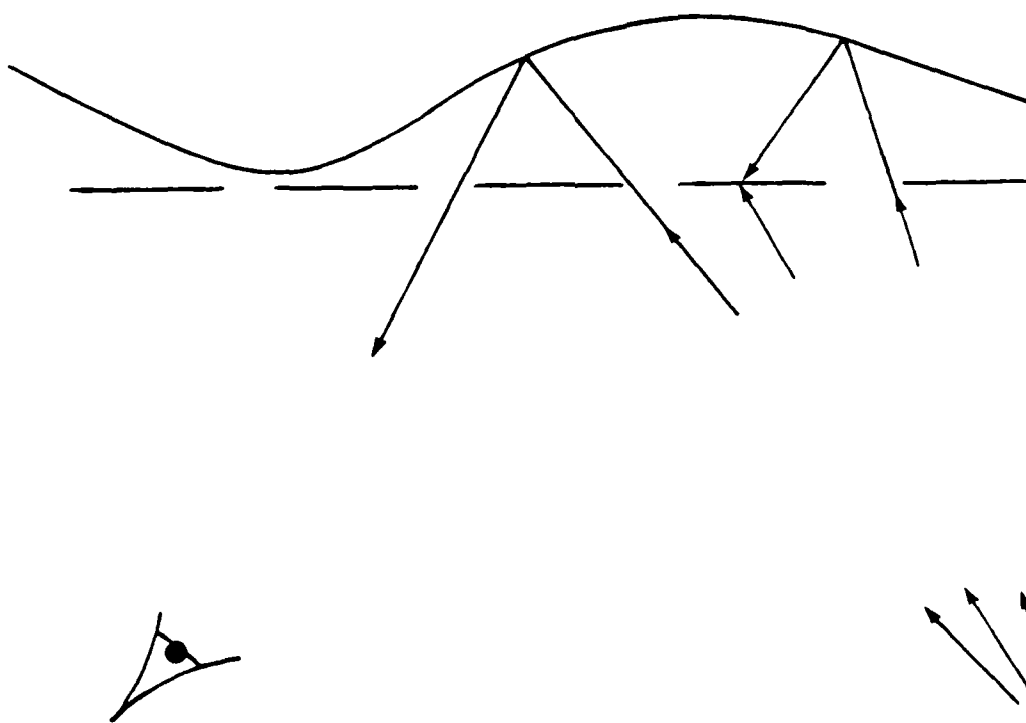


Figure 7. Diagram of Shadow Moire System.

in Figure 8. Either the grating can be reflected off two specular objects to be compared (in a fashion similar to an equal path coherent interferometer) or the master grating can be reflected off the object and imaged onto a reference grating. In either approach, the object must be specular and viewed at the specular angle. For a rotating structure, it is desirable to view the object at normal incidence to permit optical derotation. Since it would be very difficult to view the object normally and be at the specular angle of a contoured object, and because of the requirement that the object be specular, this approach is not desirable for turbine blade dynamics study.

### 3. PROJECTION MOIRE

Projection moire provides greater versatility than does either shadow or reflection moire.<sup>13</sup> A grating is projected onto the test object. This object grating is photographed at some angle other than the projection angle and compared to a master reference grating, creating the moire as shown in Figure 9. If the reference grating is made photographically, directly from the image of the object grating, the contour of the object will be subtracted out of the moire and only displacements from the reference position will be measured by the moire. Projection moire is a good candidate for turbine blade dynamics study and has been emphasized in this study.

### 4. CONTACT MOIRE

Contact moire is similar to projection moire but uses a grating applied directly to the object rather than a projected grating. The grating can then be photographed directly and compared to a reference master grating, which can be a photograph of the object grating before it is deflected, thus subtracting out the object topography, as shown in Figure 10. Only one access angle is required for this type of moire as opposed to two angles for projection moire. As an alternate approach, a second grating

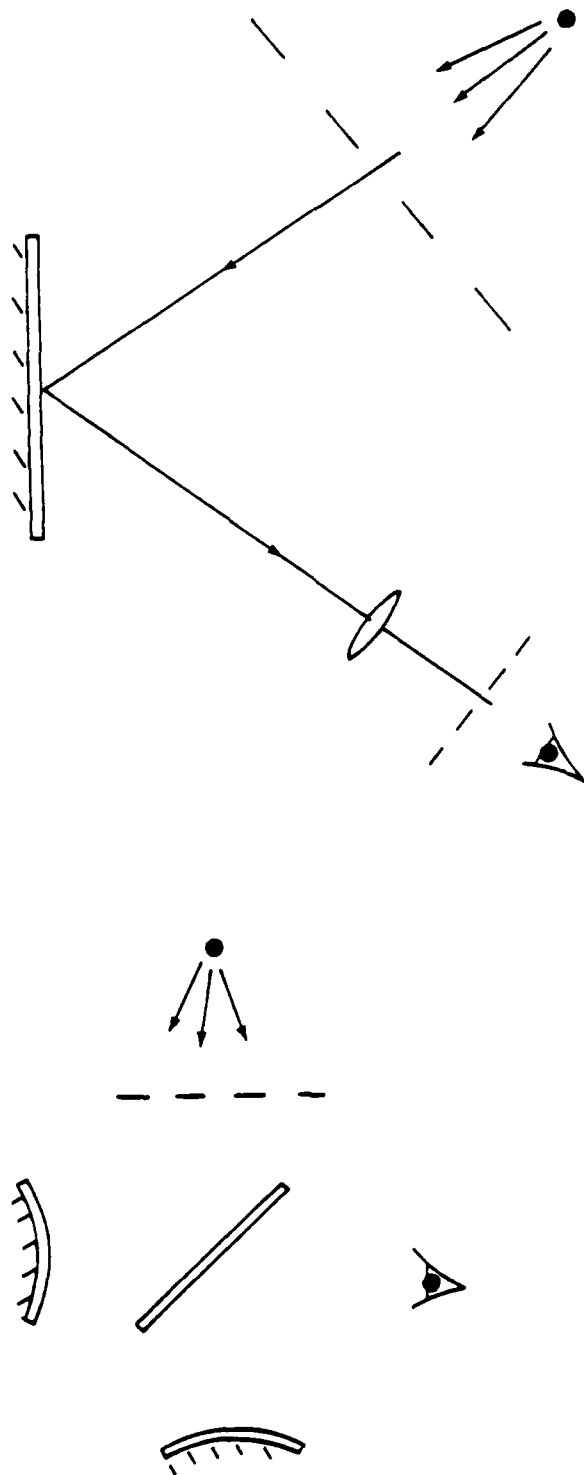


Figure 8. Diagram of a Reflection Moire System.

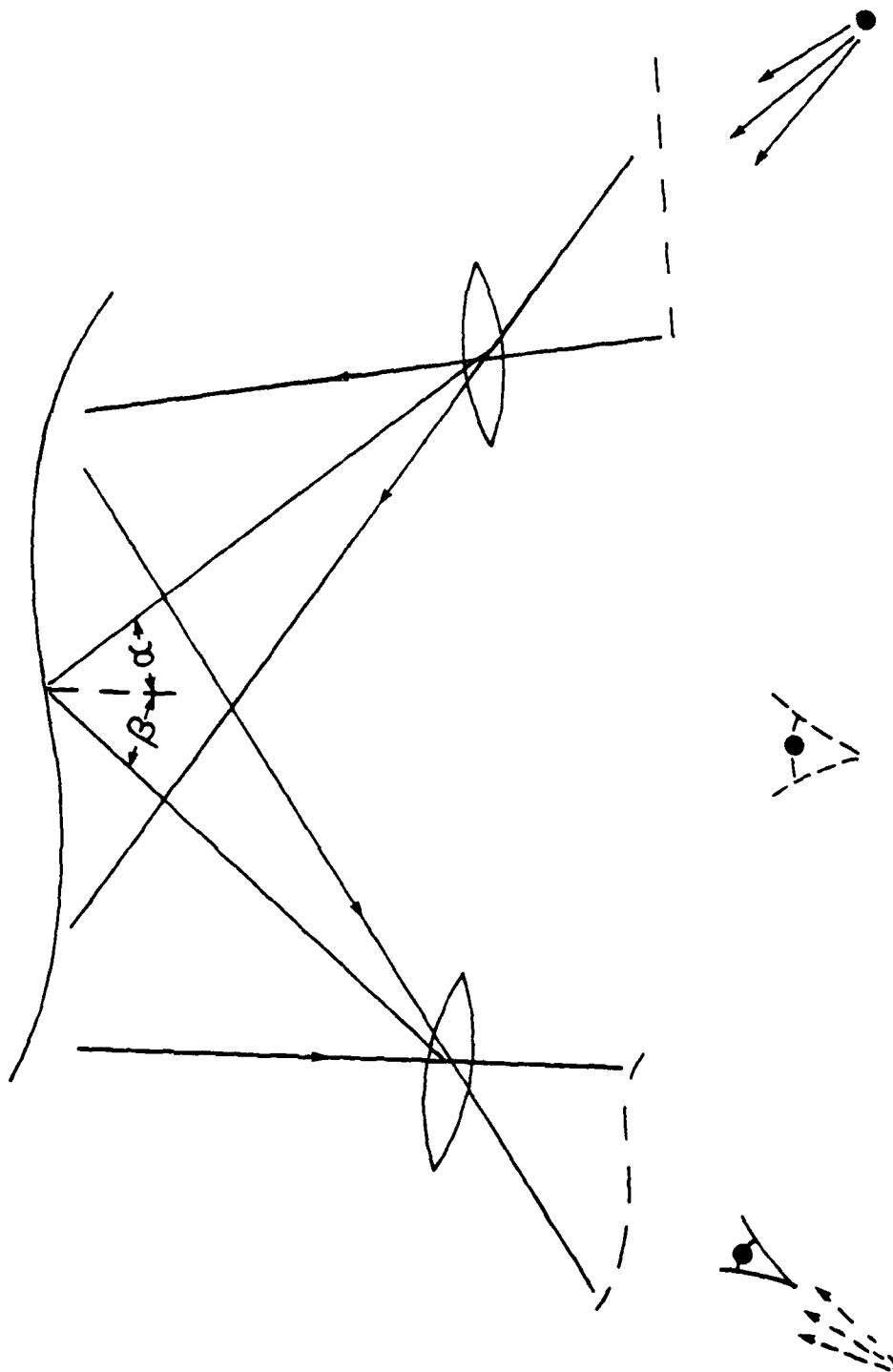


Figure 9. Diagram of Projection Moire System.



Figure 10. Diagram of Contact Moire System.

can be projected onto the contacted grating, which will create a moire directly on the object. To subtract out the object topography, this second grating would need to be made from a photograph of the underformed contacted object grating. For a rotating structure, the grating would be stationary relative to the object, so the reference grating would also need to be stationary relative to the rotating object. The major disadvantage of contact moire is that it requires the model to be prepared by glueing or painting a grating on its surface. Because the grating is attached to the object, the moire pattern will be sensitive to in-plane displacements (and therefore surface strains) in addition to the out-of-plane deflections. In fact, to be sensitive to out-of-plane deformations at all, the object must be viewed (or the second grating projected from) off normal. This requirement would prohibit derotated studies of the model under rotating conditions. Although in general in-plane information may not be desirable, there may be some tests where the need for full-field strain data would justify the model preparation work required to use contact moire interferometry.

## 5. HOLOGRAPHIC MOIRE

Holographic moire involves more sophisticated concepts than do the other approaches.<sup>14</sup> Holographic moire requires making a real-time or double-pulsed hologram of the test object and comparing the high-frequency holographic fringes with a reference grating or another set of holographic fringes (such as in sandwich holography). The basic system for holographic moire is shown in Figure 11. The sensitivity of holographic moire interferometry is determined by the period of the holographic fringes, which become finer as the amplitude of deflection increases. This would mean that higher deflections would create a more sensitive moire pattern, which is just the opposite effect to what might actually be desired. The variations in the period of holographic fringes from point to point on the object make

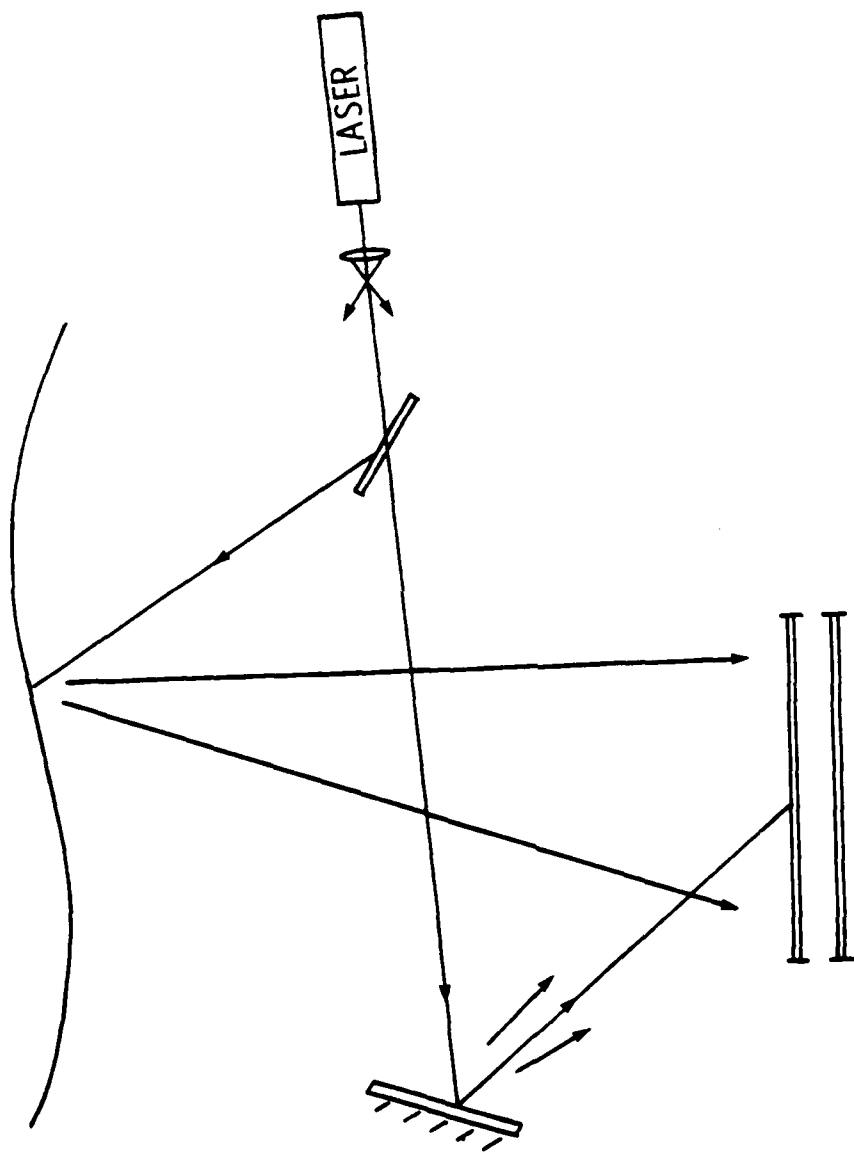


Figure 11. Diagram of Holographic Moire System.



interpretation of the resulting moire difficult. Because of the stability requirements of holography and the difficulty of interpreting the data, holographic moire is not seen as a viable option for full-scale turbine blade dynamics study, although it could be a usable tool for certain laboratory studies.

## 6. CONCLUSIONS

The above moire techniques are summarized in Table 1. An additional technique listed in the table, double exposure optically processed moire, is a variation which can be applied to most of the other five approaches. Optical processing of the moire adds the requirement of a separate optical system in which the actual moire pattern will be formed. Although optical processing adds an extra step to the test, the ability to increase the measurement sensitivity of a given moire pattern may well justify the time and effort.

Based on the above comparison of the five basic moire interferometry techniques, projection moire, possibly coupled with optical processing, provides the most versatile and easily applicable solution to turbine blade dynamics study. Projection moire requires no specific model preparation. The data recording techniques for projection moire are compatible with any high-resolution image recording system and thus are the most straightforward for larger scale structural dynamics study. Therefore, projection moire was emphasized for the remainder of this study.

TABLE 1. COMPARISON OF MOIRE TECHNIQUES

Technique	Advantages	Disadvantages	Comments
1. Shadow Moire	Simple	Limited sensitivity Requires reference grating close to object	Object and reference grating need to be in focus simultaneously
2. Reflection Moire	Simple, light efficient	Object must be specular viewed at specular angle	
3. Projection Moire	Versatile, not contour sensitive, real time	Requires high-resolution optics	Time-average moire possible with optical processing
4. Double Exposure Optically Processed Moire	Freezes motion when pulsed source is used, optical multiplication possible	Not real time, film limitations, only practical with pulsed source	A very bright pulsed source may be required though it need not be a laser
5. Contact Moire	Resolution not limited by optics, can yield in-plane deformation	Requires grating on object, geometry sensitive, must be viewed off axis or have second projected grating	Can yield high resolution when coupled with optical processing
6. Holographic Moire	High sensitivity, no high-resolution optics	Requires high stability, difficult to control sensitivity	

## SECTION V

### INTERFEROMETRY METHODS

Once the mechanism for creating the moire pattern has been established, there are three possible ways to record the moire of a dynamic object: time average, real time, or pulsed (sometimes referred to as stop action). Each method is tailored to retrieve specific types of information or reject certain information. The different recording approaches are each appropriate to different dynamic changes and test parameters.

#### 1. TIME-AVERAGE MOIRE

If a well-behaved static modal vibration of a test object is to be measured, it is often desirable to use a technique which will not record extraneous random fluctuations such as air turbulence or optical component vibrations. One method of doing this is to use time-average moire interferometry.<sup>15</sup> To make a time-average moire, an object grating is recorded on a vibrating object over a long period of time relative to the vibration period. The only points at which the grating image will be formed are at the two extremes of the vibration cycle where the surface momentarily stops moving when it changes direction. Therefore, the grating is recorded only at the two extremes of the deflection and these two grating images interfere to create a moire fringe pattern. All random movements are averaged out of this fringe data. In this manner, the maximum deflection of the object is always measured. Because of the averaging effect, time-average moire interferometry is limited to situations where a well-behaved standing wave is present.

To demonstrate time-average moire interferometry, we projected a grating onto a ten-inch steel plate. The projected grating was made using a CW Argon laser and a Wollaston prism. The Wollaston prism splits the laser beam into two beams at a small angle to each other, which interfere coherently to create

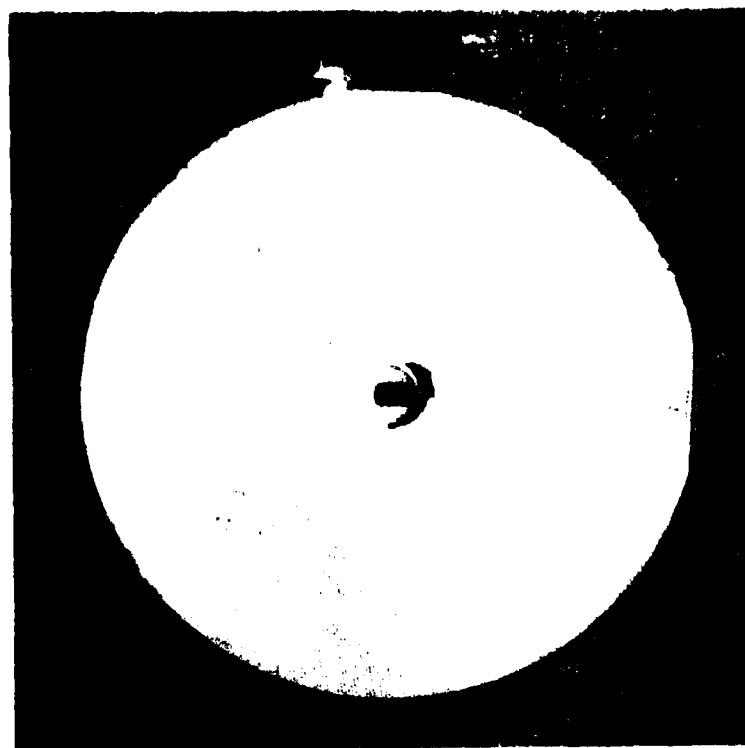
sinusoidal straight-line interference fringes. An imaging system was then used to project a constant period grating onto the plate with a frequency of about 12 lines per millimeter (300 lines per inch) at a projection angle of 45 degrees. The sensitivity of the resulting moire was 60 to 70 microns per fringe.

When the plate was driven at resonance, a low-contrast time-average moire was created (see Figure 12a). By optically filtering out the high-frequency grating information and the zero diffracted order background light from the Fourier transform of the recording, the time-average moire pattern in Figure 12b was created. This type of optical filtering enhances the moire fringe contrast without changing or losing any of the moire data.

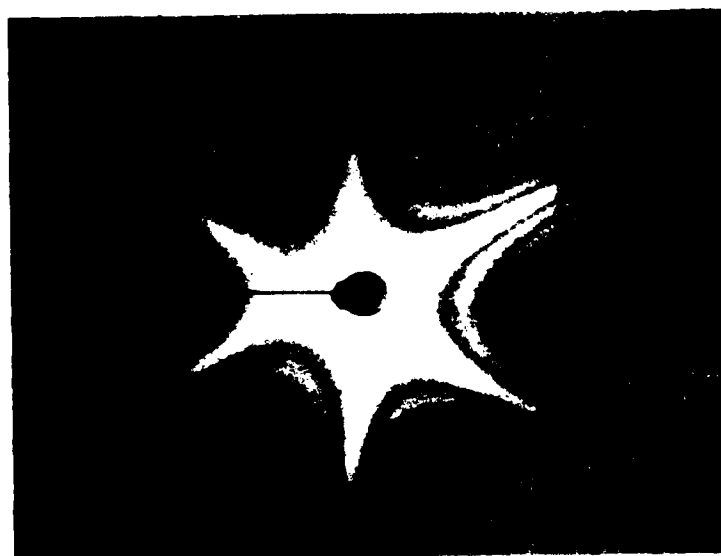
Using a slightly thicker steel disk, we obtained the time-average moire pattern of a 2-N mode pattern shown in Figure 13. The excitation frequency was 144 Hz and the sensitivity of the moire was 150 microns of out-of-plane displacement per moire fringe. The negative was again optically filtered to remove the DC background.

Time-average moire photographs of the rotating disk were made by strobing the laser at a rate of once per revolution. This approach removes the extraneous bias fringes caused by the contour of the object. The results for a series of pulse lengths from 100 to 700 microseconds are shown in Figure 14. The rotation speed was about 2,700 RPM and the excitation frequency was 237 Hz.

At 700 microseconds (see Figure 14a) the fringes started to blur near the edges, indicating the pulse length was too long to sufficiently stop the rotation of the disk. The frequency of excitation was readjusted for the 100 and 200 microsecond exposures to obtain a stronger mode. With the shorter pulse lengths the fringe patterns were clean out to the edges. However, during the long integration time needed to expose the photographic plate



a. Pattern as Recorded.



b. Pattern after optical filtering.

Figure 12. Time-Average Moiré Pattern on Metal Plate.

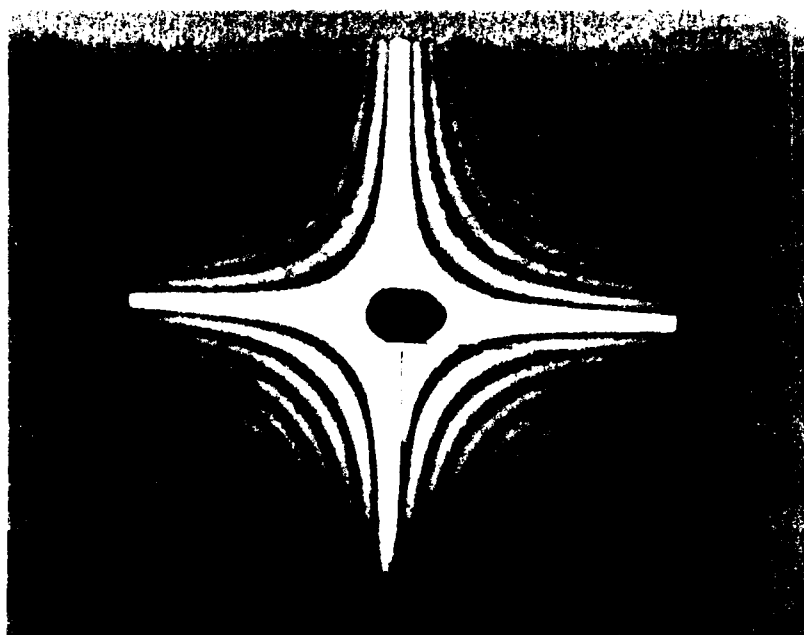
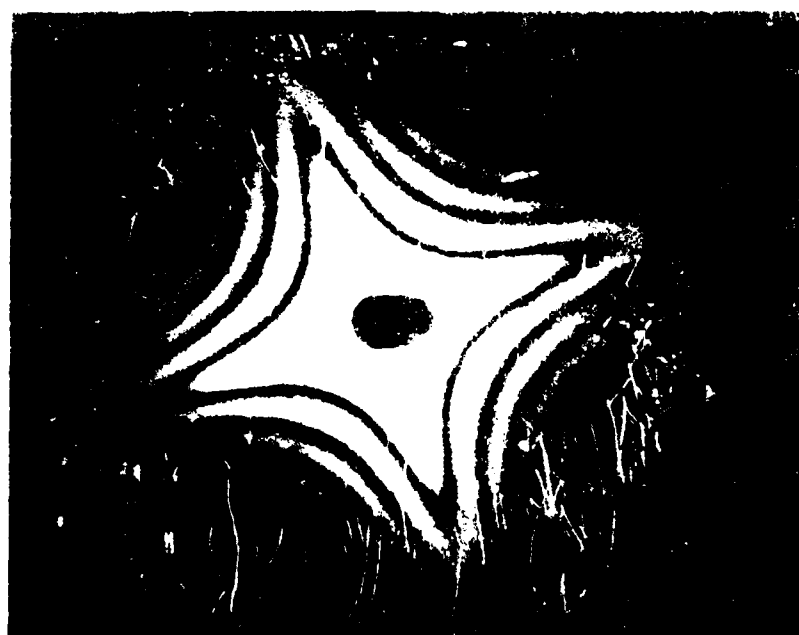


Figure 13. Time-Average Moire of Static Disk

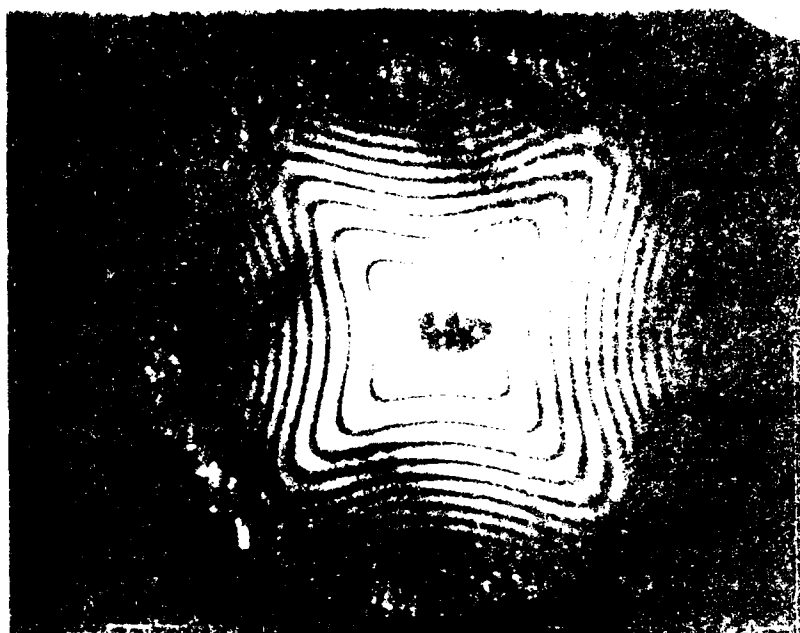


a. 700 Microsecond Pulse Length

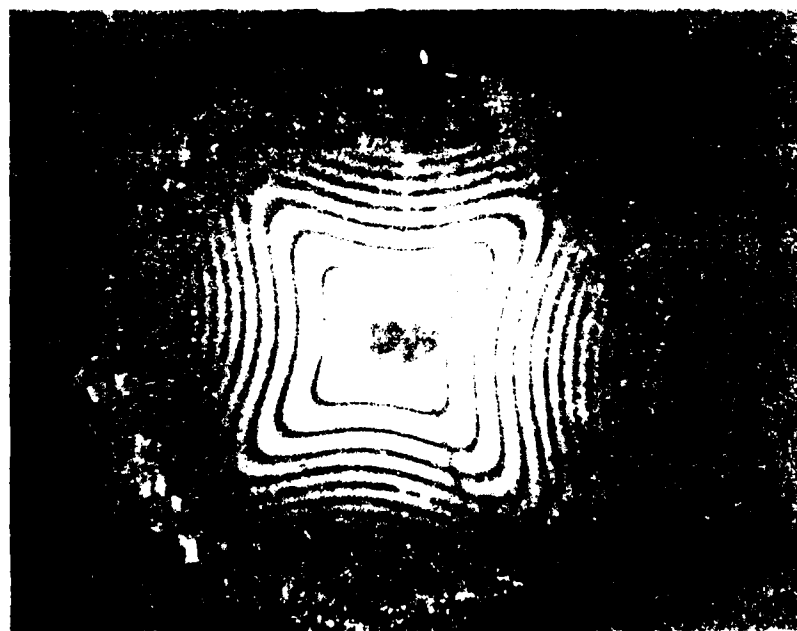


b. 500 Microsecond Pulse Length

Figure 14. Time-Averaged Micrographs of the Laser



37. 200 Microsecond Pulse Length



38. 400 Microsecond Pulse Length

FIGURE 6. The Axon-Like Motion of the  $\text{Ca}^{2+}$  Ion



(on the order of five minutes), the mode pattern apparently moved very slowly yielding the type of pattern in Figure 4c and 4d. This drift could have been caused by a drift in the speed of the disk. This rotation information could be useful in actual analysis.

## 2. REAL-TIME MOIRE

A method of moire interferometry which does not average out random vibrations, but rather is sensitive to all movements as they occur, is real-time moire interferometry.<sup>16</sup> To make a real-time moire interference pattern, the specimen grating is recorded, then repositioned so as to exactly superimpose the recorded image and the real image. The resulting moire pattern will be sensitive to all out-of-plane dimensional changes in the object (and the associate optical system) as they occur with all initial surface topography subtracted out of the data. Real-time moire provides a consecutive record of dynamic vibrations as they occur. Although good historical visualization results from the very large amount of information provided by real-time moire interferometry, it can be difficult to obtain concise quantitative data. The sensitivity of real-time moire interferometry has been demonstrated on the order of 100 microns of out-of-plane displacement per interference fringe. This sensitivity makes real-time moire a very powerful tool for measuring structural dynamics. However, this high sensitivity to all displacements in the system limits the use of real-time moire interferometry for large scale dynamic analysis. Drive motors or pump systems can often be a source of extraneous excitation. Such sources of vibration can cause the optical system and mechanical support hardware itself to vibrate. When this happens, the interference fringes will contain not only information regarding the dynamic response of the turbine assembly, but also information pertaining to the vibrations of the test equipment. The extra information obtained from vibrating mounts and optics is not pertinent to the

desired test data but will rather act to obscure the important test data with noise data.

Therefore, if real-time moire interferometry is to be used for structural dynamics testing, the optical system must be made as stable as possible. Since the optics required for moire are few and simple, this is not a large task, although special thick glass gratings may need to be produced (if a grating is used). The greater problem with any real-time test is taking into account mount vibrations and air turbulence effects. Moire interferometry is no more sensitive to these parameters than any other optical measurement scheme and much less sensitive than holography.

Real-time moire of a static and rotating disk was demonstrated using the system shown in Figure 15. A Wollaston prism was used to create the projected interference fringes, and a large aperture telescope system was used to enlarge and collimate the fringe field. Since the beam was collimated, the projected fringe period was constant for any plane. The model grating (on the disk) was then imaged onto a reference grating in front of the derotator. Since the moire was created in front of the derotator, it was not necessary to image a high-frequency grating through the derotator but rather only the moire pattern. Both the projected fringe field and the reference grating remain stationary (which is easier than rotating the grating) but the moire pattern will rotate with the disk. A strobed argon laser was used to freeze the vibration of the disk.<sup>2,17</sup> The results of the static, real-time moire are shown in Figure 16a. The excitation frequency was 144 Hz and the strobe pulse length was 300 to 500 microseconds. The real-time moire of the disk rotating at about 2,600 RPM as seen through the derotator is shown in Figure 16b. The excitation frequency for the rotating mode was 220 Hz and the sensitivity of the moire was 150 microns per moire fringe. It was very difficult to keep the mode from rotating or oscillating. Some of this rotation could have been from a drift

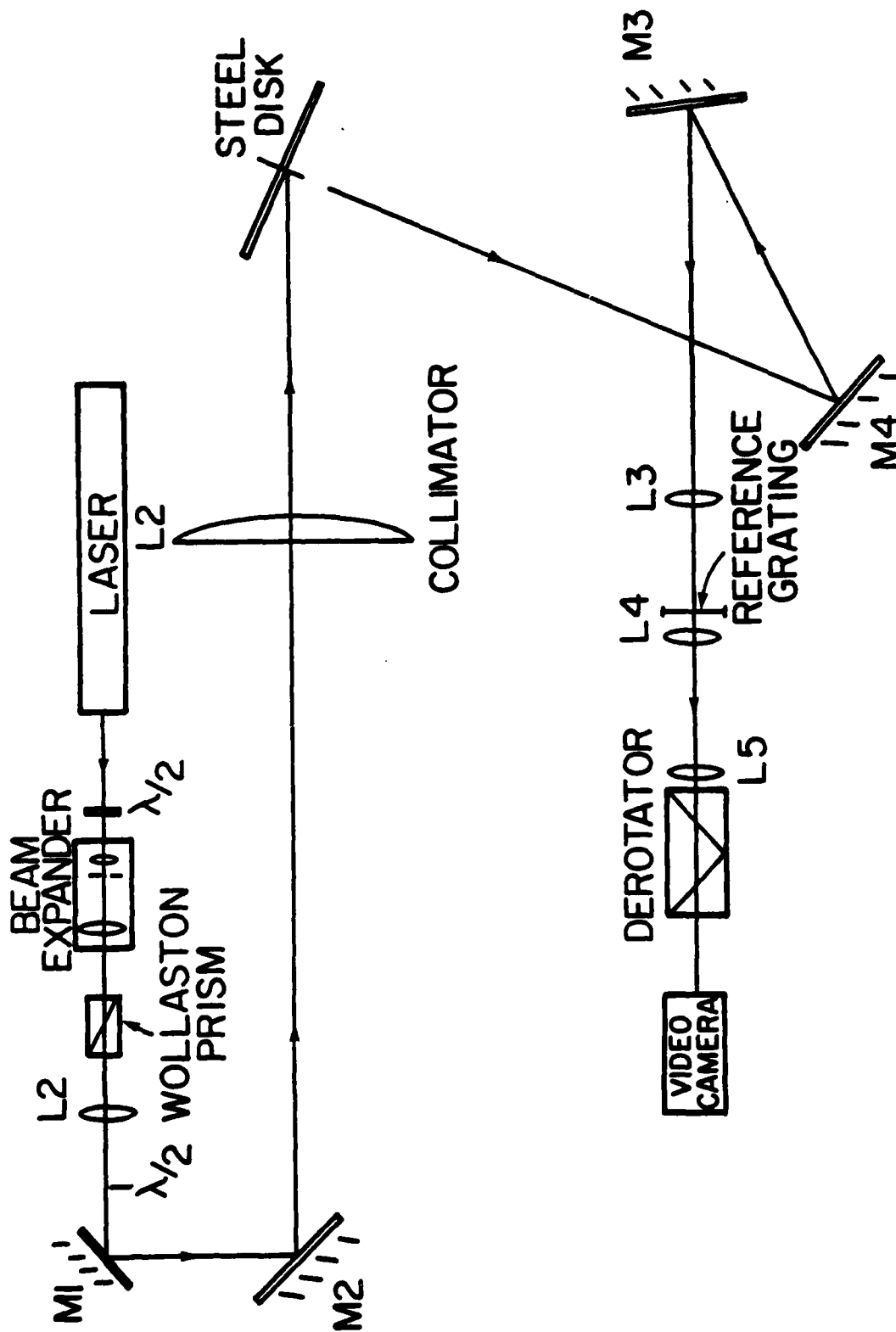


Figure 15. Schematic of Optical System for Moire Interferometry.

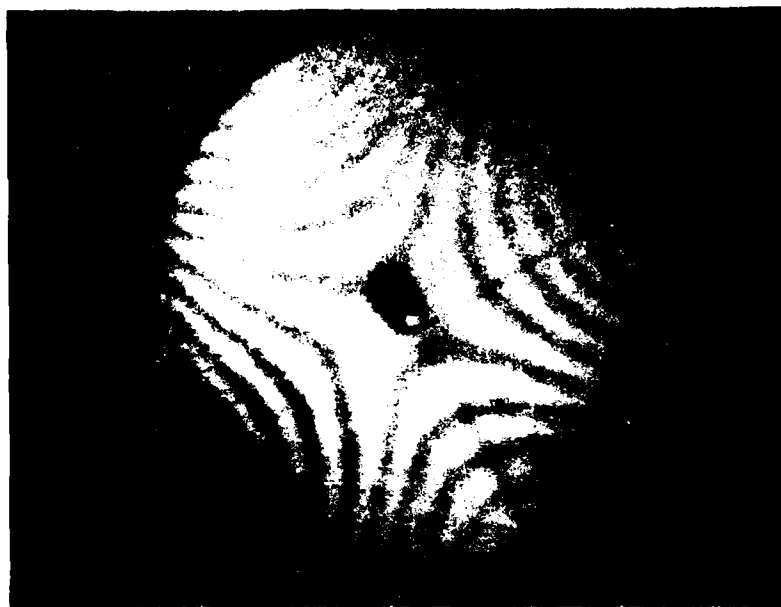


Figure 16a. Real-Time Moire of Static Disk..



Figure 16b. Real-Time Moire of Rotating Disk.

in the speed of the disk. The misalignment of the optical derotator is degrading the derotated image, but this would not be a problem with the derotator in the AFWAL/PO facility. A source with more energy in a shorter pulse would also improve the quality of the moire information.

The high sensitivity of real-time moire to all out-of-plane motions of the disk may limit its usefulness to actual testing where many motions may be involved. The real-time moire is extremely useful though for finding mode patterns and identifying what motions are present. For the purpose of studying traveling waves in a turbine assembly, real-time moire interferometry could be an invaluable tool. An example of a traveling wave mode pattern recorded with real-time moire is shown in Figure 17.

### 3. PULSED MOIRE

It is possible to lessen the complexity of the recorded data and the image blurring effects associated with real-time techniques, without being restricted to the periodic vibrations in time-average techniques, by using a pulsed-light source to create the moire interference pattern. A short-light pulse can effectively freeze the motion of the object.<sup>18</sup> If the specimen grating is recorded with a pulsed-light source at two different points in time, the moire resulting from overlaying the two recordings will map the overall change in topography of the model, not what it went through to get to that position.

There are two variations of this pulsed moire interferometry. The two grating recordings could be two exposures on the same photographic (or video) frame. The result of a double exposure is that the two grating patterns will add optically, yielding an additive moire pattern. An additive moire is inherently low contrast (see Figure 18a). If two separate exposures are multiplied together (see Figure 18b), either electronically or by overlaying two separate photographic negatives, the resulting

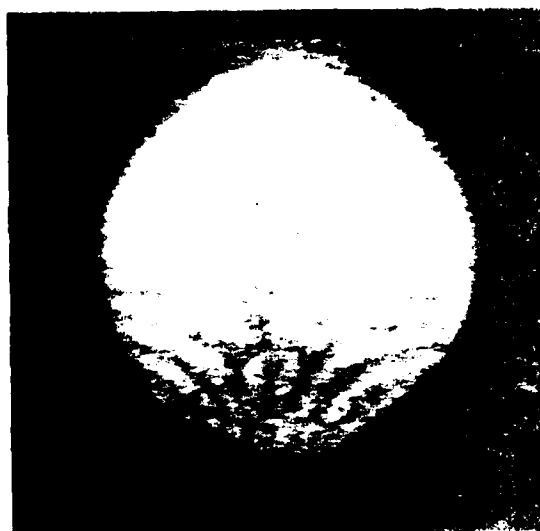
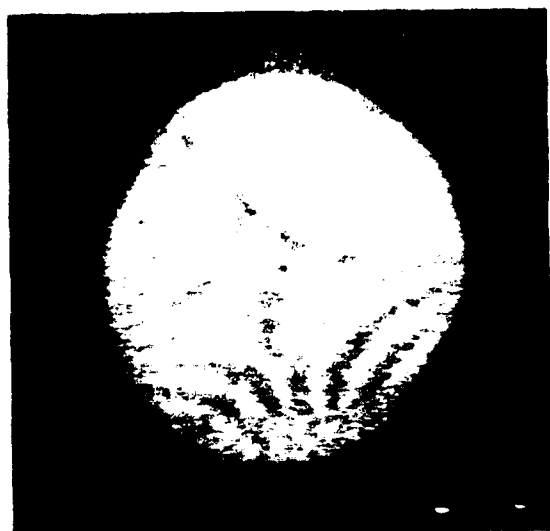


Figure 17. Traveling Wave 2-N Mode Moire Pattern.

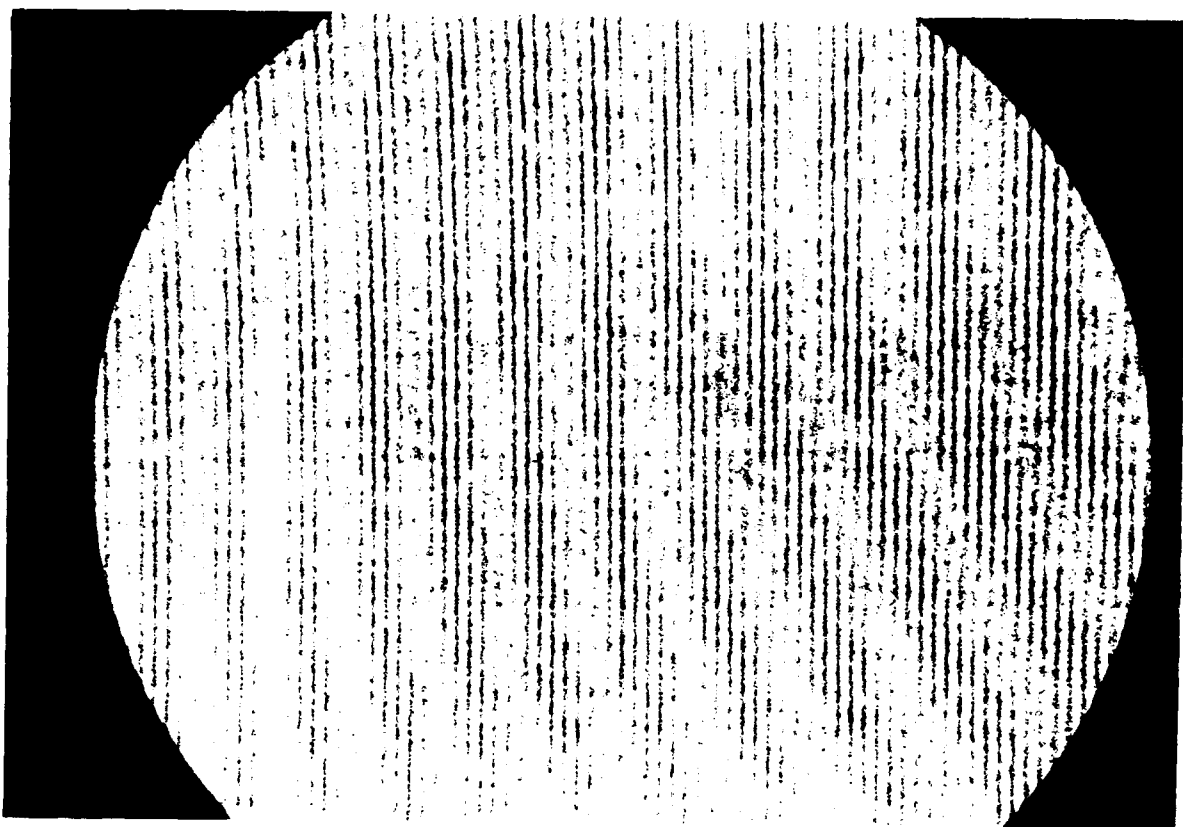


Figure 18a. Double Exposure Additive Moire.

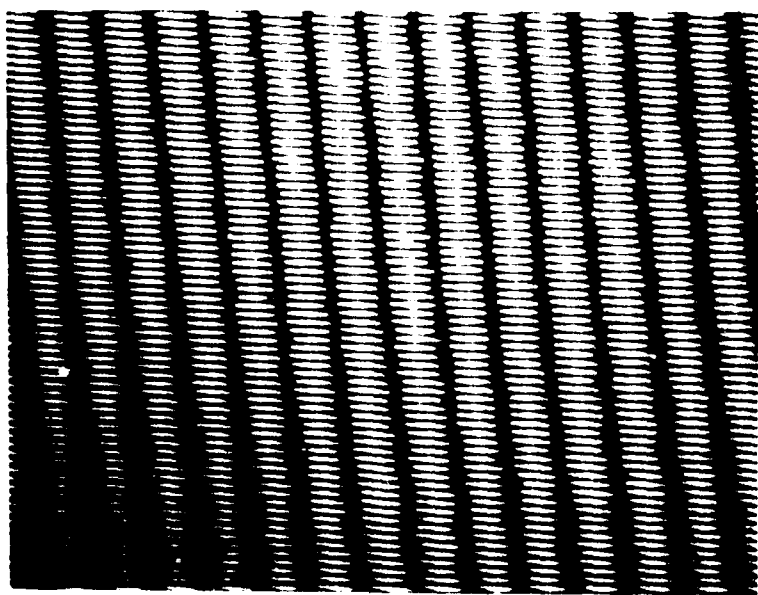


Figure 18b. Multiplicative Moire.

moire will be a multiplicative moire with potentially very high contrast. Individual grating recordings have the additional advantage that they can be optically processed to yield a higher sensitivity moire.

As a demonstration of testing dynamic objects with pulsed projection moire, we applied the technique to a ten-inch vibrating steel plate driven at resonance. The object grating was produced by imaging a Ronchi ruling onto the plate so as to have approximately a 2-line-per-millimeter (50-line-per-inch) grating on the object. The grating was photographed at various points in the vibration cycle, using a Q-switched ruby laser to freeze the motion of the plate. By taking two of the photographs 180 degrees apart in phase as referenced to the vibration cycle of the plate and laying one over the other, we obtained the moire pattern shown in Figure 19a. The sensitivity of this moire is approximately 500 microns (0.02 inches) per moire fringe.

We then multiplied the sensitivity of this moire by optical processing to obtain a sensitivity of 250 microns (0.01 inches) and 125 microns (0.005 inches) per fringe as shown in Figure 19b and 19c. The original photographs made with the ruby laser were recopied using a high-contrast process to obtain higher diffraction efficiency. The multiplication of sensitivity is accomplished by selecting out specific diffracted orders in the optical Fourier transform of the object photograph which correspond to the spatial frequency sensitivity desired. The moire is created between a master grating made in the optical processor using one of the object photographs and the image created in the optical processor of the other photograph. The direction of a deflection can be determined in the optical processor by laterally translating the master grating relative to the image of the test grating.

As an alternate approach, we made a double exposure photograph of the plate undergoing random vibrations using the ruby





a. Pattern as Recorded.

b. Pattern with 2x Multi-  
plication.



c. Pattern with 4x Multi-  
plication.

Figure 19. Pulse Moire of a Metal Plate.

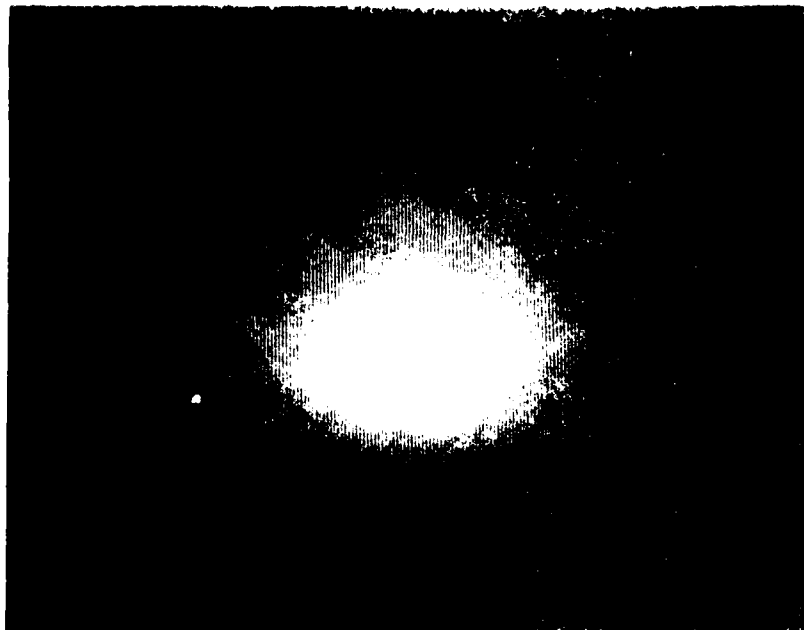
laser as the light source. A section of the double-exposure photograph is shown in Figure 20. The additive moire created in this fashion is inherently low contrast. By optically filtering out the frequency information relating to the grating and leaving only the information relating to the moire pattern, the moire pattern is effectively enhanced as shown in Figure 20. This approach permits changes on a short-time scale to be recorded.

#### 4. CONCLUSIONS

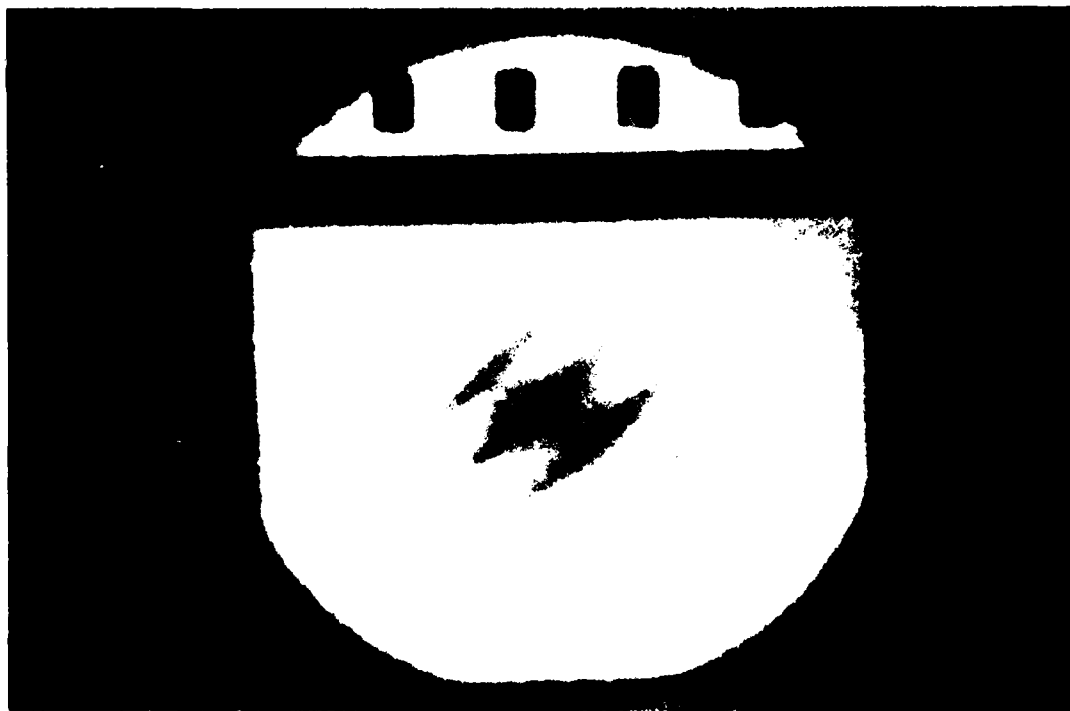
We have demonstrated three methods of projection moire interferometry as applied to studying the structural dynamics of a rotating disk: time-average, real-time, and pulsed or stop-action moire. Time-average moire interferometry can use a very simple optical system by stopping the rotation of the object with a laser strobed at once per revolution. The maximum deflections are always measured with a time-average method but the method is restricted to studying well-behaved standing wave vibrations.

Real-time moire interferometry will be limited in its usefulness to large-scale turbine blade assembly testing because of its high sensitivity to all out-of-plane motions of the object as well as to turbulence and vibrations within the optical system. As a laboratory tool, however, real-time moire can provide the flexibility to identify what motions are present as well as providing excellent historical data. The quality of the real-time moire pattern and the versatility of the method could be greatly improved by a source with a shorter pulse yet equal energy to the strobed argon used in this study (such as a metal vapor or dye laser system).

Pulsed or stop-action moire interferometry, in conjunction with optical processing, provides the most promise for large-scale turbine assembly tests. Short light pulses will freeze all the vibrations of the system, allowing for a less controlled environment than required for the other techniques. Although



a. Pattern as recorded.



b. Pattern after Optical filtering.

Figure 20. Double Exposure Pulsed Moire.

real-time feedback is not available, optical processing techniques to increase measurement sensitivity and enhance contrast can easily be incorporated into the system used to view the moire.

## SECTION VI

### DATA RECORDING

#### 1. FILM EVALUATION

If the moire pattern or gratings are to be recorded on film to permit data manipulation through the use of optical processing, the type of film best suited for the test must be considered. Many photographic films exhibit a low MTF and a high grain size. Film characteristics of this type can degrade the quality of the moire and ultimately lose important information in the noise. The photographic film should be high contrast and fast, with sufficient resolution for the type of moire. We conducted a survey of some possible films. The results are summarized in Table 2. Photomicrographs of a sinusoidal grating photographed with the various films are shown in Figure 21. The same grating period and energy were used for each original grating photograph.

The highest contrast and highest resolution were achieved with Kodak Type 1A-HRP plates (Figure 21i). This plate also had the lowest sensitivity, requiring over  $1,000 \text{ ergs/cm}^2$  to make an exposure. Holographic plates (Figure 21d) also give high resolution, high contrast, and low noise but with only slightly more sensitivity (about a factor of ten) than the type 1A plates. There are situations in which the very high resolution of the holographic plates may be desirable. The holographic emulsions are also available on a film base when a plate, although nice to work with in optical processing, may not be practical.

Of the films evaluated, Minicard II film by Kodak (Figure 21j) was found to have the highest resolution and contrast, but again relatively low sensitivity. Minicard II also has a fairly clear, noise-free base. A clear base is important in optical processing, because if the base exhibits high scattering, the coherent light used in optical processing will show up these scattering centers as noise.

TABLE 2. COMPARISON OF POSSIBLE FILMS FOR MOIRE PHOTOGRAPHS

Film	Exposure	Devel.	Comments
1. 35 mm Litho-graphic film	9 sec	Litho, 2 min.	High contrast, noise, (no ruby sens)
2. Polaroid Pos/Neg	-	50 sec	Low contrast, grainy
3. Litho Copy of Polaroid Pos./ Neg	-	-	High contrast, sensitive to irregular orig.
4. Agfa Gaveart 10 E56 Holographic Plate	1 sec	HRP, 10 min	High contrast, very fine grain
5. Technical Pan	1 sec	D-19, 6 min	Med. contrast, med. grain
6. Agfa Gaveart 10E75 copy of Technical Pan	4 sec	HRP, 8 min	High contrast, some noise from Tech. Pan base
7. Litho copy of Technical Pan	0.4 sec	Litho, 6 min	High contrast, noise from base
8. Panatomic-X	2 sec	D-19, 4 min	Low contrast, grainy
9. Kodak type 1A-HRP	1.5 min	HRP 3 min	Very high con- trast, very slow speed
10. Kodak Minicard II Film	5 sec	D-19 4 min	High contrast and resolution, clear base

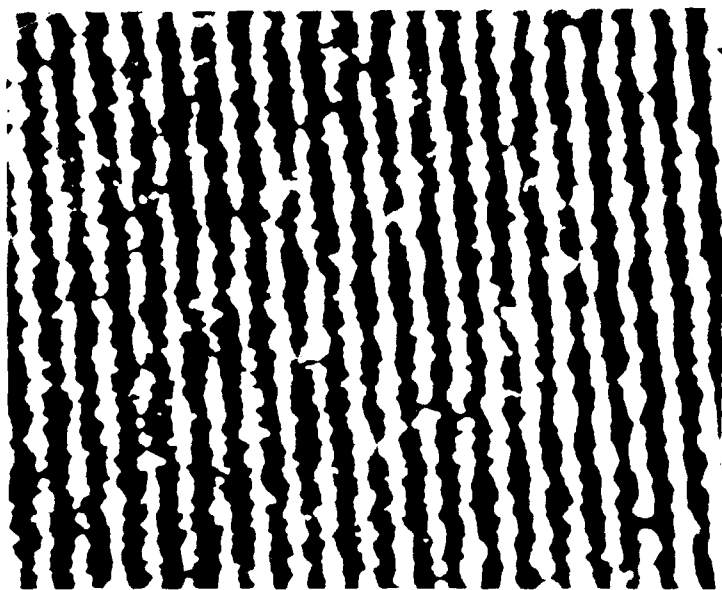


Figure 21a. 35 mm Lithographic Film Photo of Grating.

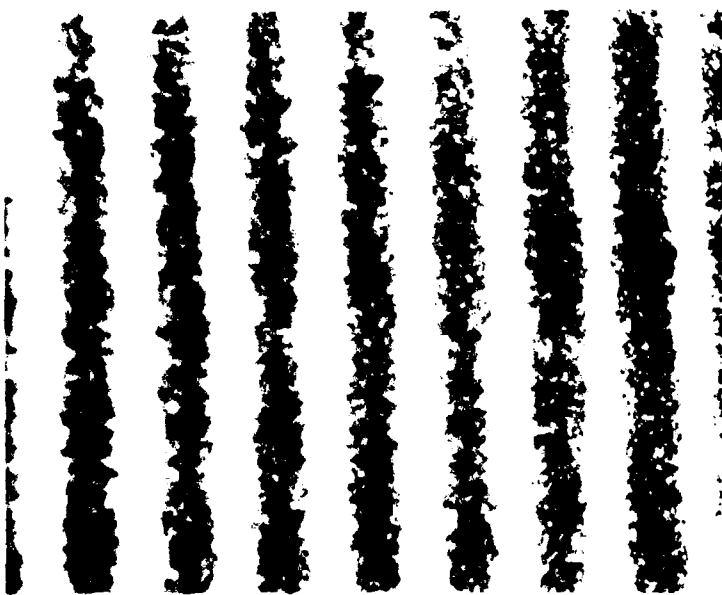


Figure 21b. Polaroid Pos/Neg of Grating.

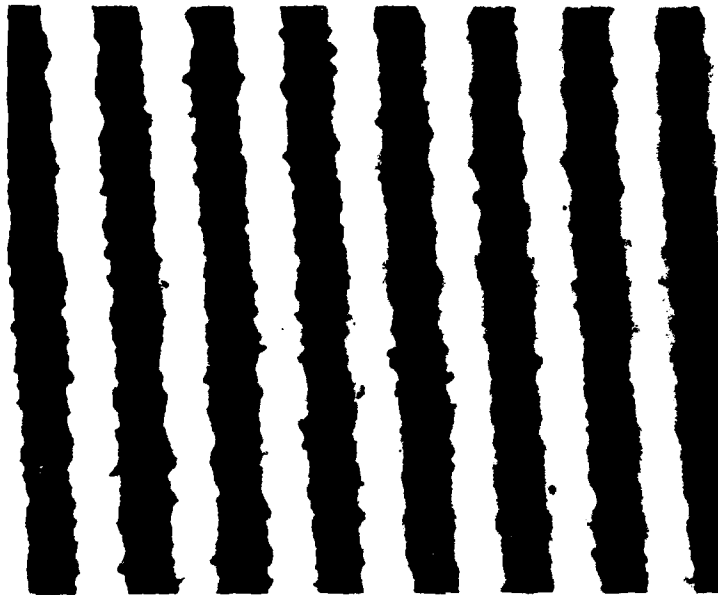


Figure 21c. Lithographic Copy of Polaroid Pos/Neg Photo.

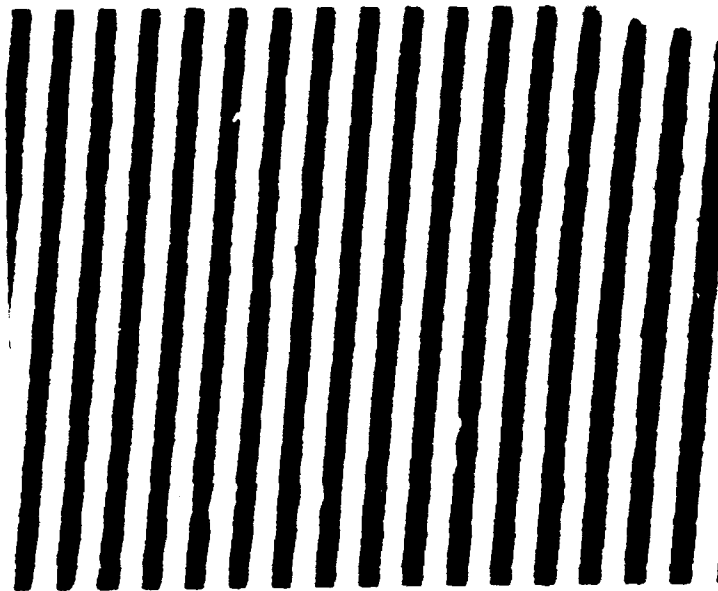


Figure 21d. Holographic Plate (10E56) Photo of Grating.





Figure 21e. Technical Pan Film Photo of Grating.

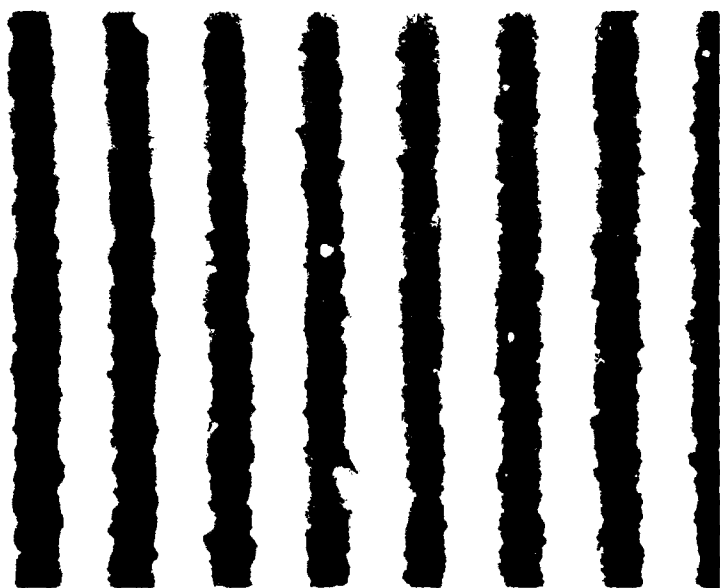


Figure 21f. Holographic Plate (10E75) Copy of Technical Pan Photo.

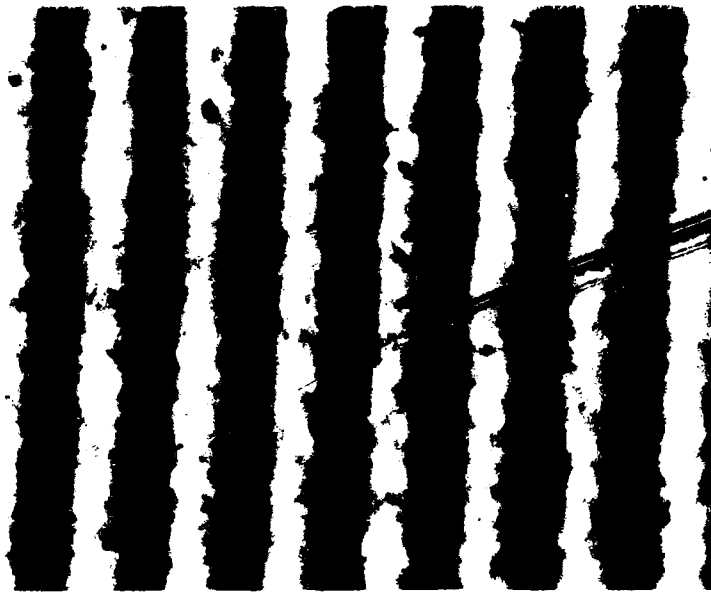


Figure 2lg. Lithographic Copy of Technical Pan Photo.

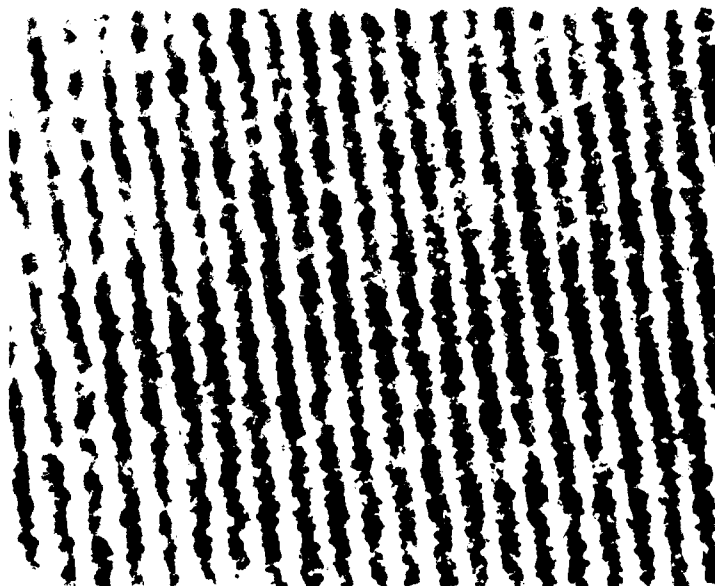


Figure 2lh. Panatomic-X Film Photo of Grating.

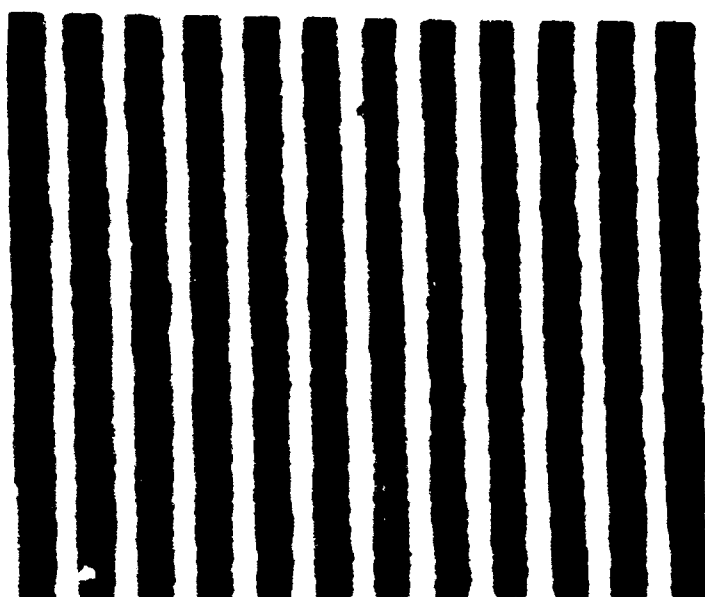


Figure 21i. HRP Type 1-A Plate Photo of Grating.

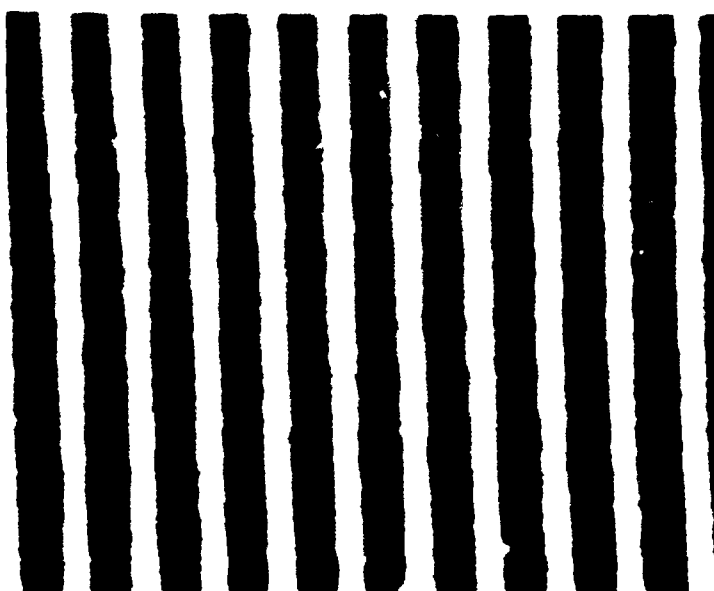


Figure 21j. Minicard II Film Photo of Grating.

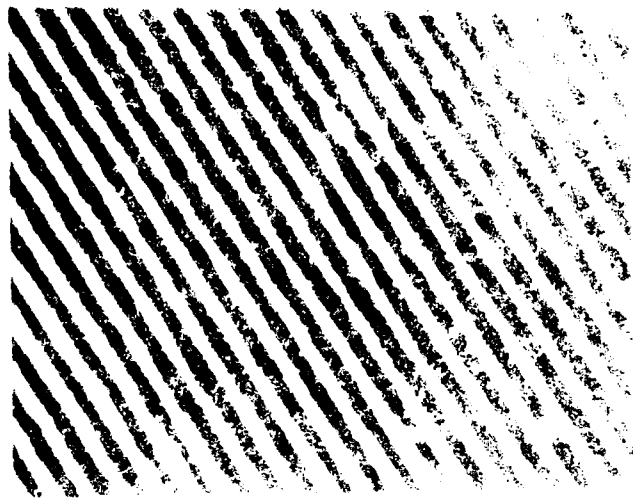
Technical Pan film by Kodak (Figure 21c) was found to give a reasonable tradeoff between speed and resolution. At the ruby laser wavelength, the Technical Pan film was found to have the highest sensitivity. Although the base of the Technical Pan film did exhibit some scattering, the emulsion exhibited a fine-to-medium grain. Many of the other films investigated exhibited a very coarse grain and generally high film noise.

In an effort to increase the contrast of the Technical Pan film, we tried recopying the photographs using contact printing techniques. Both the holographic plate copy and the lithographic film copy of the Technical Pan film (Figure 21e and 21f) showed higher contrast, thus higher diffraction efficiency, and less noise. The holographic plate had the advantage of being on a glass plate which introduced less scatter than the film base of the lithographic film.

A better recopying process was found through the use of optical processing to filter out the zero diffracted order background and the high-frequency noise. By optically processing the Technical Pan originals, we were able to achieve high-diffraction efficiency with very little noise. A comparison of a grating photograph original, copy, and optically processed copy is shown in Figure 22. Since this processing and copying require a great deal of effort, it may only be practical if data need to be extracted from (and possibly the sensitivity multiplied of) a noisy, low-contrast grating photograph. For practical purposes, the best approach would be to use the highest-contrast low-noise film that can be tolerated (perhaps a holographic film) to obtain an initially good recording. Most of the moire effects can be clearly seen and analyzed without further photographic processing.

## 2. MODEL COATING

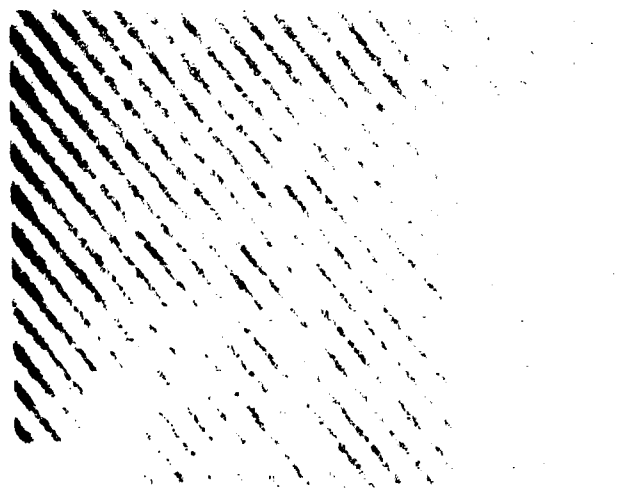
Holographic interferometry is sensitive to changes in optical path length whereas moire interferometry relies on changes in



Original Document



Copy



Original

Figure 22. Comparison of Copied Material with Original.

the intensity distribution on the model surface (the model grating). In holography work, we were therefore able to use a retroreflective coating on the model which provided high light efficiency. We can not use a retroreflective coating with the moire work since the intensity distribution would always return with the same distribution as is incident on the model, regardless of the model position or orientation. Therefore, to obtain light efficiency in moire interferometry we need a diffuse coating which will consistently reflect the majority of the light to the viewing position regardless of the incidence angle.

To this end we conducted a comparison of a number of different surface coatings. The data are summarized in Table 3. The numbers are all relative. Care was taken to ensure consistency in the measurements, particularly when comparing over-coated materials to the original materials. The important point to note is the relative relationship between the normal angle diffuse reflectance and the specular angle reflection. A more detailed graph is shown in Figure 23 for the Dutch Boy and Krylon flat white paints. The Dutch Boy paint very nearly follows the theoretical Lambertian reflectance of a cosine function. A Lambertian reflector should be insensitive to the angle of illumination with a maximum reflectance always occurring at the normal to the surface. Such a reflector is desirable for our work, since to optically derotate an object we must view it at normal incidence, but the illumination must be from off-axis to do moire testing.

The next relevant parameter is the normal angle reflectance. A relative comparison of the normal angle reflectance of various materials measured at 514 nm and 45 degree incidence angle is shown in Table 4. All numbers have been normalized to the Eastman reflectance coating which clearly had the highest reflectance. In real terms the reflectance of the Eastman coating appears to be greater than 90 percent as compared to a theoretical Lambertian reflector. The biggest limitation of the

TABLE 3

DIFFUSE REFLECTANCE OF VARIOUS MATERIALS AT A WAVELENGTH OF 0.6328 MICRONS

Surface	Incidence Angle(°)	Normal Angle Reflection	Specular Angle Reflection	Comments
Krylon Flat White (new)	45	5.9 $\mu$ W	55.0 $\mu$ W	High specular reflection.
	60	5.8	50.8	
Krylon Flat White (old)	45	5.3	13.5	Surface slightly worn, very dependent on application.
	60	5.5	18.3	
Glass Frosting on Krylon Flat White	45	5.0	12.6	Some attenuation only.
	60	5.2	18.5	
Soft & Dry on Krylon Flat White	45	5.4	5.5	Reduced specular reflection, did not improve normal reflection.
	60	5.3	4.1	
Sanded Aluminum	45	5.2	105	High specular component.
	60	3.8	120.	
Glass Frosting Over Aluminum	45	6.8	21.3	Some reduction of specular reflection.
	60	4.5	21.3	
Dutch Boy Flat White	45	7.2	5.1	Close to Lambertian, no specular component.
	60	7.1	5.0	
Eastman Chalk	45	8.1	5.5	Close to Lambertian, highest reflection.
	60	7.8	5.3	
Stripping Film on Krylon Flat White	45	2.0	24.6	Film enhances specular reflection, reduces normal reflection.
	60	1.9	32.0	

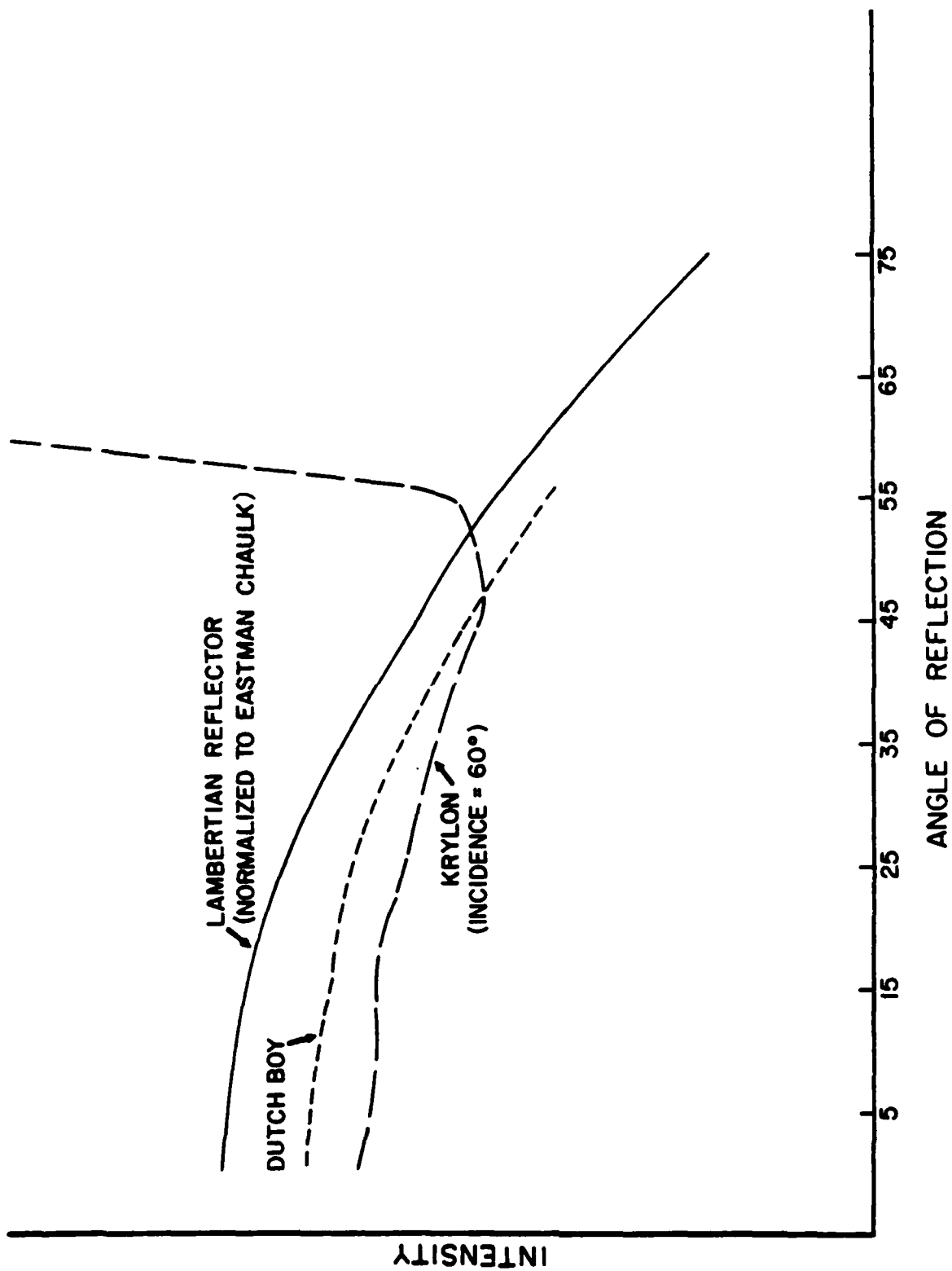


Figure 23. Reflectance Map of Selected Painted Coatings.



Eastman coating is the difficulty in application. A thick coating tends to dampen the vibration of the object. Any layer of the Eastman coating will flake off since it is only a powder. The Dutch Boy paint would appear to offer a happy medium of reflectance (between the Krylon and Eastman coatings) without the presence of an annoying specular angle reflection yet with the adhesion and durability of paint.

TABLE 4

NORMAL REFLECTION FOR 45-DEGREE INCIDENCE BEAM  
AT 514.5 nm (NORMALIZED)

Eastman Chalk	1.0
Dutch Boy Flat White	.86
Krylon Flat White	.76
Soft & Dry over Krylon	.78
Clean White Index Card	.85
Clean White Cardboard	.86
Sand Blasted Aluminum	.45 (specular .57)

## SECTION VII

### DATA INTERPRETATION

Moire interferometry offers a full-field map of out-of-plane displacement. For these data to be analyzed quantitatively one must have an understanding of what causes the various possible fringe patterns.<sup>4</sup> The discussion presented here will assume that a projection moire approach is used (thus there is no sensitivity to in-plane motion) and that the angle of projection and the period of the specimen grating are constant.

This last assumption regarding the angle of projection and period of the grating may not be absolutely true. If a grating is projected onto a 600 millimeter (2 foot) wide object from 1,200 millimeters (4 feet) away, so that at the center of the object the light is at a 25-degree angle to the average normal to the surface, then at the edges the angle of incidence could vary by  $\pm 10$  degrees. This is not a problem if the view position is symmetrically positioned on the other side of the object center from the projection port, because then the tangent of the viewing angle will increase by the same amount that the tangent of the projection angle decreases. Since the sum of the tangents is constant, the sensitivity of the moire,

$$\Delta Z = P/(\tan \theta_i + \tan \theta_v),$$

will remain constant. A similar compensation occurs if the model is tilted. If the slope of the model surface varies, there will be some small change in period, but this effect will be small. A variation in surface slope of  $\pm 5$  degrees would change the period by less than 10 percent. If this measurement were critical, a correction factor could be calculated from the known model geometry. Changes in slope due to deflection will also cause the pitch to change, but this change is what causes the desired moire. The sensitivity of the moire would change less than a percent for the expected typical deflections of less than 2 millimeters.

There are four basic motions of interest for the purpose of this study: rigid body translation, pitch, yaw, and deflection (i.e., bending of the model).

## 1. TRANSLATION

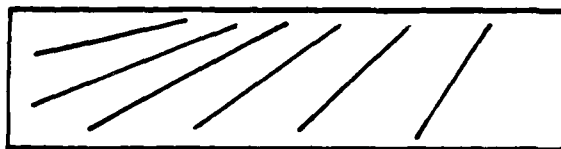
Translation of the model in the plane of the model will not produce any moire fringes since the moire is only sensitive to out-of-plane motions. If the moire is created by superimposing separate recordings of the model grating, the pictures would need to be lined up to a given point, such as the central hub and a blade tip, or referenced to a constant straight-line grating. If the gratings are not lined up, a moire will be created that maps the change in surface geometry of the overlaid points. For a rigid body out-of-plane displacement, the moire pattern will not be changed, since there is no variation in height. Only one large moire fringe covering the entire object would result from an out-of-plane translation. If a moire fringe pattern exists, it would appear to sweep across the field. Since the number and character of the moire fringes would not change, rigid body translation is not a problem in interpreting fringe data, as long as the object stays in focus.

## 2. PITCH

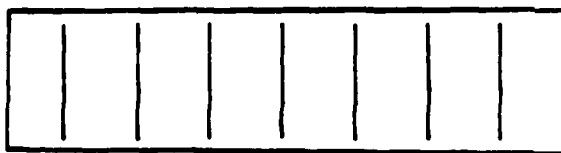
A change in pitch or tilt out of the plane of incidence of the model would create a change in out-of-plane position and hence create a fringe pattern. The moire fringes would follow contours of constant displacement which would be straight lines perpendicular to the projected grating lines (see Figure 24). From the discussion earlier in this report, we know this type of fringe is caused by a rotational mismatch of the grating lines. Since the turbine assembly model is rotationally symmetric, any tilt moire lines would cause the radially symmetric vibration mode pattern to become unsymmetric in the horizontal versus vertical directions. If the model is actually twisting, these



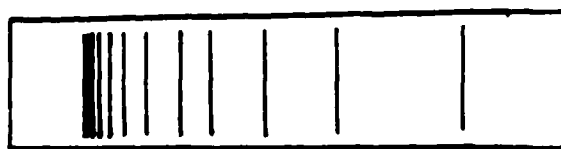
PITCH



TWISTING



YAW



DEFLECTION

Figure 24. Predicted Moire Pattern of Blade Model.

rotational mismatch fringes will not be of constant period across the model (see Figure 24), the variation in the period being a measure of the amount of twist.

### 3. YAW

Yaw or tilt of the model causes a variation in out-of-plane position in the plane of incidence (perpendicular to the projected grating lines). Since this is a linear rigid body motion, the resulting moire fringes will be a constant period bias fringe with the fringe lines parallel to the grating lines (parallel to the vertical axis) thus again causing a radially symmetric moire pattern to be unsymmetric in the horizontal versus vertical directions (see Figure 24). Since rigid body movements cause constant period bias fringes, they can be recognized and corrected in the data. If the fringe pattern is digitized and put into a computer, the rigid body bias fringes could be subtracted out just as tilt bias fringes are subtracted out of holographic interferogram data in current fringe analysis systems.<sup>11</sup>

### 4. DEFLECTION

Just as twisting introduces a varying period fringe across the model of a single blade, a deflection of the blades along their length will introduce a varying period moire fringe pattern perpendicular to the length of the blades as shown in Figure 24. The number of fringes from a chosen zero point (say the center) to a point on the blade assembly, times the sensitivity of the moire, is the deflection of the model at that point. The width of a moire fringe (dark to dark or light to light), that is, the period, minus the period of the moire at a reference point (which could be zero at the center), divided by the sensitivity of the moire, is the slope at that point on the beam, in relation to the reference point. The sign of the deflection can be determined by translating the reference grating parallel to the specimen

grating perpendicular to the grating lines so as to move the center of the reference grating toward the point of zero displacement (using the two overlaid gratings).<sup>5</sup> The moire fringes will appear to move toward the nearest point to the observer. Therefore, if the model is deflected away from the observation point, the fringes will appear to move toward the zero displacement point. This effect occurs because if the deflection is away from the observation point, the grating period will increase to the point of interest relative to the zero deflection point. The opposite effect occurs if the model is deflected toward the observation point (i.e., the period of the grating lines decreases). When the center of the master grating is moved toward the zero order or zero deflection point, the moire fringes will appear to move toward the highest frequency (smallest period) grating lines.

## 5. MEASUREMENT TECHNIQUES

A simple approach to measuring the moire fringe data would be to place a ruler along the line of interest and measure the fringe separations and count the number of fringes which intersect the ruler. These measurements describe the changes in out-of-plane position along the line of the ruler. A slightly more sophisticated method of data analysis would be to put the moire pattern on a video screen and use a simple video scan line selector to look at individual lines for different orientations of the moire pattern. As a simple automation, the video scan line could be processed using thresholding techniques to locate the one-dimensional fringe positions, which could then be fed into a computer to do the calculations. Chances are that only a few scan lines (through different diameters) would be required to yield the desired data.

These simple line intersect measurements are only valid if the moire pattern does not exhibit closed fringes and the positions of zero slope are known. If the pattern is more complicated

or if more automation is desired, the fringe pattern could be fully digitized, using high-resolution digitizing equipment, and computer analyzed. This may not always be necessary, but if a lot of test data are to be analyzed, it is very practical and cost efficient. For mode pattern visualization and qualitative measurements, simply counting the fringes and noting any asymmetries would be sufficient.

## 6. EXPERIMENTAL DEMONSTRATION

As a simple example of moire on a model, projection moire was used to measure the deflection of a styrofoam beam which was 700 millimeters (28 inches) long (which may be scalable to a single turbine blade). To provide a comparison of the moire measurements to a mechanical contact measurement, dial indicator gauges were contacted against the back of the beam at selected points along its length. This setup is shown in Figure 25. The sensitivity of the moire was approximately 0.635 millimeters (0.025 inches) per moire fringe with a variation across the field of about five percent. The sensitivity and illumination could be better controlled with higher sensitivity by specifying the required optics (we used what we had in house). A series of moire fringe photographs made with this system are shown in Figure 26. Table 5 shows a comparison of the dial indicator measurements to the moire measurements for simple deflections of (a) 25.4 millimeters (1 inch) and (b) 12.7 millimeters (0.5 inches) total deflections (shown in Figure 26a and 26b). Most of the measurements agreed to within five percent, although the position 2 moire measurement was offset by a constant +10 percent. The systematic offset errors can be accounted for by hysteresis in the particular dial indicators used, problems with the model, uncertainties in the positioning of the dial indicators, and a slight variation in the model grating period as indicated by the nonconstant period of the tilt-only moire pattern (Figure 26d). The blade model used in this demonstration was not

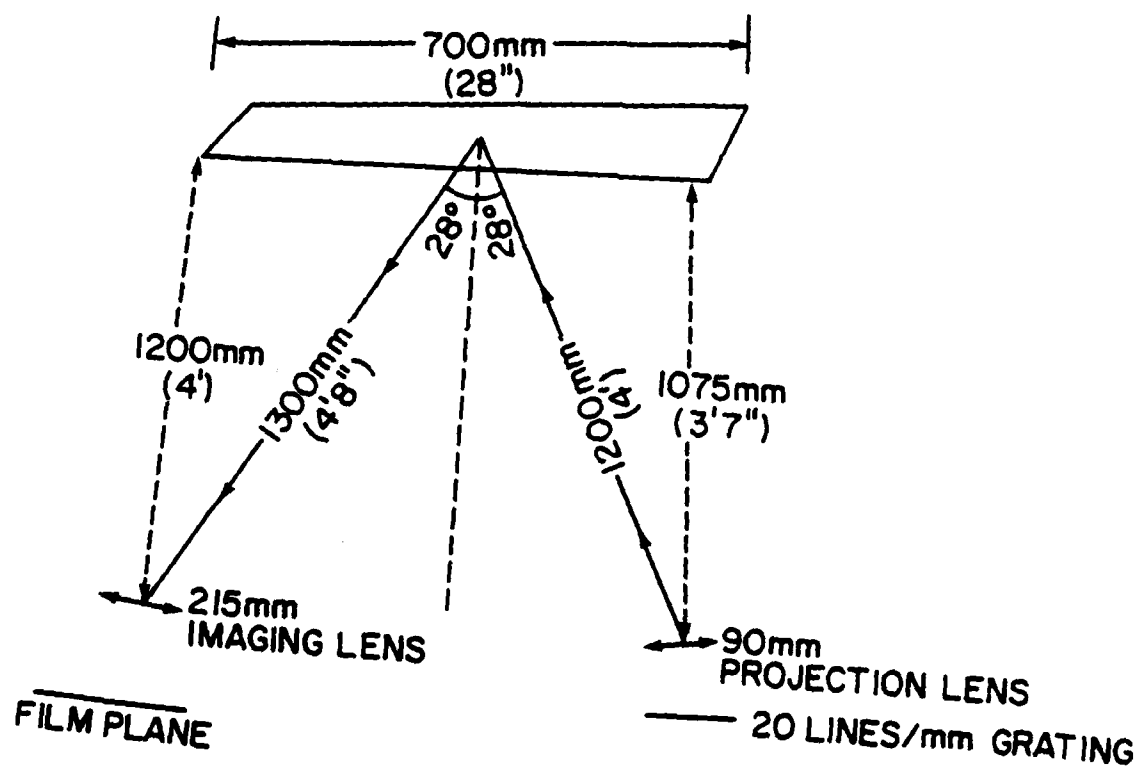
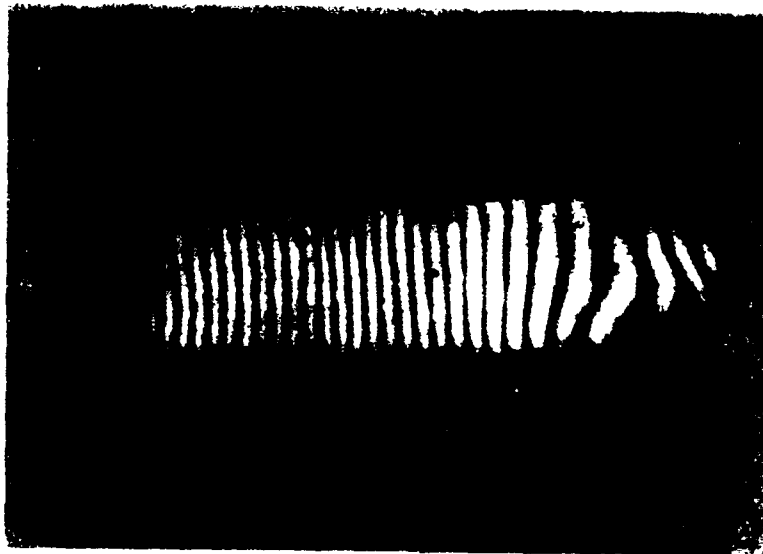
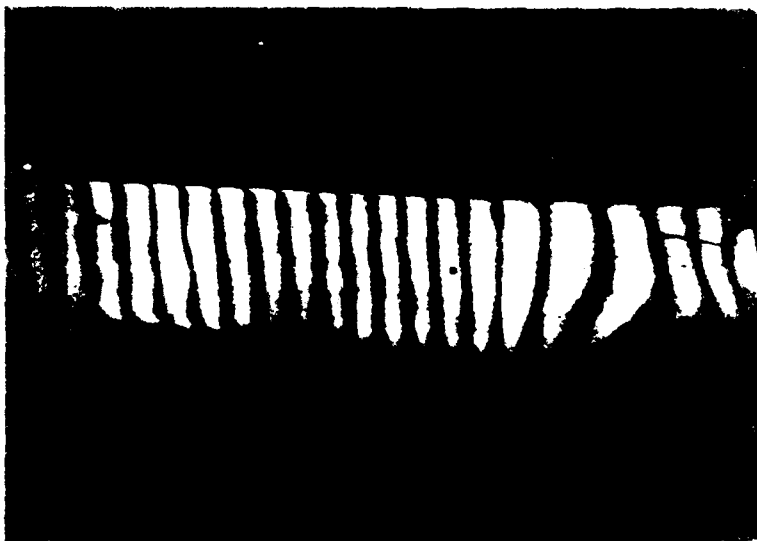


Figure 25. Setup to Demonstrate Moire on Beam Model.



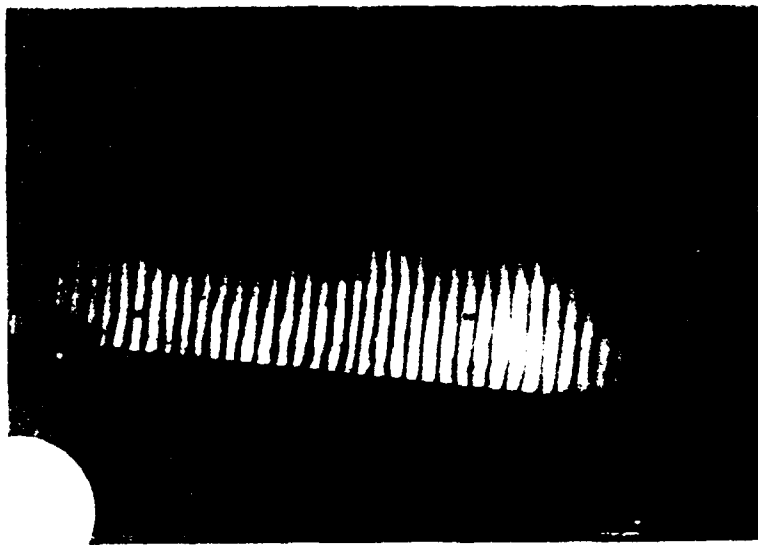


a. 25.4 mm Deflection.



b. 12.7 mm Deflection.

Figure 26. Moiré Patterns on a Beam Model.



c. +2.5 Degrees of Tilt, -12.7 mm Deflection.



d. -2.5 Degrees of Tilt.

Figure 26 (cont.). Moiré Patterns on a Beam Model.

very predictable as to what motion it would exhibit (yaw, deflection) since it exhibited hysteresis, and the surface tended to compress where the dial indicators contacted the model. Taking these facts into account, the moire gave very reliable and easily interpreted results with a manually readable sensitivity of about 0.1 millimeters (0.004 inches) without any advanced data processing.

TABLE 5. MOIRE MEASUREMENTS COMPARED TO DIAL INDICATOR MEASUREMENTS (IN MILLIMETERS) FOR SIMPLE DEFLECTION OF A BEAM MODEL

Position	1		2		3	
Case	a	b	a	b	a	b
Dial indicator	7.6	4.7	20.3	10.2	25.4	12.7
Moire	7.5	4.7	22.1	11.2	25.4	13.3

## SECTION VIII

### SPECKLE INTERFEROMETRY

#### 1. BACKGROUND

The nature of laser light is such that when used to illuminate an object, the resultant reflected light is in the form of a speckle pattern characteristic of the particular surface. If this speckle field is then referenced to some other speckle field from the same object, small lateral displacements of the object can be measured to a high accuracy.<sup>19-23</sup>

The basic premise of one technique, as described by E. Archbold, et. al.,<sup>19</sup> is that each individual area of the processed film will cause an illuminating beam to be scattered into a "diffraction halo" with a periodically varying intensity pattern. This pattern is the product of the "halo" from a single speckle pattern plus the intensity distribution produced by two points on the specklegram (which correspond to a single point on the object) which act as two point sources with the same separation as the image shift to be measured. Therefore, to observe large lateral movements of the object, a double exposure of the speckle pattern is first recorded. Then the lateral motion of the object, through the resulting image shift, can be analyzed by scanning across the recorded image and observing its optical transform at each point.

It is generally possible to calculate what the limits on the displacement to be measured would be. For a lateral displacement where

$$d = \Delta X^2 + \Delta Y^2 \quad 1/2$$

there is an image shift  $b$  of

$$b = \frac{d}{m}$$

where  $m$  is the demagnification factor relating the image

dimensions to object dimensions. This shift will give a diffraction pattern in the form of a set of Young's fringes with an angular separation of  $\alpha$  so that

$$\sin \alpha = \frac{\lambda m}{d} .$$

The direction of these fringes will be orthogonal to the direction of image motion. The limiting speckle size is determined by the f-number ratio of the camera. The allowed speckle size is then

$$\delta = 1.2 \lambda F$$

where  $F$  is the camera f-number ratio. This implies a speckle size on the object of

$$\Sigma = 1.2 \lambda m F .$$

As stated before, the lateral movements must be greater than  $\Sigma$  to be observable. As an example, for an f/4 lens system at 1:1 magnification the smallest theoretical displacement that could be measured is about 3  $\mu\text{m}$ . This then sets a lower limit on the lateral displacement that can be resolved with this technique.

An upper limit on the allowed displacement is set by the resolvability of the fringes. Experimental results found by Archbold, et al.,<sup>19</sup> indicate that the fringe spacing must be about five times the speckle diameter. For an object diameter of  $L$  we can express the speckle diameter as

$$\delta = 1.22 m \lambda / L .$$

Then for a lateral body motion of  $d$ , so that

$$\alpha \approx \frac{m \lambda}{d}$$

the fringes will just be resolvable for a lateral displacement of

$$5 \left( 1.22 \frac{\lambda m}{L} \right) = \frac{\lambda m}{d}$$

or

$$d = L/6 .$$

This limit is no great problem since for displacements greater than  $1/6$  object size the displacement could probably be more easily measured directly. An additional qualification on this, however, is that the distortion introduced by the lens would tend to wash out the fringes even more as this limit is approached.

Another important limiting condition to consider is that to get a meaningful fringe pattern, the speckle patterns being compared must remain correlated. For a noncollimated imaging system, decorrelation occurs with displacement along the line of sight. It was pointed out before that speckle interferometry is relatively insensitive to longitudinal displacements. However, due to the change in  $m$ , there is a resulting radial shear effect between the two speckle patterns. This leads to a series of rings when illumination is done with collimated light. For an axial displacement of  $Z$ , a radial distance on the object of  $R$ , a field semiangle  $\beta$  and an object conjugate  $C$ , and an apparent radial displacement of  $Z\beta = Z(R/C)$  there is a radial displacement on the film of

$$\rho = ZR/mC .$$

This would yield bright rings of diameter  $r$  so that

$$r^2 = nLC \lambda / Z_1, \quad n = (0, 1, 2, 3, \dots) .$$

The depth of focus for which the speckle patterns would remain correlated (in object space) is

$$\Delta Z = \lambda m^2 F^2 .$$

Experimental results by Archbold, et al.,<sup>19</sup>, show correlation to exist for about four times this amount. This is possible because only small angle diffraction is used in viewing the pattern while a wide cone is used to record the pattern (as suggested by Archbold, et al.). The depth of focus then is approximately the effective f-number of the observing system.

We conducted a series of experiments to determine correlation width, using holographic interferometry. This method provides a sensitive method of determining coherent correlation widths by observing the contrast of a real-time holographic interferogram. When the diffracted speckle field character changes so that the same points of light are no longer available in the field to interfere with the holographic image field, the contrast of the holographic fringes will go to zero (this is decorrelation). This information is applicable both to speckle interferometry and to holographic interferometry, though it is more restrictive than speckle interferometry requires.

We considered retroreflecting paper, diffuse aluminum, bare aluminum, and a specular surface. The results of these measurements are summarized in Table 6. The object size was about 25 millimeters.

TABLE 6  
CORRELATION WIDTH MEASUREMENTS  
(Point at which fringes lose visibility for ~f/30 system)

Surface	Z-axis	X-axis
Retroreflecting paper	4 mm	20 microns
Diffuse aluminum	4 mm	>70 microns
Bare aluminum	4 mm	>80 microns
Mirror	no decorrelation	no decorrelation

As expected, a specular surface showed no decorrelation. For the retroreflecting paper, the allowable lateral displacement was considerably less than for a diffuse surface. This effect may be due to the nature of the material to exactly retroreflect over a very limited angle rather than scatter light over a large angle.

Other limitations follow from the decorrelation problems described. For near normal incidence and viewing, the maximum allowed tilt to maintain correlation is given by

$$\delta\psi = \lambda/2m\delta$$

since  $\delta \approx 1.2 F$ , then

$$\delta\psi = \frac{1}{2.4mF} \cdot$$

For a typical  $f/4$  system and a demagnification less than ten, this sets a practical limit on tilt of about 15 mrad. The technique involved in measuring tilt is similar to the technique for measuring vibrations as described by Massey.<sup>22</sup> Take a double exposure with the camera focused some known distance in front of or behind the object,  $w$ . A measurement can then be made of the lateral displacement of the speckle pattern produced by the object as a whole compared to a reference pattern produced by focusing a beam onto the surface, which will approximate specular reflection. The patterns will displace at twice the rate of tilt due to the mirror effect being used. The tilt can then be found from geometry:

$$\delta\psi = md / 2 w$$

where  $d$  is the lateral displacement. This measurement is also limited by scattering effects. Similarly the maximum allowable rotation is limited by the maximum lateral displacement at whatever radius the fringes are being observed.



There are some other techniques in addition to the double-exposure techniques referred to that do not appear to allow any additional freedom and, in fact, tend to be a little more restrictive. One such technique is Boone's<sup>23</sup> technique, which involves illuminating the surface with two parallel collimated beams and imaging the speckle pattern on a photographic plate. Once the plate has been developed, a real-time or electronic (with a television recording) subtraction technique can be employed to see if the speckle patterns still match. The fringes due to lateral displacement are then dependent on the illuminating angle  $\frac{\theta}{2}$  and

$$2d \sin \frac{\theta}{2} = n\lambda, \quad n = (0,1,2,3\dots).$$

Bias fringes can be introduced by tilting one of the illuminating beams with respect to the other. This requires that the plate can be repositioned very accurately. A modification of this technique takes advantage of the nonlinearities of the film and the statistical distribution of the emulsion particles. This involves giving a small (couple of speckle) lateral displacement to the object between a double exposure to produce a one-dimensional grating and again obtaining Young's fringes. The recording is then reimaged using just the  $\pm 1/2$  order recorded beam (by spatial filtering).

These techniques have the advantage that, theoretically, very high contrast fringes can be obtained. The fringes can be analyzed either by examining the film with some small viewing aperture or by reilluminating the film and selecting an area by spatial filtering. The sensitivity of the techniques is adjustable by varying the demagnification factor of the system, thereby varying the Young's fringe spacing  $\alpha$ . By doing this, a sensitivity range of a few microns to about  $1/6$  the object size can be obtained.

There are also some very restrictive limitations. A certain amount of mechanical and coherence stability is required which

limits the "in factory" type use. Due to resolution and correlation requirements, the magnitude of displacement that can be tolerated is somewhat limited (tilt of about 15 mrad and a lateral displacement of about 1/6 the object size). There is also a relative insensitivity to line-of-sight movement. This movement, however, can introduce a certain amount of error into lateral displacement measurements. Because of this problem the applicability of this technique to vibration analysis would be limited.

## 2. CONCLUSIONS

The main limitation of speckle techniques is their relative insensitivity to longitudinal movement along the line of sight. Other basic limitations are inherent in this type of interferometry.

a. Distortion introduced by the lens of the camera used for recording the phenomena will limit the range of displacement that can be measured accurately (even if other aberrations are negligible).

b. A fine-grain film is required to resolve the speckle.

c. The image movement must be greater than one speckle for any observable results.

d. The speckle patterns must remain correlated.

In the Aero Propulsion Laboratory derotator system, these limitations would be severe. Because of the very high f-number of the optical system, the sensitivity of the speckle interferometry would have a lower limit of about 50 microns. The aberrations through the derotator would limit the movement even more by effectively enlarging the size of the speckle. For the purpose of vibration analysis, the out-of-plane displacements are typically larger than the in-plane displacements. From a geometric point of view, the minimum out-of-plane displacement to obtain the required in-plane displacement would be a few

millimeters, probably enough to decorrelate the speckle pattern (beyond the depth of focus) or at least introduce a large error factor. Therefore, it may not be possible to obtain a clear derotated speckle pattern. The potential solution to this sensitivity to in-plane but not out-of-plane movement is to use a white light speckle projected from off-axis so that it moves laterally relative to the surface, due to an out-of-plane movement. This is what moire interferometry does, without the limitations and errors associated with speckle interferometry since it does not rely on the surface structure as a measurement standard.

# SECTION IX

## MULTIPLE WAVELENGTH INTERFEROMETRY

### 1. MULTIPLE WAVELENGTH CONTOURING

Multiple wavelength holographic contouring is a similar approach to the problem of deflection measurements without the problems associated with projecting a clear grating on the object as required with moire.<sup>24-26</sup> For this technique, a hologram is made of the object, then reconstructed in real time using a wavelength different from that used to make the hologram. A variation of this would be to make a double exposed plate using a different wavelength for each exposure and then reconstructing with either. The sensitivity of this technique is given by (fringe-to-fringe spacing)

$$P = \lambda_1 \lambda_2 / 2 | \lambda_1 - \lambda_2 | .$$

Using an Argon laser, fringe spacings of a few microns to about twenty-five microns can be obtained, as shown in Table 7. A more continuous range could be obtained using a dye laser. A dye laser for this application would probably be more trouble than it would be worth.

TABLE 7  
FRINGE SPACING FOR MULTI-WAVELENGTH CONTOURING

<u><math>\lambda_1</math></u>	<u><math>\lambda_2</math></u>	<u>Fringe Spacing</u>
488 nm	514.5 nm	4.75 microns
488 nm	496.5 nm	12.25 microns
488 nm	476.5 nm	10.1 microns
501.7 nm	496.5 nm	23.95 microns
514.5 nm	496.5 nm	7.99 microns
514.5 nm	476.5 nm	3.22 microns
514.5 nm	501.7 nm	10.08 microns

A typical optical system for the multiple wavelength technique is shown in Figure 27. First, a hologram is made of the object at a wavelength of  $\lambda_1$ . Then the developed hologram is accurately repositioned and the hologram and object are illuminated at some other wavelength  $\lambda_2$ . The holographic image is displaced from the object in the x, y, and z direction due to the dispersion property of the hologram. By changing the angle of the reconstruction beams to the holographic plate, the lateral displacement of the holographic image relative to the object can be corrected, yielding a holographic image which is superimposed over the object but slightly displaced along the line of sight. This small z-axis displacement causes the holographic image to appear to be a different size than the object. When the two images are viewed together, a contour of the object is seen like the contour of a sphere that is seen when it is cut by a series of planes or spherical surfaces of a different curvature. It is important that the object be viewed at normal incidence for this contour, or a lateral displacement will still exist and introduce additional bias fringes. These bias fringes would make the contour difficult to interpret.

To make a double exposed hologram of the object, a second plate is exposed right after the first. The first plate is developed and used to reposition the holographic image over the object to obtain a clear contour. A second exposure is then made on the second plate at the new wavelength. When this plate is developed, it can be viewed with either wavelength independent of the object and the holographic image will show contour fringes.

To view these contours, both images must be in focus at the same time. This puts a limit on the resolution which can be obtained in viewing the object since high resolution permits a smaller depth of focus. An opaque yet finely diffuse coating would greatly decrease the noise in the holographic image and make the contours more visible. As with the moire, the resolution

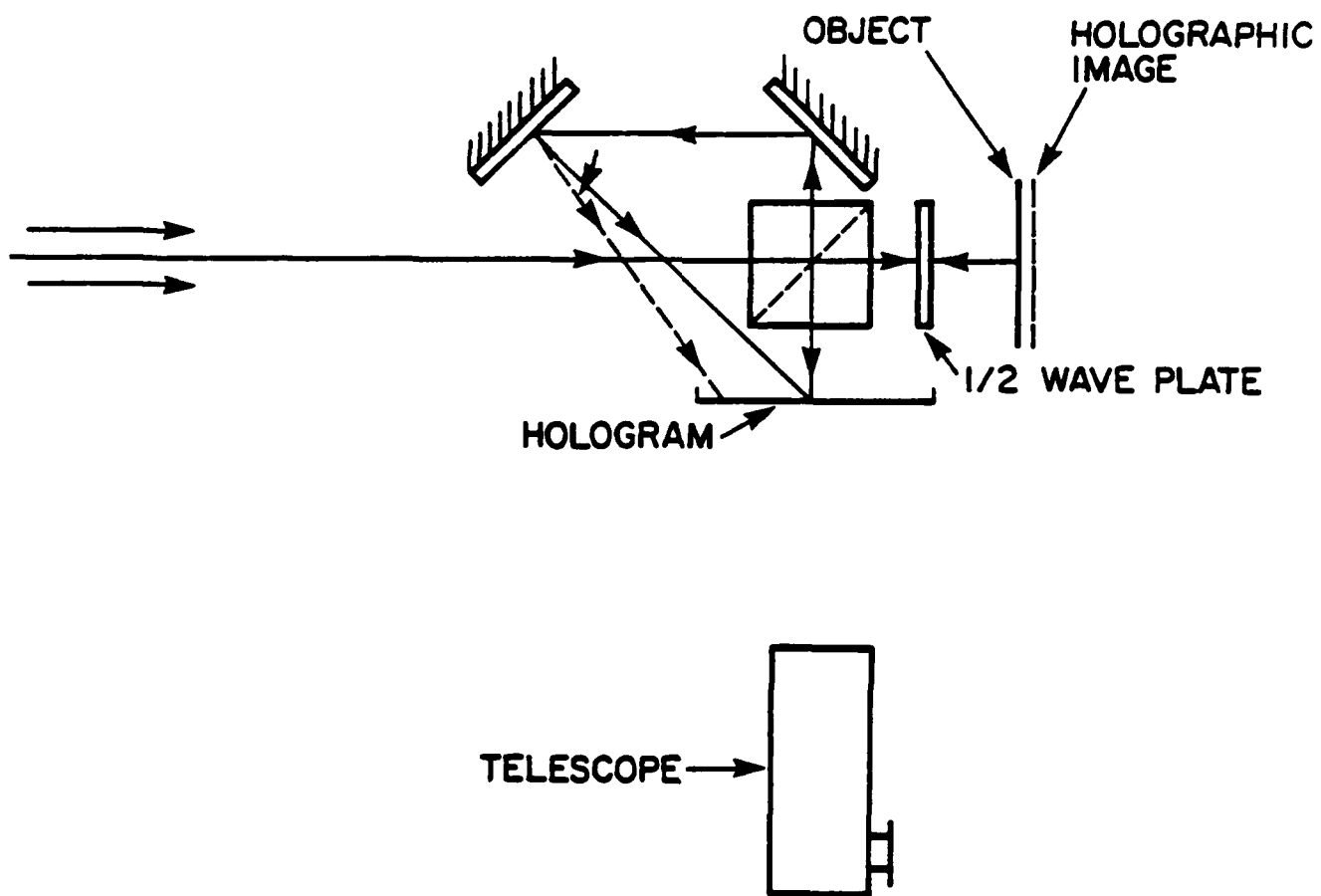


Figure 27. System for Multiple Wavelength Contouring.

and hence the rate of change of a contour and the size of a structure which can be viewed at one time are limited by the depth of field required for the area of interest to be in focus.

The allowable depth of focus for a required resolution is given by (object in air)<sup>27</sup>

$$\text{depth of focus} = \pm \lambda / 2 \sin^2 U$$

where  $\lambda$  is the wavelength of illumination and  $U$  is the largest ray angle accepted by the optical system. If the holographic image moves more than this, both images can not be viewed at the same time and no contour is seen. The equation for this displacement is

$$\Delta Z = Z[(\lambda_1/\lambda_2)-1] = \text{Optical Path difference}$$

where  $Z$  is the distance from the hologram to the object. For a typical system this would be on the order of 1/8 to 1/4 inch. Therefore, to see fringes clearly the depth of focus and hence the resolution are limited by this constraint to a resolution of about 300 microns. If an optical system is devised so as to locate the hologram very close to the object or image the object close to the plate, the resolution could be increased and a contour would be easier to view.

## 2. MULTIPLE WAVELENGTH SPECKLE

A technique related to speckle interferometry but using multiple wavelengths to achieve the effect is that described by Jones and Wykes.<sup>28</sup> This technique involves making a hologram of a specular master object using two wavelengths  $\lambda_1$  and  $\lambda_2$ . The hologram can then be reconstructed and a comparison made of either the master or some nonspecular object of the same geometry (to compare to the geometry of the master) using speckle interferometry. In particular, video techniques can be used to

electronically subtract the intensity distribution of the  $\lambda_2$  illumination from that of  $\lambda_1$ , illumination. This yields:

$$I_1 - I_2 = 4A_R^2 A_S^2 \cos \phi \sin \left[ \psi + 2 \pi \left( \frac{1}{\lambda_1} - \frac{1}{\lambda_2} \right) q \cos \alpha \right]$$

where  $A_S$  = speckle amplitude,  $A_R$  = reference beam amplitude,  $\phi$  = random phase factor,  $\psi$  = average phase difference between object and reference beams,  $q$  = normal distance between the object and master wavefront, and  $\alpha$  = angle of illumination between illuminating wavefront and surface normal. Dark fringes occur when  $q \cos \theta/2 = \Lambda_{12}$  where

$$\Lambda_{12} = \lambda_1 \lambda_2 / 2(\lambda_2 - \lambda_1).$$

The sensitivity of the system is then adjusted by changing  $\lambda_2$  and  $\lambda_1$  relative to each other. This is ultimately limited by the surface roughness of the object under test in that  $\Lambda_{12}$  must be greater than eight times the mean surface roughness. A workable sensitivity range of 7  $\mu\text{m}$  to 25  $\mu\text{m}$  was found by Jones and Wykes.

A number of limitations and possible sources of error could make this technique very cumbersome for the results obtainable. The limitations of speckle testing as discussed before will still hold in general. The area of inspection is limited by the aperture and depth limitations of the hologram. There is also a problem with error fringes caused by inaccurate replacement of master or object to be compared; errors in reconstruction beam, emulsion shrinkage; and other related factors. However, these error fringes can be minimized. The sensitivities possible are limited by the available wavelengths. There is also the problem that the master needs to be specular to obtain good fringes, and this still does not guarantee high contrast due to the surface roughness of the object to be compared.



### 3. RESULTS AND CONCLUSIONS

Multiple wavelength holographic contouring (MWHC) has a number of limitations. Because MWHC is a holographic process, it requires holographic tolerances and stabilities. This requirement would limit its use in actual turbine blade tests to static situations. MWHC is also contour sensitive. The contour information is superfluous to the deflection data and can be an annoyance. This problem was encountered at APL when doing pulsed holography of a contoured bladed disk with a ruby laser which was not operating in a single longitudinal mode (see Figure 28). If the object surface is not smooth, MWHC can generate a highly complex pattern of fine contour lines. To obtain actual deflection data, two contours would need to be made (before and after deflection) and superimposed to form a moire. The sensitivity of the moire would be determined by the original contour interval. For a rough surface, the MWHC fringes would be very high frequency and low contrast. The additive moire that would be formed between two contours would be even lower contrast. For a displacement which is large compared to the contour interval, the moire may not be visible because of depth-of-focus limitations imposed by the high-frequency contour.

A possible approach, which could make either MWHC or high-frequency holographic interferometry fringes useful, would be to moire the holographic fringes against a higher frequency known linear grating. The moire would then have the sensitivity of the known grating which could be adjusted as desired. This system would still be limited to laboratory type applications. However, if the range of contour fringes is large, the resulting moire may often be too fine to be useful.

Experimental investigations of MWHC have shown that it is difficult to obtain high-contrast contour fringes over a diffuse large area object due to the depth-of-focus limitations and chromatic aberrations introduced by the derotator optical system.

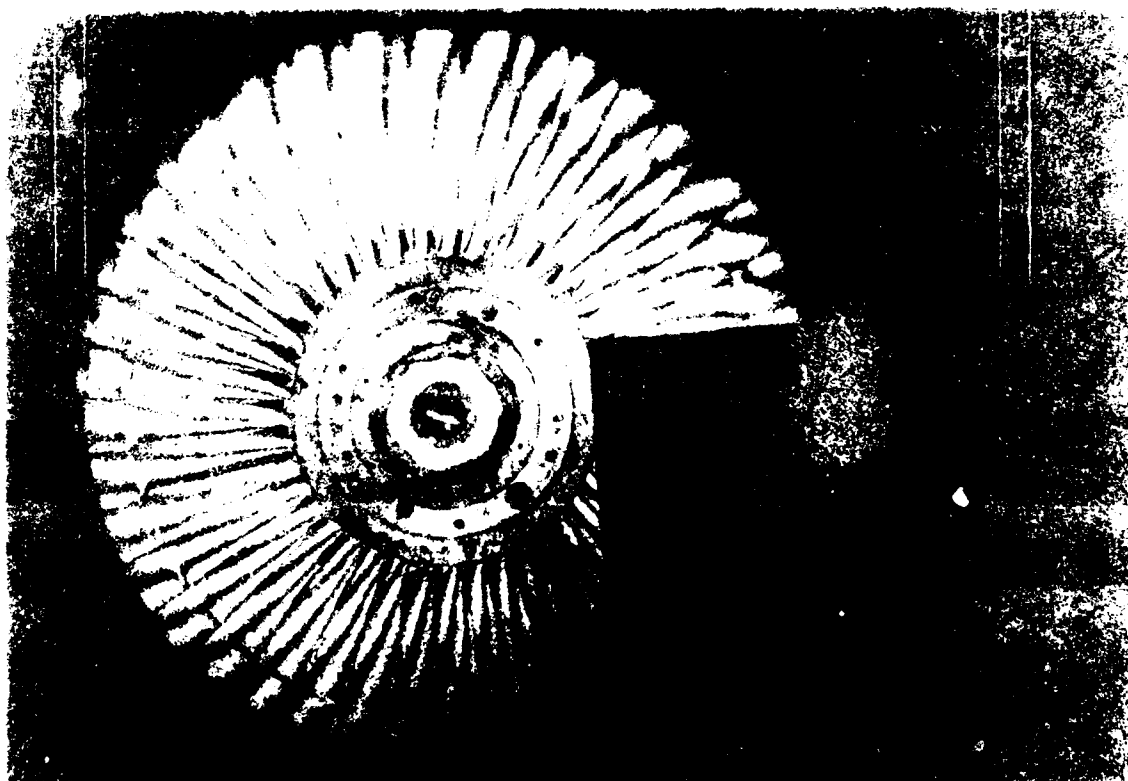


Figure 28. Multiple Wavelength Contouring Program (F. X. X.)

AD-A122 403

DEVELOPMENT OF NEW NONDESTRUCTIVE TESTING TECHNIQUES  
FOR USE IN BLADED-DI...(U) DAYTON UNIV OH RESEARCH INST  
K G HARDING ET AL. SEP 82 UDR-TR-82-46 AFWAL-TR-82-2081  
F33615-80-C-2011

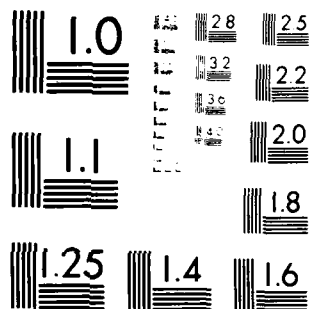
2/2

UNCLASSIFIED

F/G 20/6

NL

													END DTIC FILMED 1-85 DTIC



MICROCOPY RESOLUTION TEST CHART  
 NATIONAL BUREAU OF STANDARDS-1963-A

We were able to obtain a clear contour of specular objects with a contour sensitivity of 20 microns per fringe. Because of the sensitivity of MWHC to surface roughness, we were not able to obtain a clear contour on a painted surface (the fringes contour the roughness of the surface). This problem would be even more severe if retroreflecting paper was used since the specular spheres which make up the surface are large compared with the contour interval. Because of the depth of focus, contour sensitivity, data interpretation difficulty, and the need for an expensive wavelength adjustable laser (like a dye laser), multiple wavelength techniques would not be a viable approach to real structural dynamic response study.

SECTION X  
SUMMARY AND RECOMMENDATIONS

1. ANALYSIS OF REAL-TIME SYSTEM

The resolution of the real-time derotator system is currently about 5 LP mm. This can be increased to 60 LP mm and the illumination field enlarged by replacing the present imaging optics with larger aperture flat-field lenses and replacing the current one-inch polarizing beam splitting cube with a larger aperture beam splitter. We procured these items and verified these improvements.

The University also developed a speed controller to provide a more exact setting of the object speed. To provide increased excitation force and permit operation in a vacuum chamber, we developed a set of externally cooled magnets. These improvements will permit more reliable results to be obtained with greater ease in the APL real-time holographic test facility.

2. NEW TECHNIQUES FOR BLADED-DISK DYNAMICS MEASUREMENTS

Both speckle interferometry and multiple wavelength interferometry have some serious restrictions. Speckle interferometry is not directly sensitive to out-of-plane displacements. The amount of movement required to obtain displacement data would probably decorrelate the speckle patterns. Speckle interferometry is best suited for in-plane deformations under static conditions. Multiple wavelength interferometry creates a contour of the object, thereby requiring four separate holographic exposures to obtain data. A rough object surface or large deformation may reduce the contrast of the deformation fringes below a usable level. Because of the limitations imposed on the objects, the cost of the required equipment, and the difficulty in obtaining results, multiple wavelength holographic interferometry is not foreseen as a viable technique except for specific laboratory experiments.

Moire interferometry is a much simpler, less costly technique than the others considered, and it requires much less stability and fewer optics. Projection moire interferometry offers the most versatility of the moire systems investigated. A lower range of sensitivity with projection moire was found to be 20 to 50 microns (one to two mils). Projection moire requires no special model preparation (as does contact or reflection moire) and is compatible with the derotator imaging system. To enhance the fringe data, optical processing can be easily applied to the projection moire data.

We demonstrated three methods of projection moire interferometry as applied to studying the structural dynamics of a rotating disk: time-average, real-time, and pulsed moire. Time-average moire is simple to do and measures the maximum deflections but is restricted to studying well behaved standing waves. Real-time moire may provide too much extraneous information for large-scale testing but is a powerful laboratory tool for obtaining historical data of structural dynamics. The versatility of real-time moire could be increased by using a shorter pulsed (high repetition rate) laser than was available for this study. Single or double-pulsed moire would be the most appropriate approach for larger scale, nonlaboratory testing, although real-time feedback is not available.

### 3. SYSTEM RECOMMENDED FOR APL FACILITY INSTALLATION

We have investigated two potential projection moire interferometry systems for application to the Aero Propulsion Laboratory test facility: a telescope system and a single tilted lens system. These two systems are shown in Figures 29 and 30. Both systems use projected interference fringes. The primary advantage of the telescope system is that the fringe field at the object is collimated. Collimation ensures that the projected fringe period is constant for any plane. Because of the

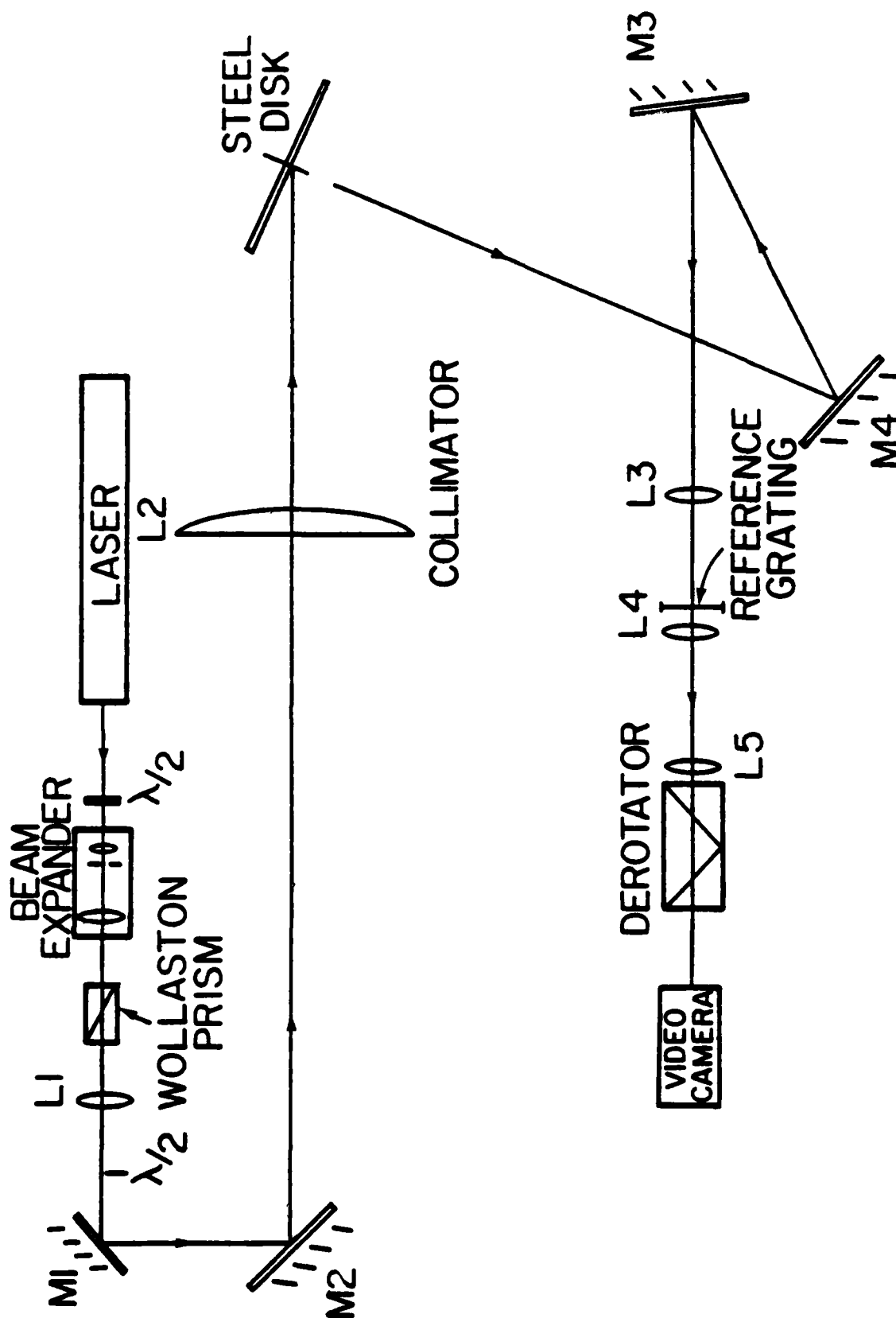


Figure 29. Collimating Telescope System for Projected Interference Fringe Moiré.



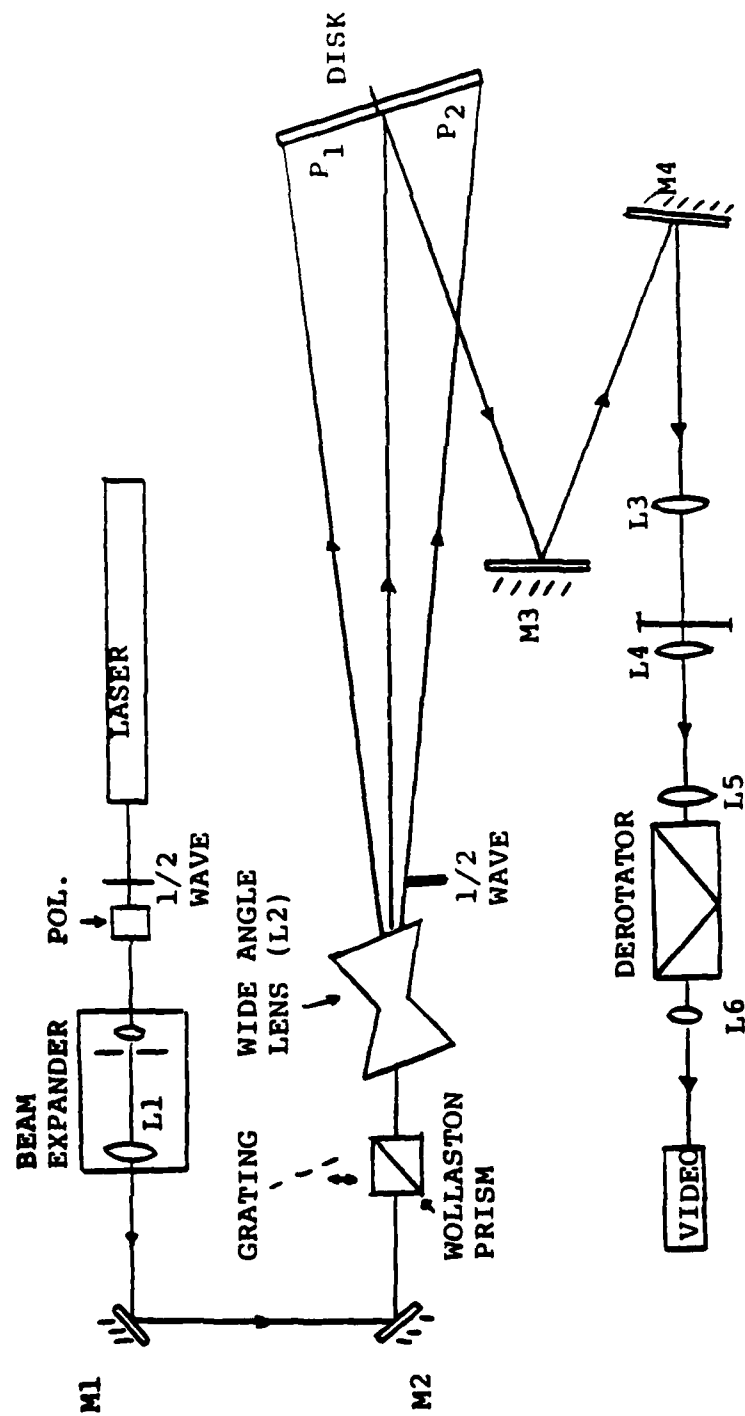


Figure 30. Single Tilted Lens System for Projected Interference Fringe Moiré.

divergence of the light in the single lens system there will be some variation in angle of incidence from one side of the object to the other. This can be compensated for by introducing a variation in the projected grating period across the object such that

$$P_1 / \tan \theta_1 = P_2 / \tan \theta_2$$

where the period on the object  $P_1 = P_0 / \cos \theta_1$  ( $P_0$  is the normal incidence period). Another advantage of the telescope system is a collimated beam passing through a thick tilted window (such as the vacuum chamber window) will gain no aberrations except those inherent in the window. A tilted thick window will cause the apparent focus of a horizontal fan of rays to shift relative to the focus of a vertical fan of rays, thus introducing astigmatism and coma (much like a tilted lens). If both focus points are at infinity (i.e., the beam is collimated) then these aberrations will not be introduced at all. The actual implication of these aberrations on the projected fringe field may be questionable. Since we are using a one dimensional grating, the difference in magnification along the length of the grating lines versus the period is inconsequential. However, we would expect a bowing of the grating lines from top to bottom which would be nice to avoid (i.e., a different period in the middle versus the edges).

The telescope system has one important limitation in that the size of the object is limited by the size of the collimating lens. For application to the current APL test facility, this is not a real limitation since the size of the object is already limited by the size of the vacuum chamber window. Another limitation of the telescope system is that it can not practically image a Ronchi ruling onto the object (while the single lens system can easily do so). For some applications, it may be possible to spread out the telescope system to make this practical, but it would not easily fit on a single optics table.

This is not a problem for the current application since we are using interference fringes which exist everywhere in space and do not need to be imaged. The principle advantages and disadvantages of each system are summarized in Table 8.

Based on this comparison, the best projected fringe system for the Aero Propulsion Laboratory test facility would be the collimating telescope system. This system is the easiest to set up and the data would be the easiest to interpret. A single lens imaging system may be more desirable for large objects since a large collimator would not be required, (a holographic optical element may also be useful).

TABLE 8  
COMPARISON OF PROJECTED FRINGE OPTICAL SYSTEMS

Description	Advantages	Disadvantages
Nonimaging, collimating telescope system	<ol style="list-style-type: none"> <li>1. Yields a collimated beam so has a constant period and sensitivity at any plane.</li> <li>2. Aberrations due to a thick window minimal.</li> </ol>	<ol style="list-style-type: none"> <li>1. Size of object field limited by size of collimating lens.</li> <li>2. Does not image a Ronchi ruling onto object (not practical).</li> </ol>
Single tilted lens imaging system	<ol style="list-style-type: none"> <li>1. Easily scalable to large objects.</li> <li>2. Can be compact.</li> <li>3. Can use white light to image Ronchi ruling on object.</li> </ol>	<ol style="list-style-type: none"> <li>1. Variation in angle of incidence across object requires a calculated variation in period for constant sensitivity.</li> <li>2. Aberrations due to a thick window could be detrimental.</li> </ol>

## REFERENCES

1. J. C. MacBain, J. E. Horner, W. A. Stange, J. S. Ogg, "Vibration Analysis of a Spinning Disk Using Image-Derotated Holographic Interferometry," Experimental Mechanics 19, (1), 67 (1979).
2. J. C. MacBain, W. A. Stange, and K. G. Harding, "Real-Time Resonant Response of a Rotating Disk Using Image Derotated Holographic Interferometry," Experimental Mechanics 21, (1), 34 (1981).
3. D. M. Meadows, W. O. Johnson, and J. Ballen, "Generation of Surface Contours by Moire Patterns," Appl. Opt. 9, p. 942 (1970).
4. F. P. Chiang, "Moire Methods for Contouring Displacement, Deflection, Slope, and Curvature," Proc. Soc. Photo-Opt. Instrum. Eng., 153 (1978).
5. F. P. Chiang, B. S. Parker, D. W. Oplinger, and J. M. Slepetz, Theory and Technology of Moire Methods, Army Materials and Mechanics Research Center, AMMRC SP80-4, April 1980.
6. F. P. Chiang, B. S. Parker, D. W. Oplinger, and J. M. Slepetz, "Multipurpose Optical Moire Processor," Optical Engineering, 18, pp. 456-459 (1979).
7. G. L. Cloud, "Simple Optical Processing of Moire-Grating Photographs," Experimental Mechanics, 20, No. 8 (1980).
8. J. Grinberg, A. Jacobsen, W. Bleha, L. Miller, L. Fraas, D. Boswell, and G. Meyer. "A New Real-Time Non-Coherent Light Valve Image Converter - The Hybrid Field Effect Liquid Crystal Light Valve," Opt. Eng. 14 (1975).
9. W. P. Bleha, L. T. Lipton, E. Wiener-Avnear, J. Grinberg, P. C. Reif, P. Casasent, H. P. Brown, and B. V. Marhavitch, "Application of the Liquid Crystal Light Valve to Real-Time Optical Data Processing," Opt. Eng. 17, p. 371, (1978).
10. J. Feinlieb and D. S. Oliver, "Reusable Image Storage and Processing Device," Applied Optics 11, p. 2752 (1972).
11. A. T. Glassman, "Automated Interferogram Reduction," Presented at Soc. Photo-Opt. Instrum. Eng. Meeting, Washington, D. C., April 19, 1979.
12. P. Mengers, "Low Contrast Imaging," Electro-Optical System Design, Oct. 1978.

13. W. T. Welford, "Some Applications of Projected Interference Fringe," Optical Acta, 16, p. 371 (1969).
14. S. H. Rowe, "Projected Interference Fringes in Holographic Interferometry," J. Opt. for Am. 66, p. 1599 (1971).
15. R. Ritter and H. Meyer, "Vibration Analysis of Plates by a Time-Averaged Projection-Moire Method," Applied Optics, 19, No. 5, (1979).
16. J. C. MacBain, W. A. Stange, and K. G. Harding, "Analysis of Rotating Structures Using Image Derotation with Multiple Pulsed Lasers and Moire Techniques," presented Spring 1981 SESA Meeting, Detroit, MI.
17. J. S. Harris, R. L. Fusek, J. S. Marcheski, "Stroboscopic Interferometer," Applied Optics, 18, (14) 2368 (1979).
18. J. P. Sihora and D. W. Taylor, "Deflection of Rotating Marine Propellers Using Projected Grid Moire Techniques," Presented at May 1980 SESA Meeting, Boston, MA.
19. E. Archbold, J. M. Burch, and A. E. Enno, "Recording of In-Plane Surface Displacement by Double Exposure Speckle Photography," Optica Acta 17, 883 (1970).
20. J. A. Liendertz, "Interferometric Displacement Measurement on Scattering Surfaces Utilizing Speckle Effect," J. Phys. E., Sci. Instrum. 3, 214 (1970).
21. J. N. Butters and J. A. Leindertz, "A Double Exposure Technique for Speckle Pattern Interferometry," J. Phys. E., Sci. Instrum. 4, 277 (1971).
22. G. A. Massey, Study of Vibration Measurement by Laser Methods, NASA Report. No. NASA CR-985 (1968).
23. P. M. Boone, "Holographic Determination of In-Plane Deformation," Opt. Tech. 2, (24) (1970).
24. H. J. Caulfield, Handbook of Optical Holography, Academic Press, New York, p. 595 (1979).
25. C. M. Vest, Holographic Interferometry, John Wiley & Sons, New York, p. 388 (1979).
26. R. K. Erf, Holographic Nondestructive Testing, Academic Press, New York, p. 122 (1974).
27. W. R. Smith, Modern Optical Engineering, McGraw Hill, New York, p. 133 (1966).

28. R. Jones and C. Wykes, "The Comparison of Complex Object Geometries Using a Combination of Electronic Speckle Pattern Interferometric Difference Contouring and Holographic Illumination Elements," Optica Acta 25, 449 (1978).

APPENDIX A  
OBJECT MOTOR SPEED CONTROLLER

## APPENDIX A

### OBJECT MOTOR SPEED CONTROLLER

The object motor speed controller was built to provide accurate and easy setting of the object speed. This capability is important in obtaining resonant frequency data about rotating objects. The speed controller uses a signal directly from the optical encoder on the object spindle to provide feedback data which continuously corrects and stabilizes the object speed to the preset value. The speed can be set by the thumbwheel controls to within 1 rpm, and the electronics maintain this speed to within  $\pm 2$  rpm. The schematic drawings for the object motor speed controller are shown in Figures A.1 through A.8 (Drawings 1 through 8) and Figure A.9 lists the Pin assignments.



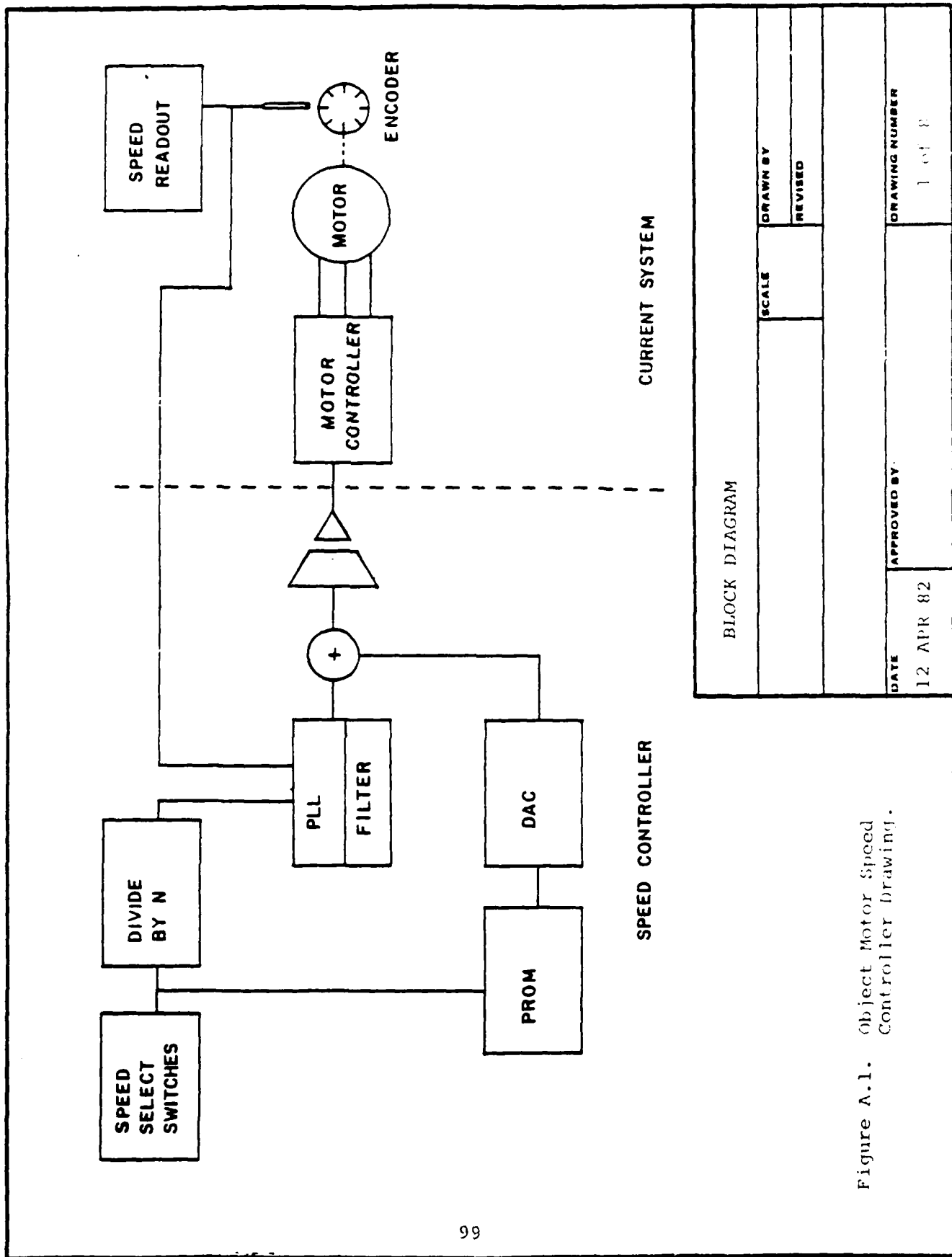
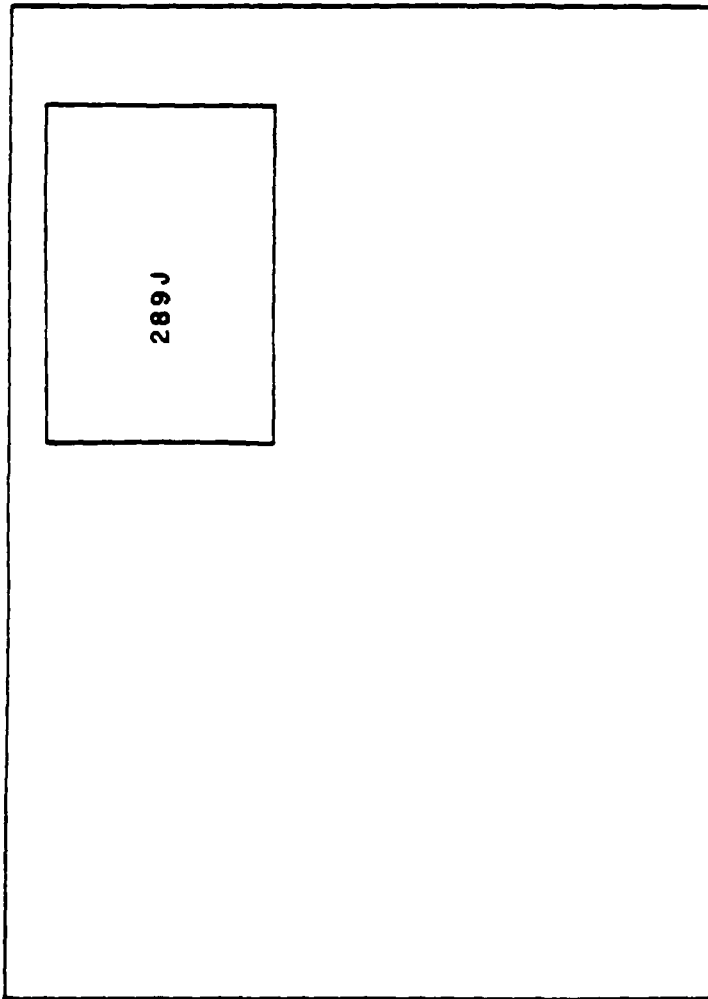


Figure A.1. Object Motor Speed Controller Drawing.



ISOLATION AMPLIFIER			
SCALE		DRAWN BY	
		REVISED	
DATE		APPROVED BY	
12 APR 82			
		DRAWING NUMBER	
		2 of 8	

Figure A.2. Object Motor Speed  
Controller Drawing.

100

MADE IN U.S.A.

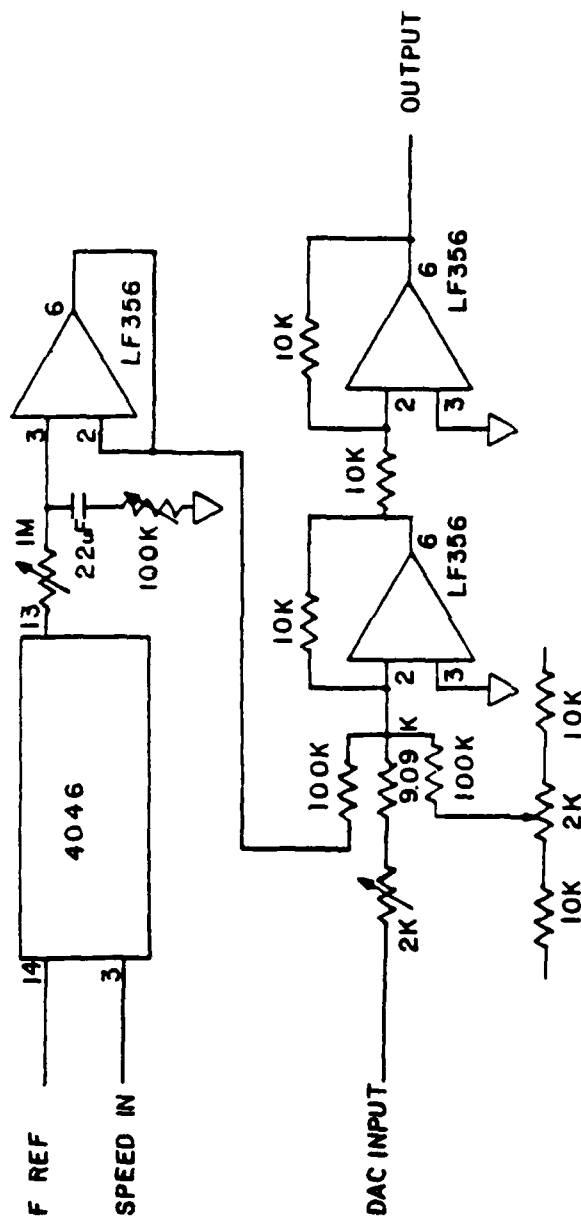
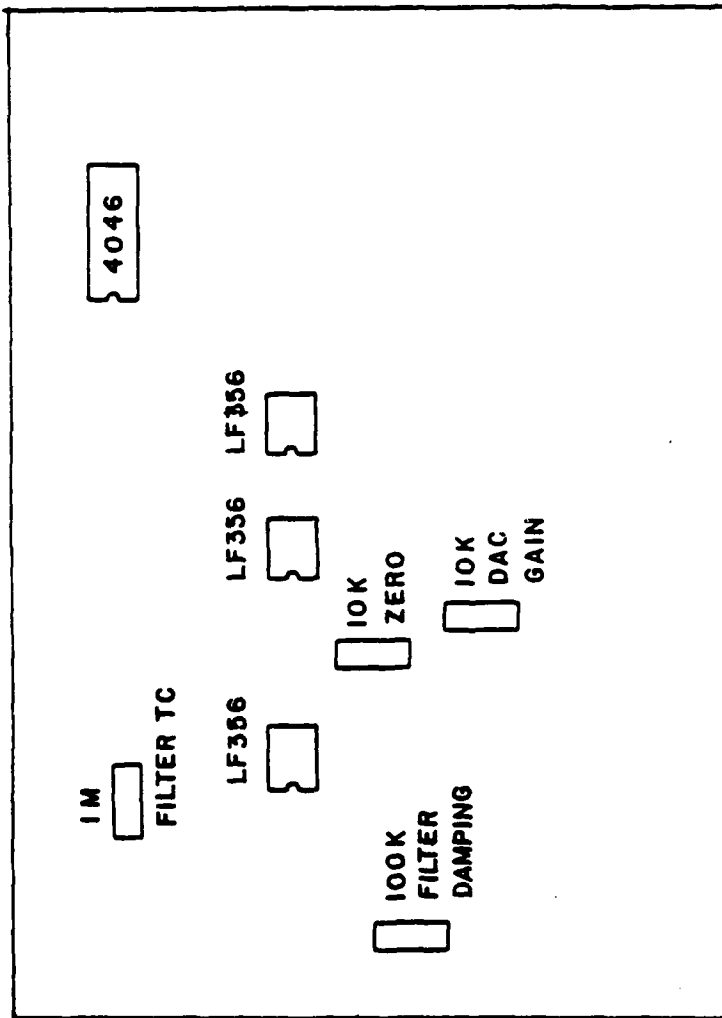


Figure A.3. Object Motor Speed Controller Drawing.

ANALOG BOARD			
SCALE	DRAWN BY	REVISED	
DATE		DRAWING NUMBER	
12 APR 82		1118	
APPROVED BY			

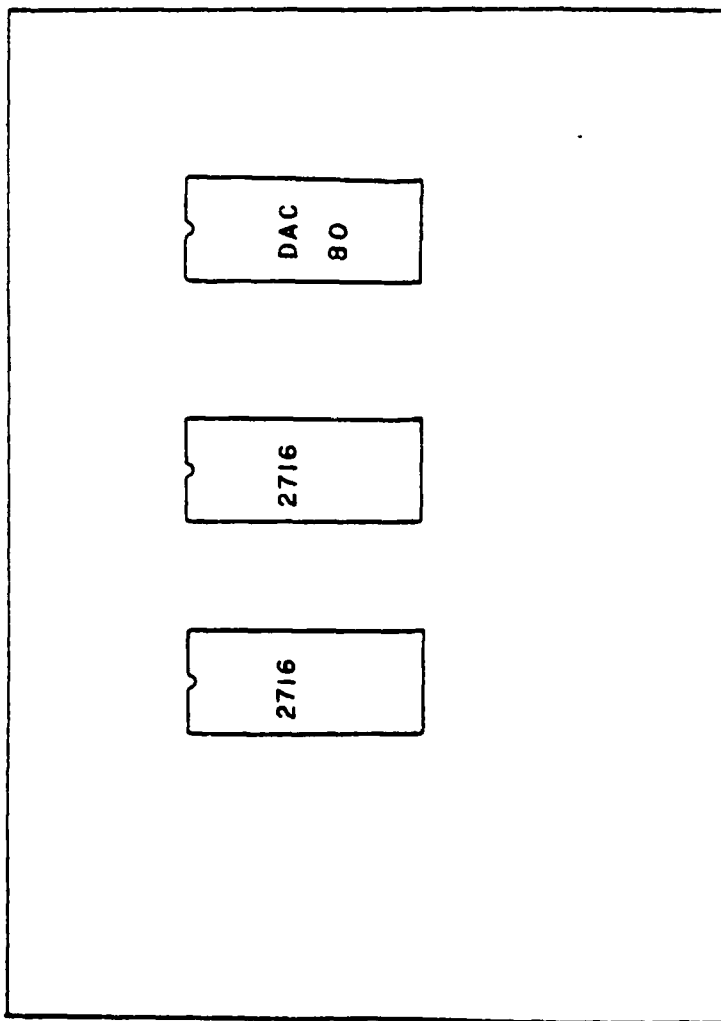
MADE IN U.S.A.



ANALOG BOARD			
SCALE	DRAWN BY	REVISED	
DATE		DRAWING NUMBER	
12 APR 82		4 of 8	

Figure A.4. Object Motor Speed Controller Drawing.

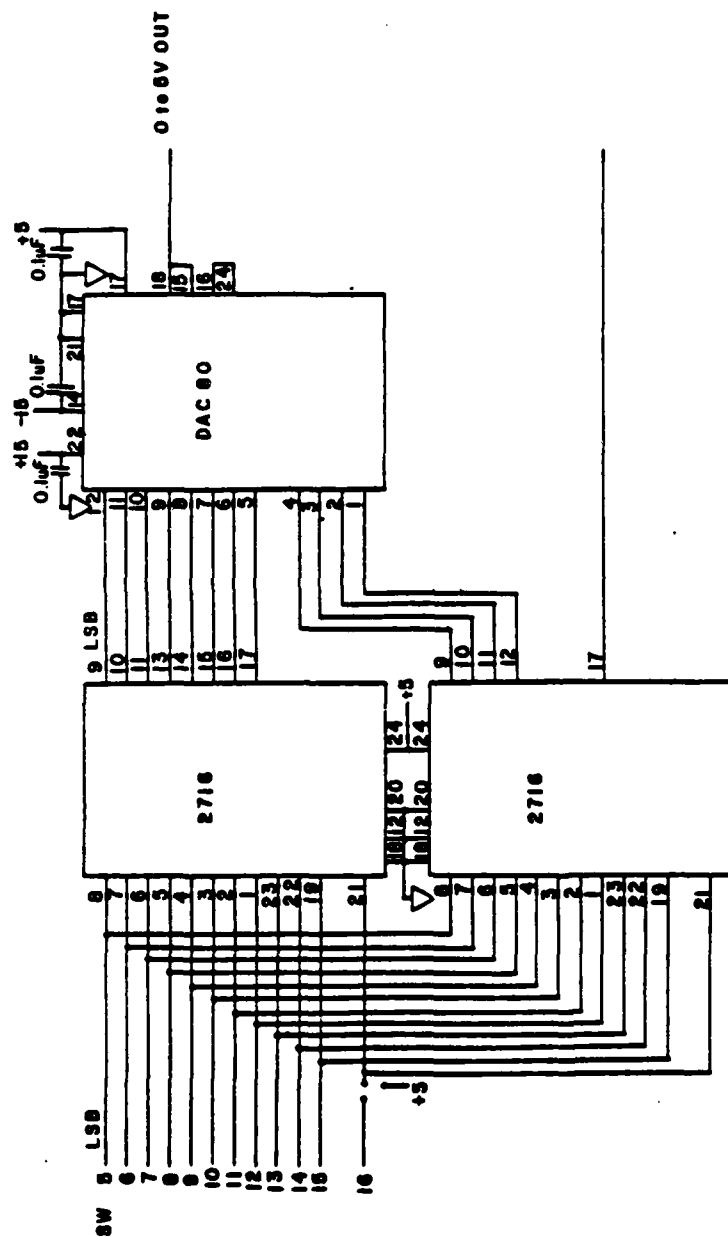
MADE IN U.S.A.



DAC BOARD			
		SCALE	DRAWN BY
			REVISED
DATE	APPROVED BY	DRAWING NUMBER	
12 APR 82		1018	

Figure A.5. Object Motor Speed Controller Drawing.

MADE IN U.S.A.

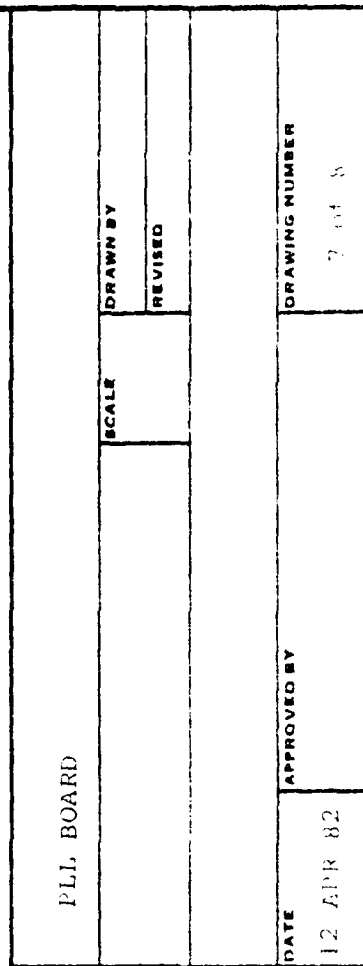


DAC BOARD	
SCALE	DRAWN BY
	REVISED
APPROVED BY	
DATE	DRAWING NUMBER
12 APR 82	6 of 8

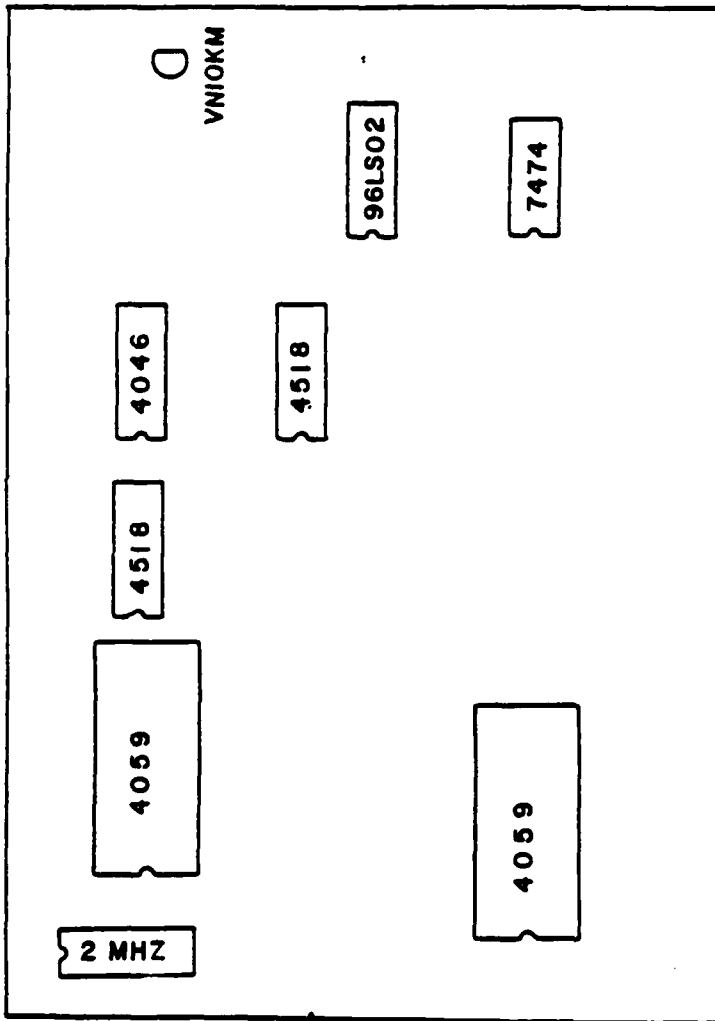
Figure A.6. Object Motor Speed Controller Drawing.

100-ALPMPNF 10 10 10 10

MADE IN U.S.A.



**MADE IN U.S.A.**



PLL BOARD			
SCALE		DRAWN BY	
		REVISED	
DATE		DRAWING NUMBER	
12 APR 82		8 of 8	

Figure A.8. Object Motor Speed Controller Drawing.

MADE IN U.S.A.



# DTOR CONTROLLER MOTHER BOARD PIN ASSIGNMENT

12/14/81

Figure A.9.

PIN #	DAC	SYNTHESIZER	PLL	ISOLATOR
1	NC	SW 1	NC	NC
2	NC	SW 2	NC	NC
3	NC	SW 3	NC	NC
4	NC	SW 4	NC	NC
5	SW 5	SW 5	NC	NC
6	SW 6	SW 6	NC	NC
7	SW 7	SW 7	NC	NC
8	SW 8	SW 8	NC	NC
9	SW 9	SW 9	NC	NC
10	SW 10	SW 10	NC	NC
11	SW 11	SW 11	NC	NC
12	SW 12	SW 12	NC	NC
13	SW 13	SW 13	NC	NC
14	SW 14	SW 14	NC	NC
15	SW 15	SW 15	NC	NC
16	SW 16/NC	SW 16	NC	NC
17	ERROR	NC		
18	DAC OUT	NC	V IN	
19		F OUT	F REF	
20		PHASE P		
21			SPEED IN	SPEED OUT
22			V OUT	
23				EXT IN +
24				EXT IN -
25				
26	-15	-15	-15	-15
27	+15	+15	+15	+15
28	GND	GND	GND	GND
29	GND	GND	GND	GND

APPENDIX B

MAGNETIC TRANSDUCER, HIGH FORCE, HIGH FREQUENCY

## APPENDIX B

### MAGNETIC TRANSDUCER, HIGH FORCE, HIGH FREQUENCY

The principle concern in the design of this transducer was to maximize the force that it can exert on the target disk or beam. The maximum force results from producing the maximum possible magnetic field at the target surface. The biggest single complication in the design arose from the requirement for large force at relatively high frequencies. Several refinements were incorporated to minimize the limiting effects and to maximize power transfer to the magnetic field.

The basic geometry of this transducer is that of a relatively long iron core with a multilayer coil of copper wire wrapped around it. This assembly is contained within a closed, externally threaded housing to allow for cooling and mounting. The actual core is square in cross section and is contained within a cylindrical coil form. This configuration allows freon to be circulated between the core and the coil in order to cool the windings. The freon removes much of the heat generated by  $I^2R$  losses, permitting a higher current to be driven through the wire coils, thus resulting in a higher magnetic field. Figure B.1 shows a schematic cross section of the cooling flow configuration.

At frequencies above several tens of Hertz, eddycurrent losses become significant. These occur in any conductor placed within a changing magnetic field, such as the core of a transformer, or the core of this transducer. As the operating frequency is increased, the eddycurrent losses also increase. This eddycurrent effect can be reduced appreciably by constructing the core of thin, electrically isolated laminations of the core material, again much as within a transformer. The higher the required operating frequency, the thinner the laminations must be.

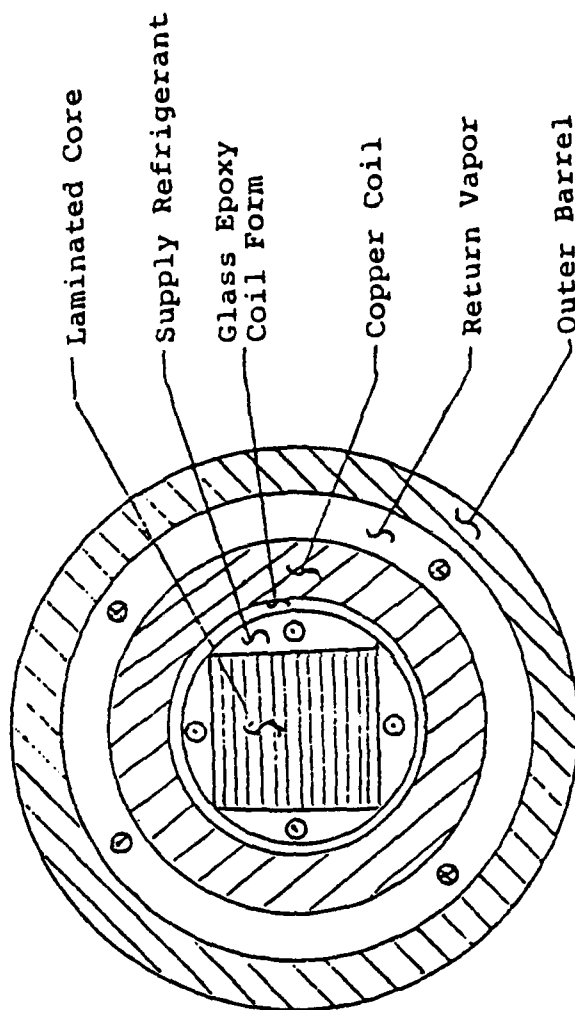
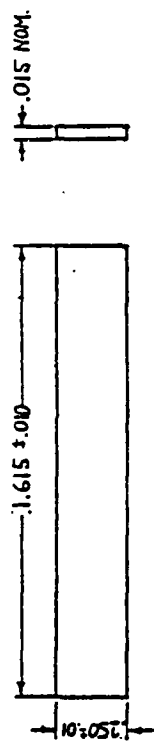
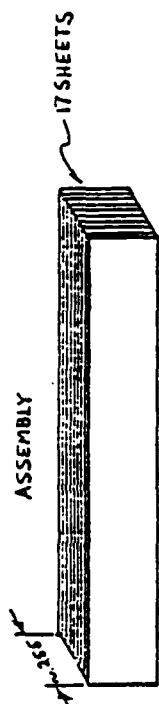


Figure B.1. Schematic Cross Section of Transducer  
Showing Coolant Flow

The core was constructed from 0.015" thick silicon-iron transformer sheet steel to produce a nominal 0.25" x 0.25 x 1-5/8" core, laminated parallel to the long direction (see Figure B.2. The laminations are pressed into a glass-epoxy coil form with a thin layer of electrical tape to fill in the slight gap which resulted from the core's not having a perfectly square cross section. The back end of the core is almost in contact with the transducer body, providing a magnetic flux return path through the transducer body. The front of the core is pressed against a ~ 0.015" thick nonmagnetic stainless steel membrane. This end provides the external magnetic field to the target disk.

The coil consists of eight layers of 30 gauge enameled wire with a copper-constant and thermocouple embedded between the fourth and fifth layers. The resistance of the coil is nominally 12.5 ohms. Fusing current for 30-gauge wire is approximately 10 amperes. To avoid possible damage to the coil, six amperes peak current should not be exceeded under any circumstances. At an ambient temperature of 27°C, the cooling should be adequate for currents up to the above recommended limit. During operation in high temperature environments the coil temperature, monitored by the thermocouple, should not be permitted to exceed 85°C.

Figure B.2 through B.7 show the design drawings of the parts of the transducer assembly. Preliminary performance results on the new transducer design are shown in Figures B.8 through B.11. Figure B.8 shows the Oersteds versus D.C. current input into the transducer. Oersteds are a measure of the magnetic field strength. Figure B.9 illustrates the increased power of the transducer as a function of increasing D.C. bias current at a constant A.C. drive voltage. The acceleration output was measured by an accelerometer mounted on a standard aluminum beam. Figure B.10 illustrates the effect on the drive power of an A.C. voltage increase to the transducer with a constant D.C. bias current. Once again the acceleration is monitored on an aluminum beam which is being excited by the transducer.



TOLERANCES		REVISIONS		MAGNETIC TRANSDUCER	
PROPERTY AS NOTED		NO.	DATE	BY	
DECIMAL		1	Feb. 24, 81	RHWS	
FRACTIONAL		2			
ANGULAR		3			
		4			
		5			
		6			
		7			
		8			
		9			
		10			
		11			
		12			
		13			
		14			
		15			
		16			
		17			
		18			
		19			
		20			
		21			
		22			
		23			
		24			
		25			
		26			
		27			
		28			
		29			
		30			
		31			
		32			
		33			
		34			
		35			
		36			
		37			
		38			
		39			
		40			
		41			
		42			
		43			
		44			
		45			
		46			
		47			
		48			
		49			
		50			
		51			
		52			
		53			
		54			
		55			
		56			
		57			
		58			
		59			
		60			
		61			
		62			
		63			
		64			
		65			
		66			
		67			
		68			
		69			
		70			
		71			
		72			
		73			
		74			
		75			
		76			
		77			
		78			
		79			
		80			
		81			
		82			
		83			
		84			
		85			
		86			
		87			
		88			
		89			
		90			
		91			
		92			
		93			
		94			
		95			
		96			
		97			
		98			
		99			
		100			

Figure B.2. Magnetic Transducer Core Sheet

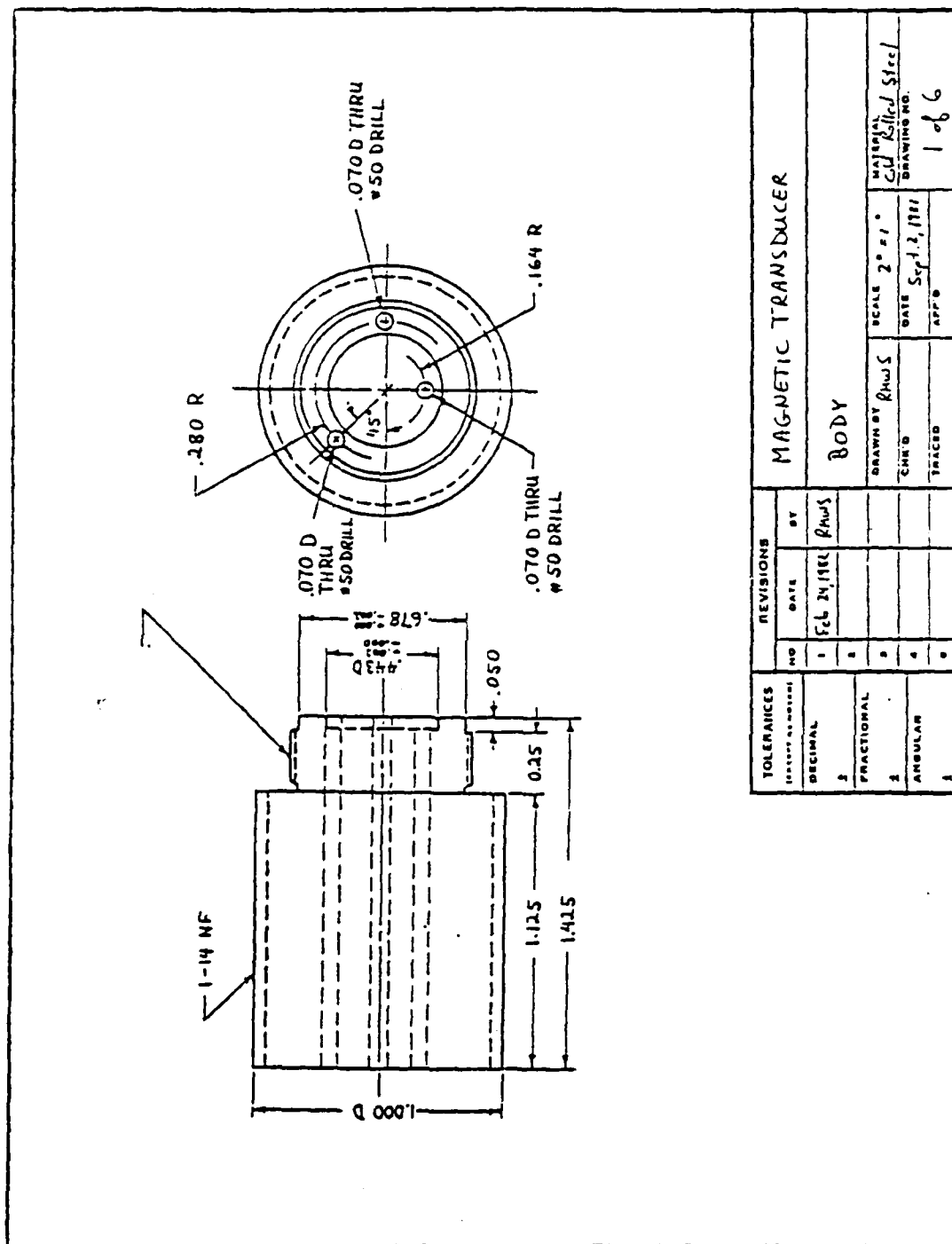
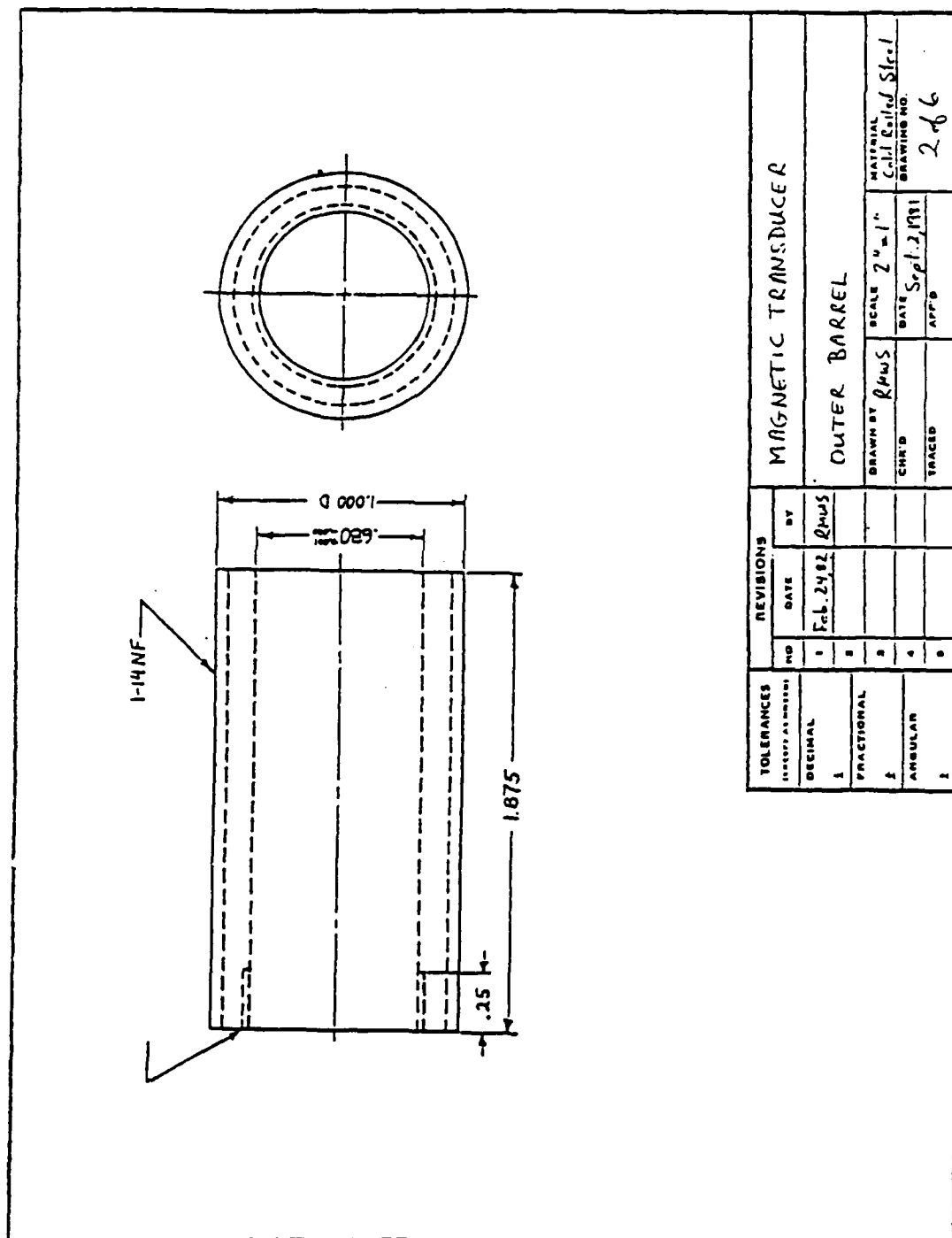
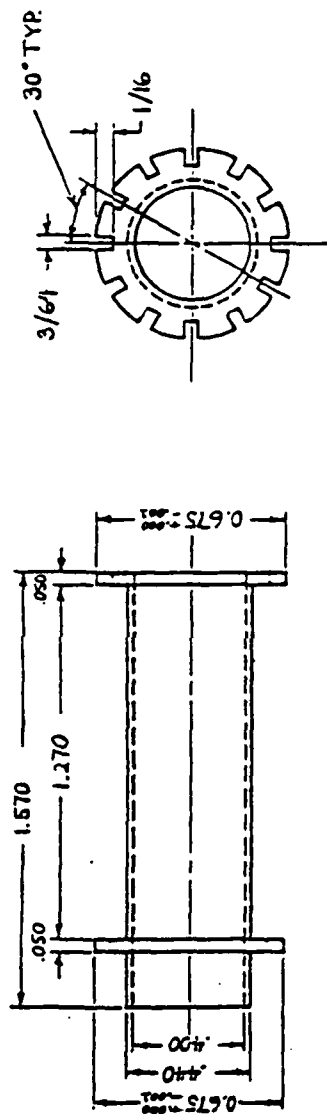


Figure B.3. Magnetic Transducer Body



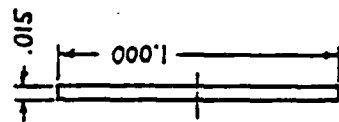
**Figure B.4. Magnetic Transducer Outer Barrel**





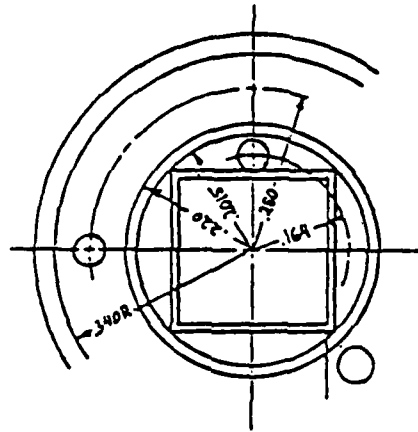
TOLERANCES (Unless Indicated)	REVISIONS			MAGNETIC TRANSDUCER
	NO.	DATE	BY	
DECIMAL	1	Feb. 24, 82	RHWS	COIL FORM
FRACTIONAL	2			
ANGULAR	3			
	4			
	5			
				DRAWN BY RHWS
				CHK'D
				TRACED
				SCALE 2" = 1"
				DATE Sep 2, 1981
				MATERIAL Class EPO-3
				DRAWING NO. 3 of 6

Figure B.5. Magnetic Transducer Coil Form



TOLERANCES		REVISIONS			MAGNETIC TRANSDUCER	
(UNLESS OTHERWISE SPECIFIED)		NO.	DATE	BY		
DECIMAL	1	Feb 24 82	RHW		END CAP	
2						
FRACTIONAL	3					
1						
ANGULAR	4					
2						
		DRAWN BY RHW		SCALE $\approx 2" = 1"$	MATERIAL	
		CHK'D		DATE Sep 2 82	Stainless Steel	
		TACED		APP'D	DRAWING NO.	
					506	

Figure B.6. Magnetic Transducer End Cap



TOLERANCES		REVISIONS		MAGNETIC TRANSDUCER			
DECIMAL	FRACTIONAL	NO	DATE	BY	Hole Spacing Sketch		
1		1			DRAWN BY	RMJS	MATERIAL
2		2			CHK'D		DATE
3		3			TRACED		Sept. 1, 1981
4		4					DRAWING NO.
5		5					6 of 6
6		6					

Figure B.7. Magnetic Transducer Hole Spacing Sketch

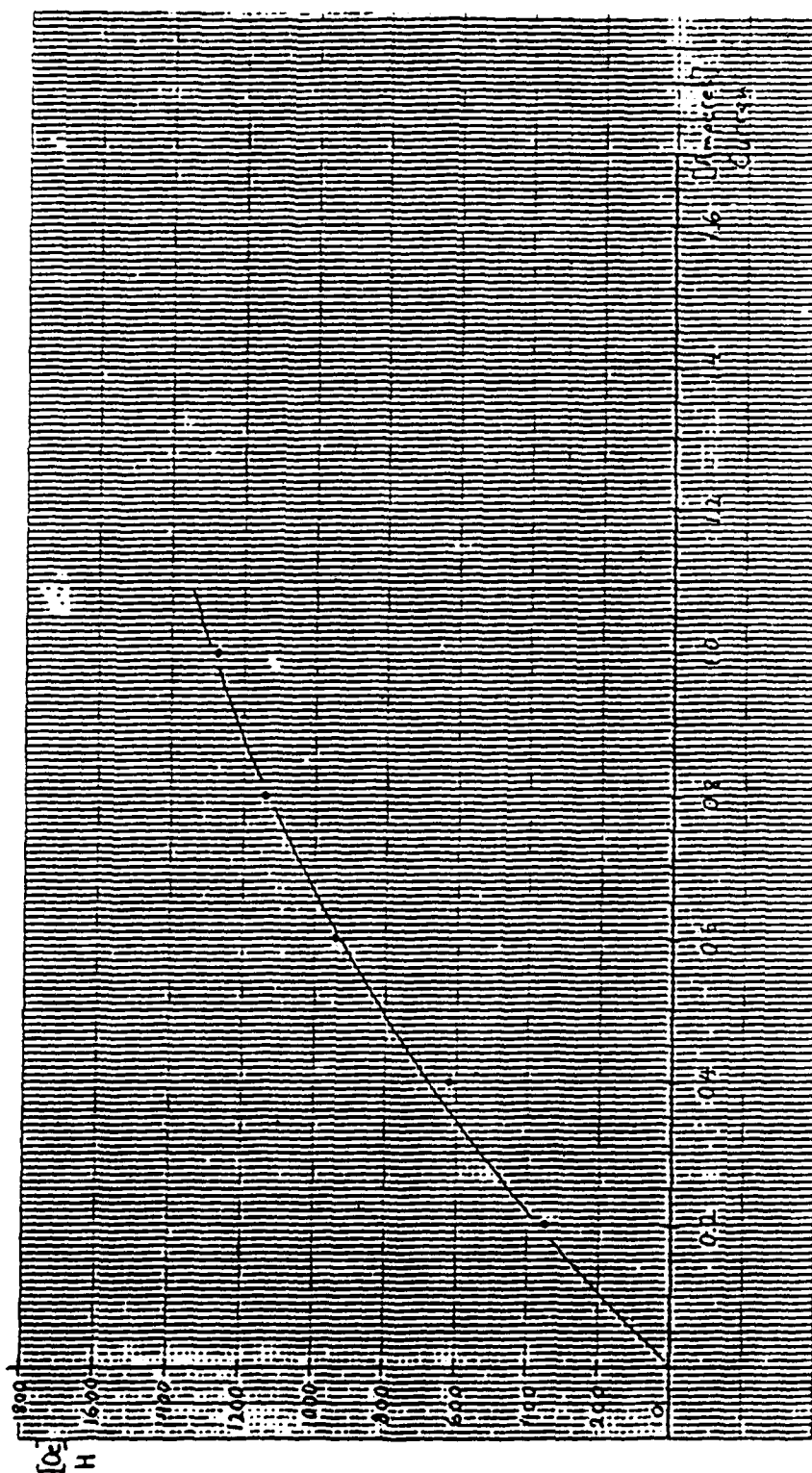


Figure 1.8. Oersted vs D.C. Current Into the Transducer

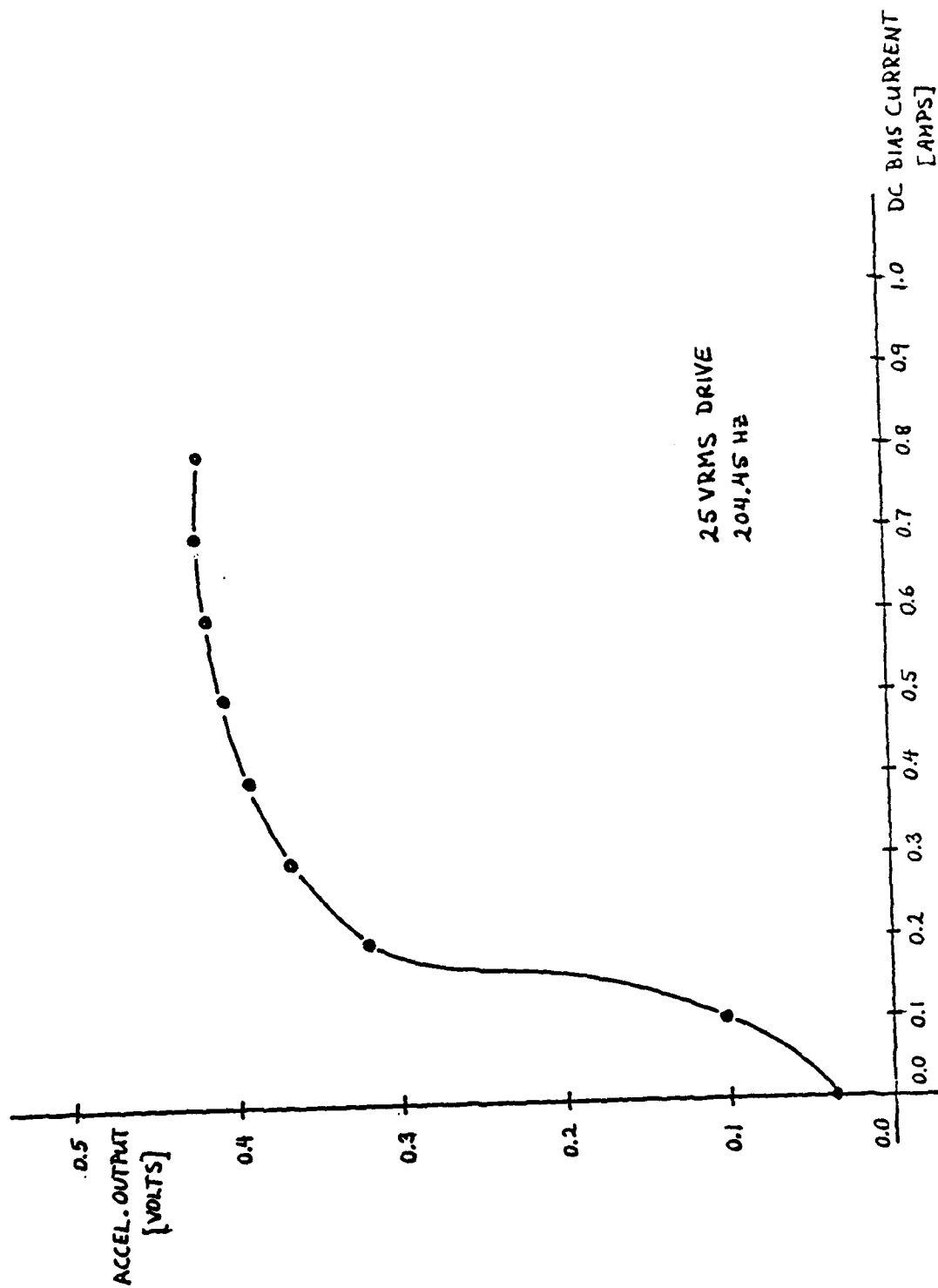


Figure B.9. Acceleration Response vs D.C. Bias at a Constant A.C. Drive Level

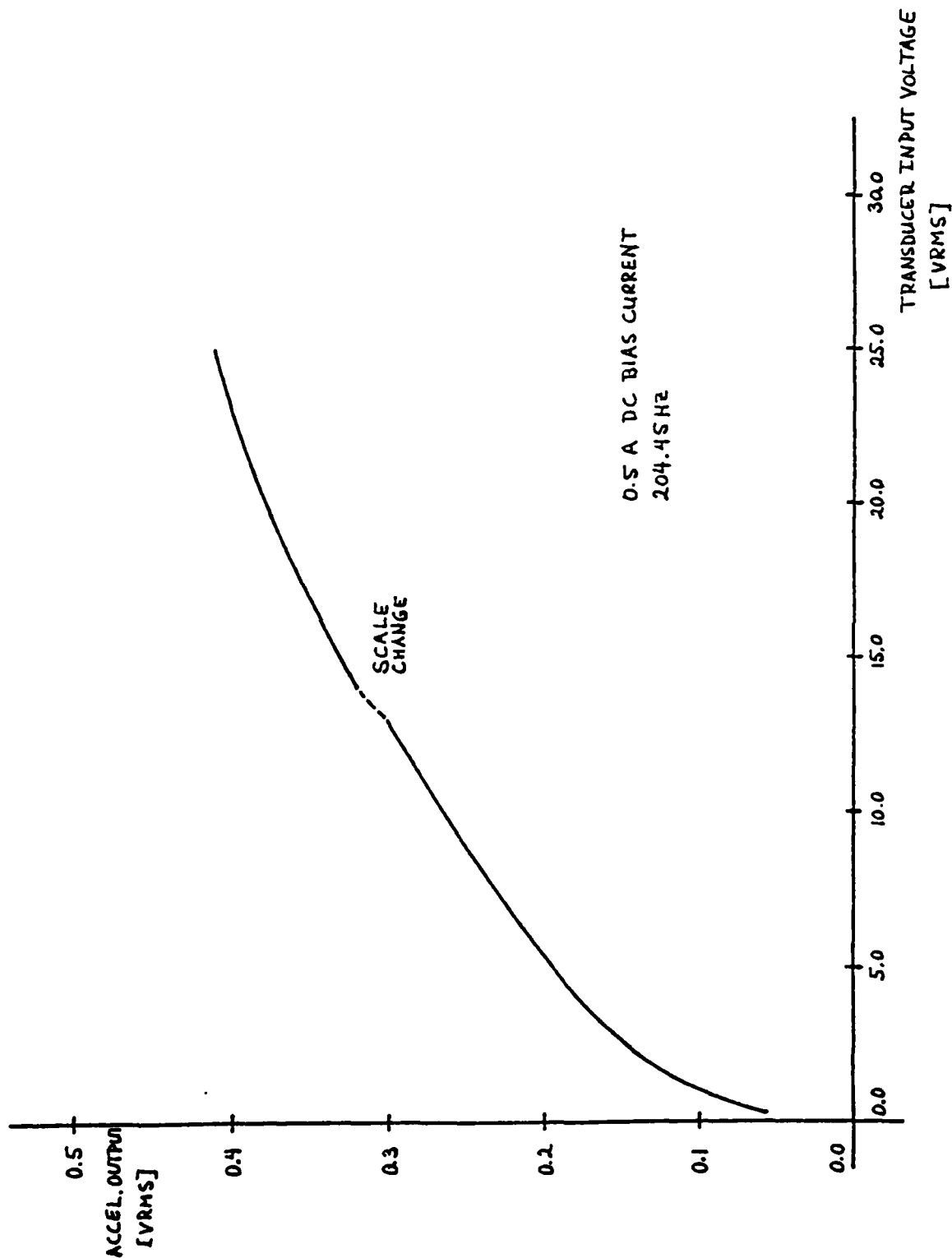


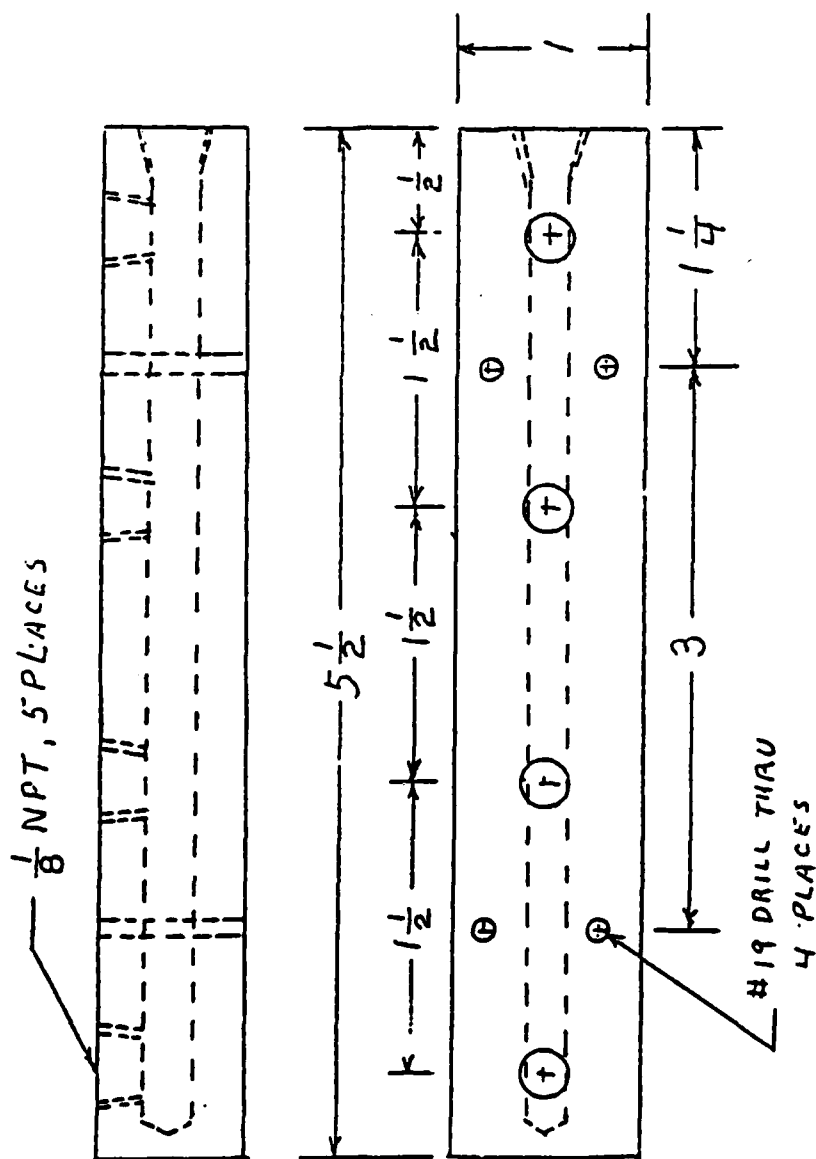
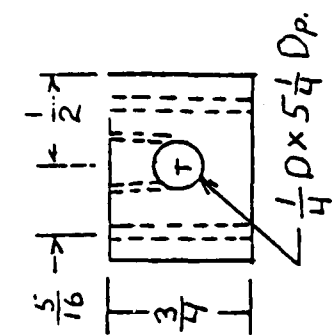
Figure B.10. Acceleration Response vs A.C. Drive Voltage at a Constant D.C. Bias Current

## B.1 COOLING SYSTEM

A cooling system, fabricated to cool the transducers manufactured for the Propulsion Laboratory, was delivered with the transducers. The system was built around a Copeland Model FBAH 0050 LAA compressor/condenser unit. The system is designed to provide cooling for two to eight transducers. Refrigerant flow rate is controlled by metering valves in the supply and return lines, a thermostatic expansion valve, and the amount of freon charge in the system. Distribution of refrigerant among transducers is provided by manifolds (Figure B.11) between the supply and the return line and the transducers. One set of manifolds was provided with the transducer mounting plate to be used on the bladed-disk fixture.

Since it is anticipated that the system will occasionally be subjected to contamination, principally due to connecting and disconnecting transducers, two filter-driers were installed. A filter-drier, having 9 cubic inches desiccant and 21 square inches filter surface, installed in the liquid line, would normally be adequate to provide long-term protection to the system. However, anticipating the probability of refrigerant contamination, not only by moisture but also by solid particulates, a larger filter-drier having 30 cubic inches desiccant and 53 square inches filter area was installed in the suction line. The larger filter drier was placed in the suction line to trap contaminants before they enter the compressor.

A schematic diagram of the refrigerant circuit is provided in Figure B.12. Refrigerant vapor is drawn into the compressor. The heat of compression is dissipated in the air-cooled condensor and liquid refrigerant flows through the receiver and liquid line filter to the expansion valve. The expansion valve regulates the flow of liquid refrigerant to the transducers in response to the temperature of the vapor return line from the transducers which can be considered an evaporator. Two sets of control valves and



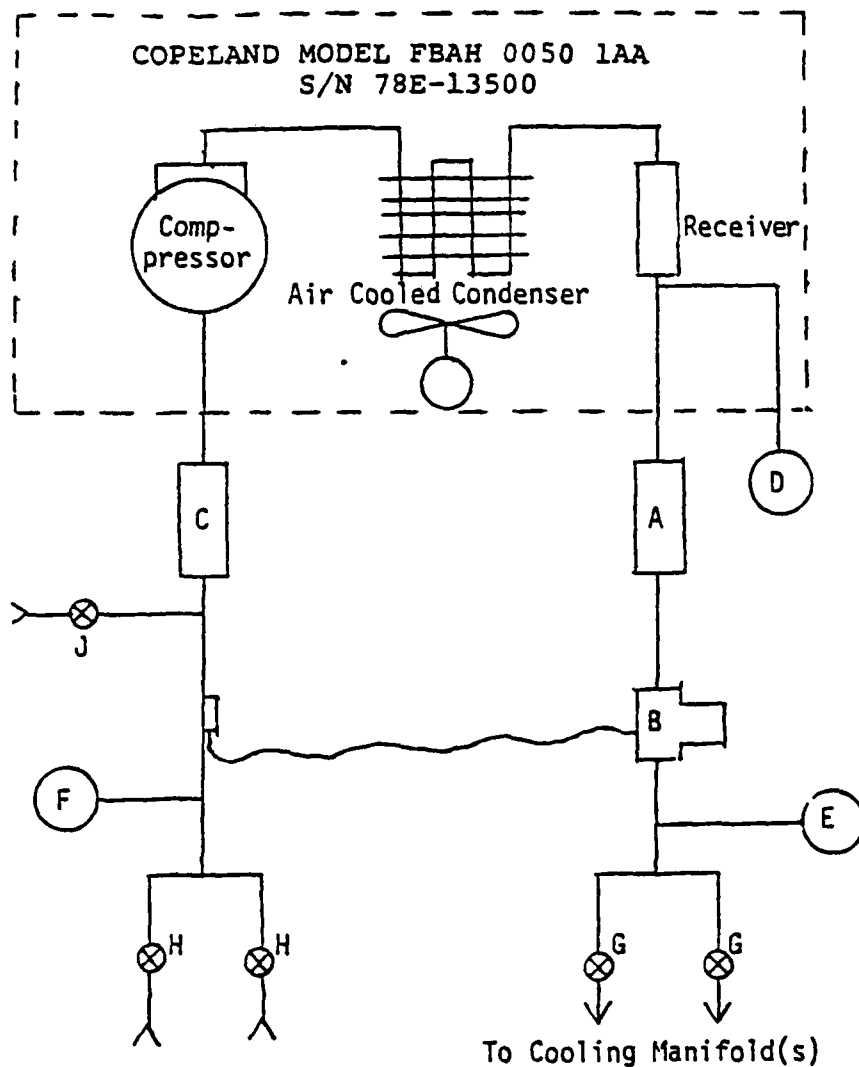
MANIFOLD, COOLANT

MAT'L: AL.

2 REQ'D

Figure B.11. Coolant Manifold





- A. Filter-Drier, Sporlan, Type C082
- B. Thermostatic Expansion Valve, Sporlan, Type FF-1/2-C
- C. Filter-Drier, Sporlan, Type C305
- D. Gauge, Head Pressure, 0-160 PSI
- E. Gauge, Supply Pressure, 0-160 PSI
- F. Gauge, Vapor Pressure, 0-100 PSI
- G. Valve, Transducer Supply
- H. Valve, Transducer Return
- J. Valve, Charging

Figure B.12. Schematic of Cooling System

connections have been incorporated to provide flexibility for cooling a variety of transducer configurations.

#### B.a Transducer Connection

During long quiescent periods, the system will leak down to one atmosphere (0 PSI gage pressure). Connecting lines and transducers to the system could introduce ambient air to the system resulting in overburdening filter/driers. To minimize contamination, the following purge procedure is recommended.

- Connect required number of transducers to manifolds.
- Connect supply lines loosely to supply fittings.
- Connect vapor return lines securely to return fittings.
- Open charge valve to purge room air from transducers and lines.
- Secure supply lines to fittings.
- Close charge valve.

The above procedure results in a clean system with the exception of atmospheric contamination (approximately 0.7 in<sup>3</sup>) entrapped between the supply fittings and supply valves.

#### B.b Operation

The system should function satisfactorily, regardless of the number of transducers being cooled, if after turning the system on, the charge valve is opened until the HEAD PRESSURE gauge registers 120 PSI. Operation for prolonged periods may require opening the charge valves occasionally to balance the system due to slight leakage at the many mechanical connections of the system.

The following procedure is recommended for satisfactory operation of the system.

##### Start-up:

- Open (CCW) valve F-12 cylinder.
- Open (CCW) supply and return valves required.

- Turn on AC power switch.
- Open (CCW) charge valve until head pressure builds up to 100-120 PSI.
- Close (CW) charge valve.

During operation the supply pressure gage should indicate 30-60 PSI and return pressure gage should indicate 0-20 PSI.

Shut-down:

- Turn off AC power switch.
- Close (CW) supply and return valves.
- Close (CW) valve on F-12 cylinder.

DATE  
ILME  
— 83